UCRL-18967

cy. 2

RECEIVED
LAWRENCE
RADIATION LABORATORY

OCT 22 1969

LIBRARY AND
DOCUMENTS SECTION

CYCLING ZONE ADSORPTION SEPARATION BY THERMAL-WAVE PROPAGATION

Burke Baker III

(Ph. D. Thesis)

September 1969

AEC Contract No. W-7405-eng-48

TWO-WEEK LOAN COPY

This is a Library Circulating Copy which may be borrowed for two weeks. For a personal retention copy, call Tech. Info. Division, Ext. 5545

LAWRENCE RADIATION LABORATORY
UNIVERSITY of CALIFORNIA BERKELEY

UCRL-18967 cy. 2

DISCLAIMER

This document was prepared as an account of work sponsored by the United States Government. While this document is believed to contain correct information, neither the United States Government nor any agency thereof, nor the Regents of the University of California, nor any of their employees, makes any warranty, express or implied, or assumes any legal responsibility for the accuracy, completeness, or usefulness of any information, apparatus, product, or process disclosed, or represents that its use would not infringe privately owned rights. Reference herein to any specific commercial product, process, or service by its trade name, trademark, manufacturer, or otherwise, does not necessarily constitute or imply its endorsement, recommendation, or favoring by the United States Government or any agency thereof, or the Regents of the University of California. The views and opinions of authors expressed herein do not necessarily state or reflect those of the United States Government or any agency thereof or the Regents of the University of California.

To Professor Pigford, who was often there
and always willing to listen,

and

to Betty, who was often willing to listen
and always there.

ABSTRACT

It is demonstrated that proper utilization of the wave-propagational properties of fixed-bed adsorption systems can result in separation processes based on the imposed cyclic variation of certain intensive variables in the system. Mathematical and experimental evidence for this conclusion is presented, and a cyclic temperature-driven process based on this conclusion is proposed.

TABLE OF CONTENTS

	Page
ABSTRACT.	ii
LIST OF FIGURES	vi
INTRODUCTION AND BACKGROUND	1
CHAPTER 1. A QUALITATIVE DESCRIPTION OF CYCLING ZONE ADSORPTION	4
CHAPTER 2. THE MATHEMATICAL MODELLING OF CYCLING ZONE ADSORPTION	15
The Derivation of the Equations	15
General Equations	15
Equilibrium-Theory Equations.	19
The Equilibrium-Theory Solution	24
Linear Isotherm	26
Optimum Cycling Frequency	29
Multiple-Zone Case.	30
Amplification by Thermal-Wave Velocity	33
Nonlinear Isotherm.	37
Multiple-Zone Case.	42
Amplification by Thermal-Wave Velocity	46
Comparison of Multiple-Zone and Travelling-Wave Cases	47
CHAPTER 3. THE PERTURBATION SOLUTION OF THE GENERAL EQUATIONS OF CYCLING ZONE ADSORPTION.	48
CHAPTER 4. THE SEPARATION OF ACETIC ACID AND WATER WITH CYCLING ZONE ADSORPTION - THE EXPERIMENTS	57
The Experimental System	57

TABLE OF CONTENTS continued

Page

CHAPTER 4
continued

The Experimental Apparatus. 61

Column Section. 65

Peripheral Equipment. 67

Feed Supply and Effluent-Removal System . 67

Square-Wave Temperature-Generation System 67

Measurement Systems 68

Temperature 69

Concentration 69

Data Reduction. 73

CHAPTER 5. THE SEPARATION OF ACETIC ACID AND WATER WITH CYCLING ZONE ADSORPTION. THE RESULTS AND COMPARISON WITH THE THEORY. 74

Applicability of Equilibrium Theory 74

Single-Zone Standing-Wave Experiments 79

Single-Zone Travelling-Wave Experiments 84

Double-Zone Standing-Wave Experiments 86

Double-Zone Travelling-Wave Experiment. 88

Appendix to Chapter 5: Details of Experimental Conditions. 92

CHAPTER 6. CONCLUSIONS 95

NOMENCLATURE. 98

REFERENCES. 103

APPENDIX A. THE CALCULATION OF TRANSPORT PROPERTIES AND HEAT OF ADSORPTION EFFECTS FOR THE PROCESS. 106

Transport Parameters. 106

TABLE OF CONTENTS concluded

Page

APPENDIX A cont.

Heat of Adsorption Effects. 107

APPENDIX B. THE USE OF INTERSTAGE HEAT REGENERATORS TO INCREASE THE THERMAL EFFICIENCY OF THE PROCESS. 111

Axial Dispersion. 113

Radial Thermal Losses 115

Dual-Zone Experiment with Regenerator 118

APPENDIX C. THE EXPERIMENTAL PRODUCTION OF TRAVELLING THERMAL WAVES OF ARBITRARY VELOCITY 120

ACKNOWLEDGMENT. 122

INTRODUCTION AND BACKGROUND

The ability of certain solids to adsorb substances preferentially from gas and liquid streams onto their surfaces has led to their use in widely varying separation and purification processes. However, due to the mechanical difficulties involved in moving settled beds of solid granules, countercurrent operation has only rarely been employed. One example is the hypersorber, discussed by Berg (1946). Instead, some fixed-bed process is usually used which must be operated cyclically, rather than in the steady state. The various cyclic operations may be summarized in the following three categories.

In conventional adsorption, occasionally called frontal adsorption, a feed stream is fed to a column of particles which adsorb the solute until the entire bed has become at least partially saturated. At this point the bed is regenerated by feeding a new stream of different composition, devoid of the adsorbed solute, to the column.

In elution chromatography, pulses of the components to be separated are introduced into a sweep gas or liquid and are carried through the bed, where they separate because of their varying affinities for the solid. This method, long an analytical technique, has recently been scaled up for commercial production, as described by Timmins et al. (1969).

The chemistry of these adsorption processes can be found in the books by Ross and Oliver (1964) for gas-solid systems, by Kipling (1965) for liquid nonelectrolyte-solid systems, and by Helfferich (1962) for ion exchange. Engineering applications and design techniques can be found in Mantell (1951) and Section 16 of Perry (1963) by Hiester, Vermeulen and Klein.

The third and more recent category are processes in which there is a periodic reversal of the fluid velocity in phase with imposed changes in a thermodynamic gradient, usually owing to pressure or temperature. The "parametric pumping" processes of Wilhelm and his co-workers (Rolke and Wilhelm, 1969; Sweed and Wilhelm, 1969; Wilhelm et al., 1966; Wilhelm et al., 1968) are in this class as are the similar processes of Bohrer (1965), Skarstrom (1959), and Jenczewski and Myers (1968).

This thesis will propose a process similar to this class but with an important difference. Although it has been suggested by Wilhelm et al. (1968) and by Sweed (1969) that the above separations depend on a periodic reversal of fluid velocity, it will be shown that this is not necessary and, indeed, it may be a disadvantage owing to the limits on production rates which it imposes. Furthermore, a general principle concerning the interactions between the imposed potential and the resulting separation will be derived and discussed which leads to a much more efficient separation.

The new process, cycling zone adsorption, uses temperature cycling to achieve a separation. In comparison with other thermal processes such as distillation, it requires less thermal energy because no phase changes are involved. It may have advantages over the first category of adsorption processes because it requires no chemical regenerant or extreme temperature conditions for regeneration. It does not require a sweep fluid, which has to be recovered and recycled as in the case of chromatography. Its main potential disadvantage is that, like other adsorption processes, the mass-transfer rates are usually low, making large throughput rates difficult to obtain. Also, it may be very difficult to obtain nearly complete separations.

In Chapter 1 a qualitative discussion of the new process will be given. Chapter 2 includes a general mathematical model of the system and a solution to a simplified version of the model. Chapter 3 contains a linearized frequency analysis of the process to examine the interphase mass transfer effects. Chapters 4 and 5 report the experimental aspects of the study, including the equipment and results. Following the conclusion section, Appendices A and B report some peripheral calculations for the process and Appendix C concerns a proposal for future experimentation.

CHAPTER 1

A QUALITATIVE DESCRIPTION OF THE CYCLING ZONE ADSORPTION PROCESS

Consider the fixed-bed process shown in Figure 1-1, in which a fluid having a constant solute concentration, y_f, is passed through a bed of solid particles (Pigford et al., 1969b). Suppose the system can be shifted between two equilibrium distribution relationships, lines T_C and T_H in Figure 1-2, by a shift in some thermodynamic potential. Temperature, pressure, concentrations of third substances, or, possibly, electrical and magnetic fields are candidates for causing such a shift and thus creating a cycling zone adsorption process. In this thesis, only temperature changes are considered, so Figure 1-2 is a plot of the distribution isotherms at the operating temperatures T_C and T_H.

Suppose the system is initially held at the constant low temperature T_C. After a long time, the effluent solute concentration must eventually become y_f. If at this time the temperature is raised to T_H, solute which was previously stored on the solid is now expelled into the fluid. The effluent has a concentration y_h for some time, t_c, which depends on the relative volumetric ratios of fluid and solid and on the equilibrium distribution coefficient. Finally, the concentration returns to y_f. Now if the temperature is decreased to T_C, the solid takes up solute from the fluid, and the depleted effluent concentration becomes

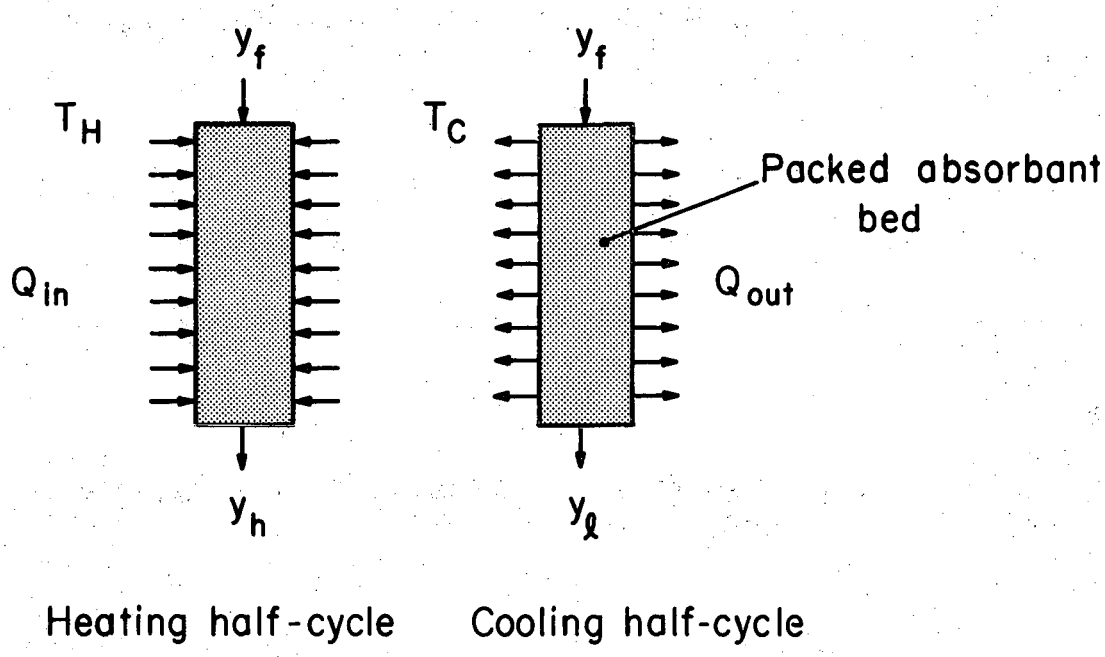

XBL694-2395

Figure 1-1. Single-zone, standing-wave operation of cycling zone adsorber.

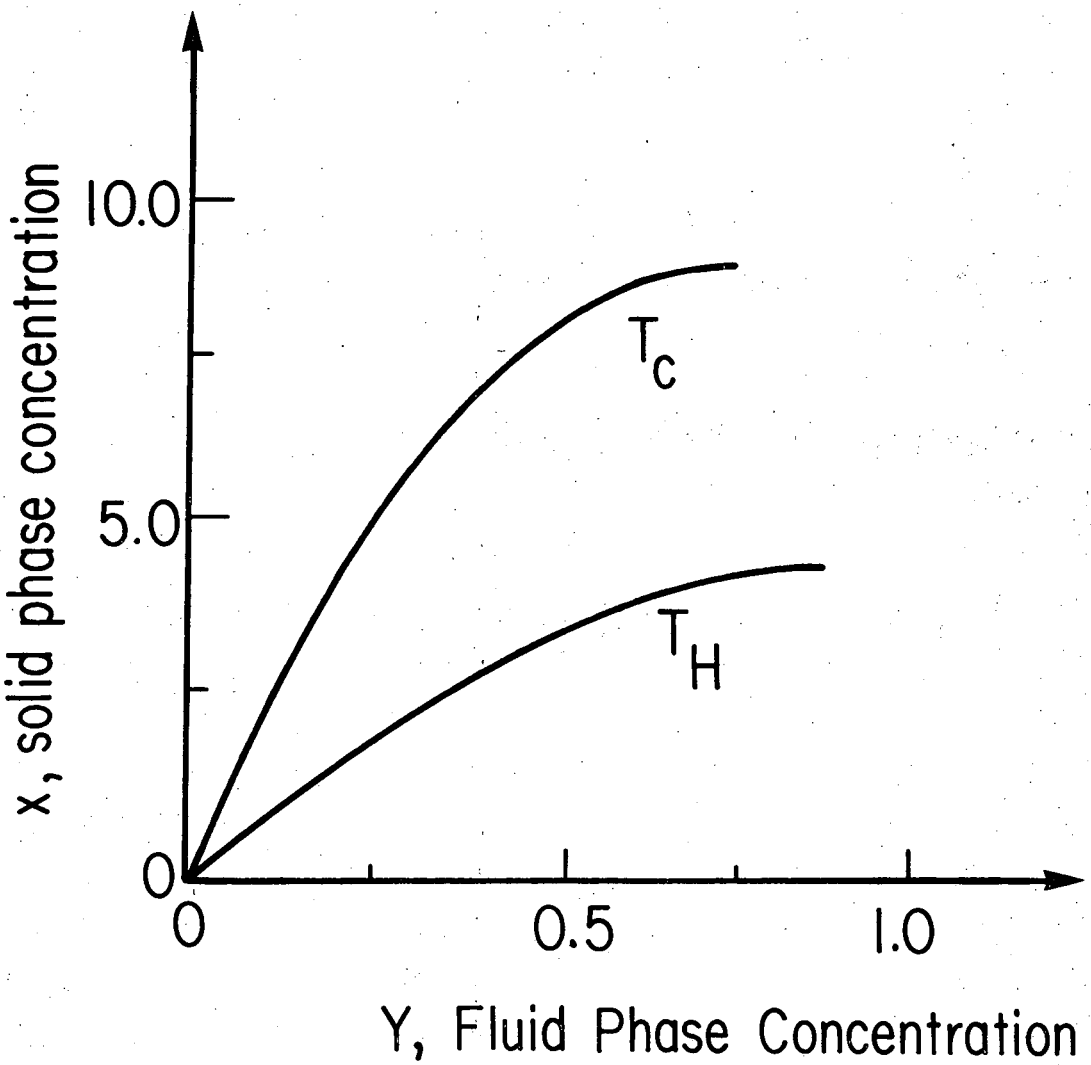

XBL 697-933

Figure 1-2. Solid-fluid equilibrium distribution isotherms.

y_ℓ. After a certain period, t_c, the concentration again returns to y_f and the cycle must be repeated. If parallel twin columns are used, as in Figure 1-3, one exactly one-half cycle out of phase with the other, a separation can be achieved by periodically switching the output of each column as shown in the diagram. The result is a continuous production of two streams of different concentrations, one higher and one lower than that of the feed. It will be shown that the process has an optimum cycle time which depends on the time of passage of a wave of fluid concentration through the bed; this is analogous to the optimum flow-temperature relationship of parametric pumping discussed by Wilhelm et al. (1968).

The type of operation illustrated in Figure 1-1 will be referred to as a single-stage or single-zone process. The separation factors which can be achieved may be interesting if the change in the adsorption equilibrium distribution coefficient is great enough between the low and high temperatures, but this usually does not seem to be the case (Kipling, 1965; Kraus and Raridon, 1959; Rolke and Wilhelm, 1969; Sweed and Wilhelm, 1969; Weiss et al., 1965; idem, 1966; Weiss, 1965).

The separation can be improved considerably, however, by operating two or more single zones in series, the temperature change in each zone being a half cycle out of phase with those in the adjacent zones, as in Figure 1-4. The increase in the separation factor obtained in this way

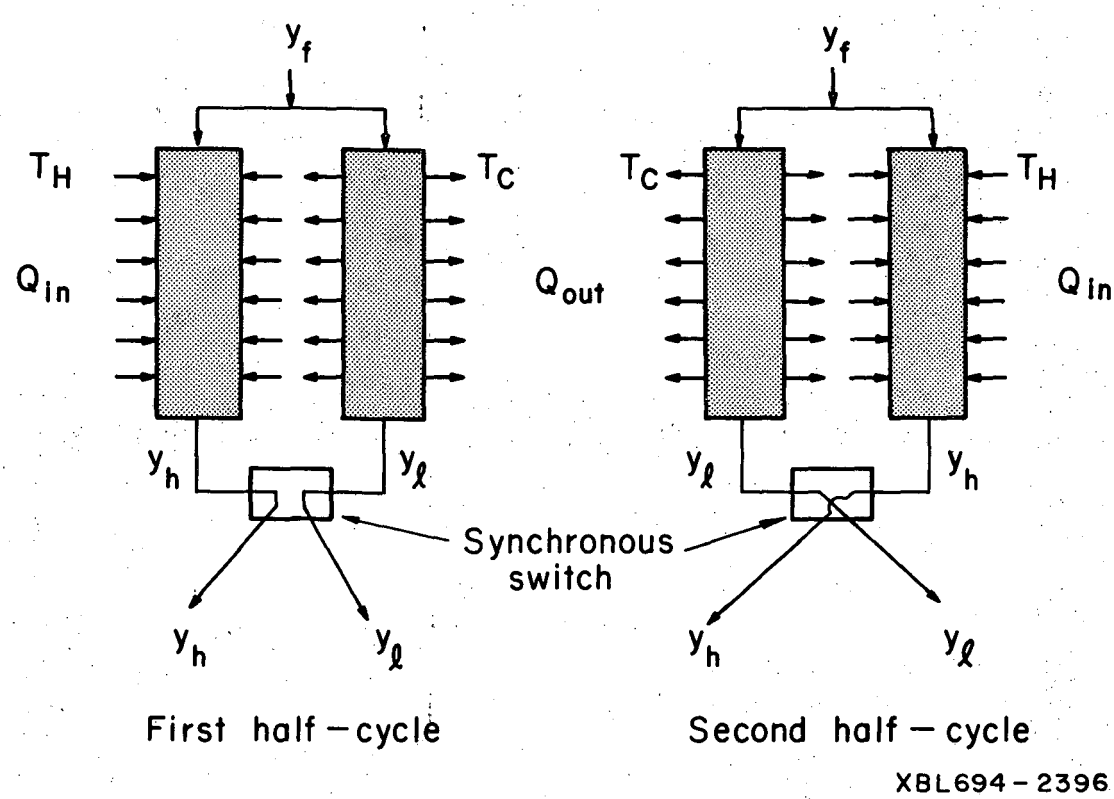

Figure 1-3. Single-zone, standing-wave operation of cycling zone adsorber for continuous production.

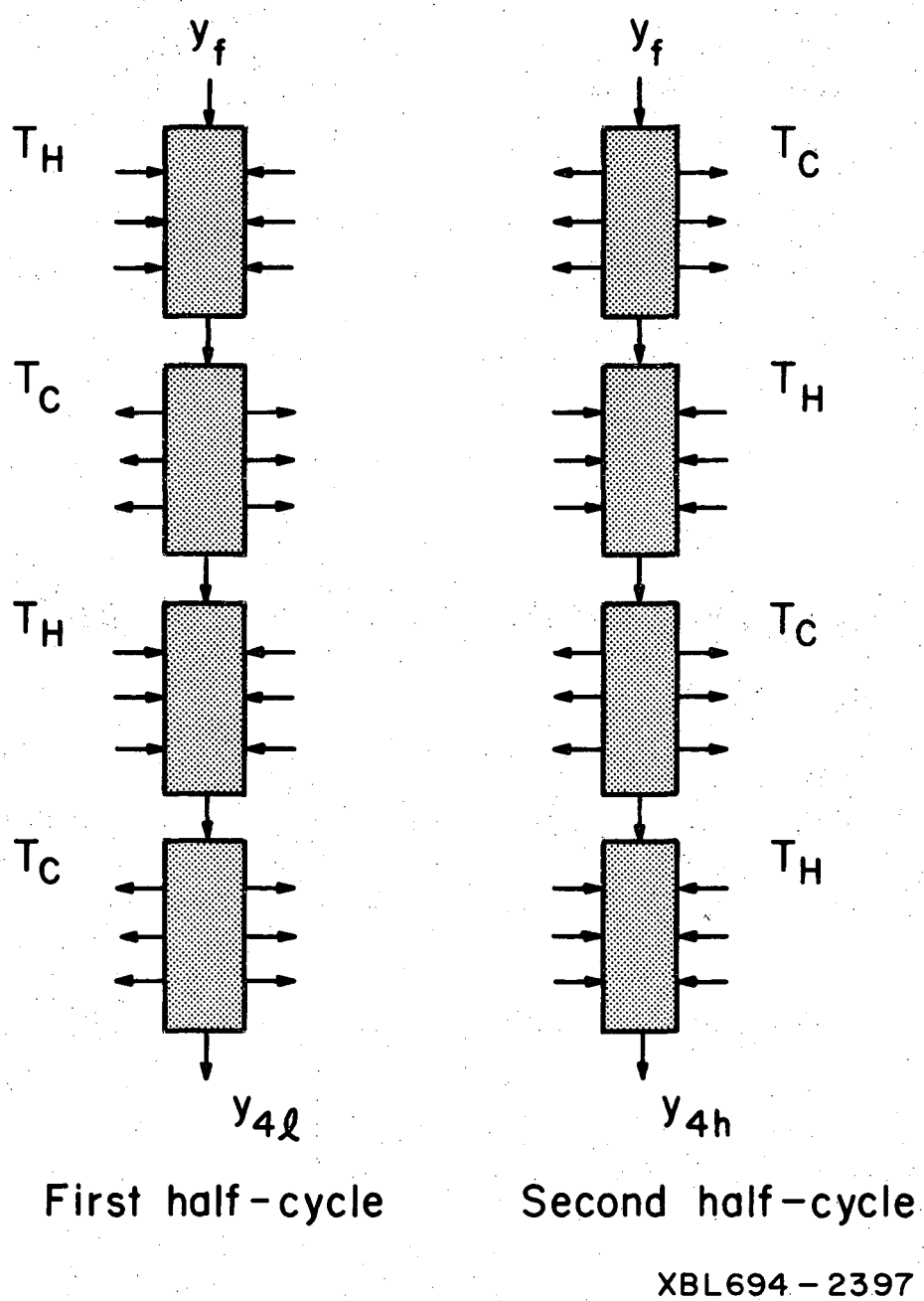

Figure 1-4. Multiple-zone, standing-wave operation of cycling zone adsorber.

will be shown to be comparable to those obtained in the direct mode of parametric pumping by Pigford et al. (1969a). In fact, the number of zones, n, is analogous to the number of batch cycles, n, of parametric pumping. The advantage of the cycling zone adsorber is that it operates without flow reversal and therefore produces enriched and depleted. products continuously.

The question of heating and cooling these beds is an important one. The direct mode of operation shown in Figure 1-1 is one in which there is a standing temperature wave within the bed. Such operation may not be practical on a commercial scale, however, owing to the thermal resistance of the packed bed itself.

There is another method of heating and cooling the solid in which there occurs a travelling wave of temperature changes that moves through the bed owing to the fluid velocity. This occurs when the column is insulated and the input stream is alternately heated and cooled in ordinary heat exchangers located outside the packed bed, as in Figure 1-5. Wave fronts separating hot and cold fluid travel through the bed at a speed determined by the ratio of the volumetric heat capacities of the flowing and stationary phases. For a liquid-solid system, this speed is about one half the fluid velocity; for a gas-solid system the thermal velocity may be three orders of magnitude smaller. If the time of passage of the thermal wave through the bed is not too much less than one half the

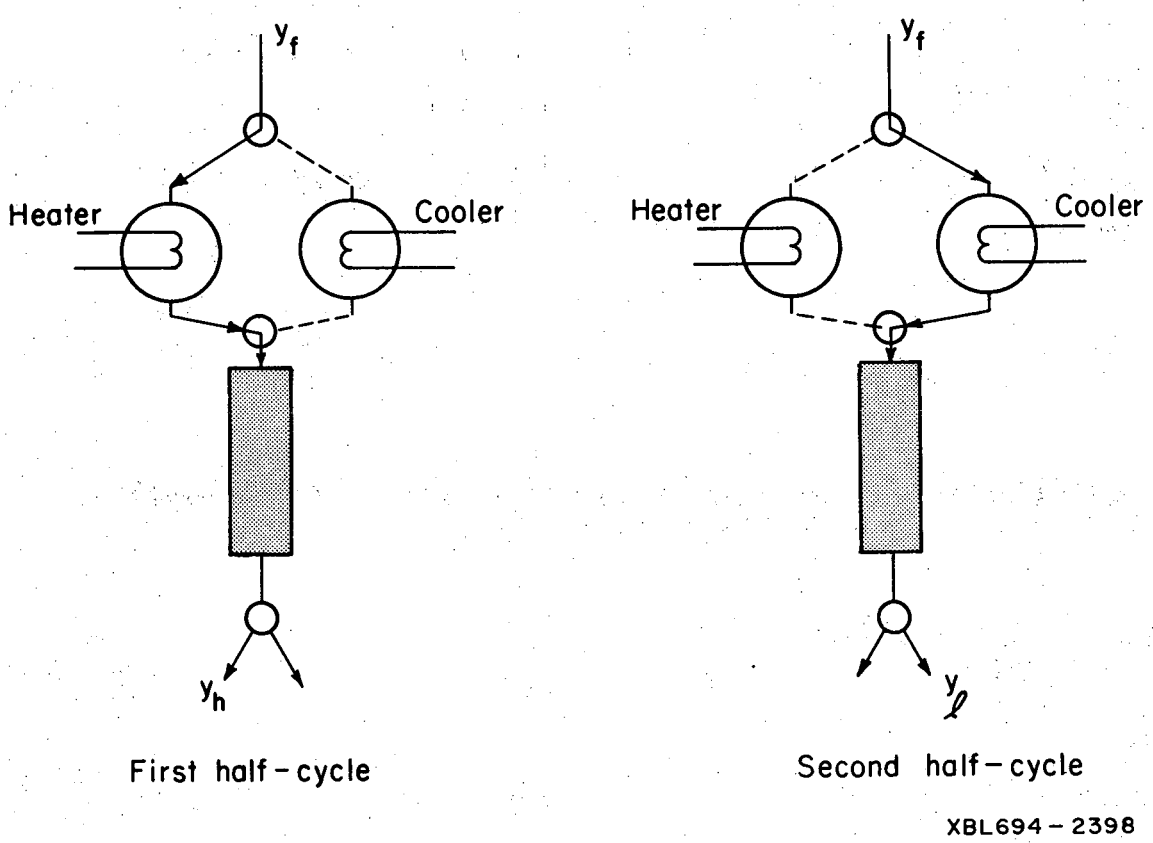

Figure 1-5. Single-zone, travelling-wave operation of cycling zone adsorber.

cycle time, as is easy to achieve with liquid-solid systems, the separation will be as good as if the heat transfer had occurred through the walls. Furthermore, the enormous fluid-solid contact area provides for very efficient energy transport. This, then, is travelling-wave heating and cooling and is a second mode of operation of the cycling zone adsorber.

There is a complication in the use of multiple zones with the travelling wave mode because of the requirement that adjacent zones be out of phase in their temperature cycles. The phase of the thermal wave must be reversed between zone columns, but this can be done using interstage heaters or coolers. In order to reuse the heat supplied in the feed stream, the exchange could be done with other streams in the process. Another way to reuse the heat is to use insulated interstage heat regenerators filled with inert particles having thermal capacity but no adsorptive ability, to delay the thermal waves until they are needed for proper temperature-concentration phasing.

Finally, in generalizing the case of the travelling thermal wave, it is found that a considerable amplification of the separation effect can be obtained if the thermal velocity approaches the concentration velocities in the column. This occurs because although the return of the effluent to y_f occurs about the same time, t_c, after a temperature shift in either the standing or travelling wave cases, the shift to the high or low concentration

does not occur in the travelling wave case until the travelling thermal wave reaches the exit of the column, t_T. It occurs immediately after the temperature switch in the standing wave case. Since the same total amount of solute is rejected or adsorbed by the solid in the two cases, the concentration shift in the travelling-wave case must be greater, since it occurs over a shorter period of time. The idealized exit concentration profiles are shown in Figure 1-6 in which the column, held at T_H or T_C, is back to y_f at $t = 0$. The heating half cycle results from switching from T_C to T_H at $t = 0$. The cooling half cycle results from switching from T_H to T_C at $t = 0$. In the travelling-wave case, the temperature wave takes half the heating or cooling period to pass through the column, emerging at t_T; as a result, the concentration shifts are doubled.

Although imposing an arbitrary thermal velocity on the column may be difficult to do physically, since it requires overcoming the natural thermal velocity of a wave in the column, the incentive for attempting it is quite large. It is shown in the mathematical section that multiple-zone cycling zone adsorption is really an approximate way of obtaining this effect.

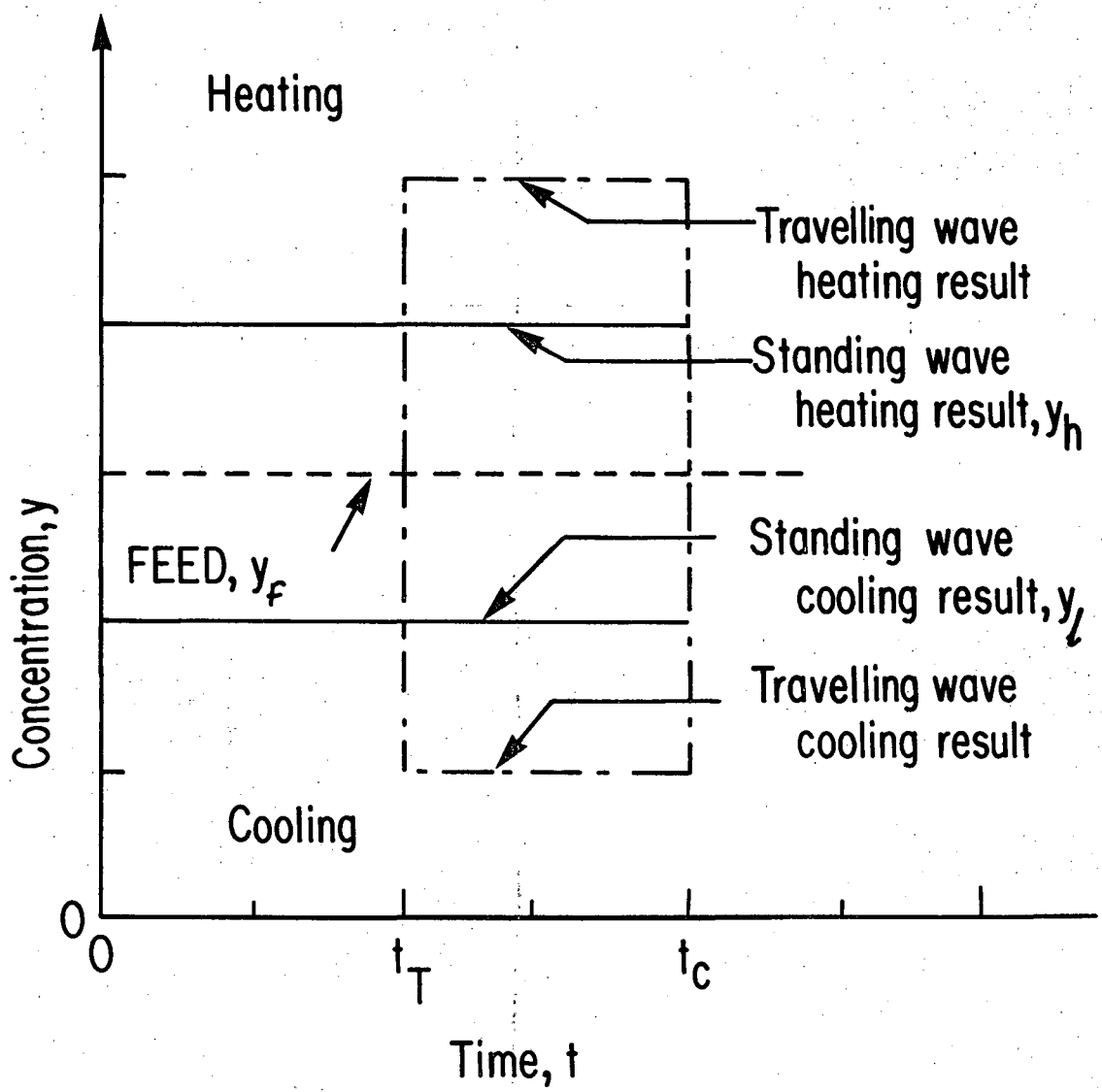

XBL 697-934

Figure 1-6. Idealized effluent concentration profile from single-zone operation illustrating amplification effect of travelling wave - step forcing.

CHAPTER 2

THE MATHEMATICAL MODELLING OF CYCLING-ZONE ADSORPTION

The Derivation of the Equations

General Equations

The equations governing the process are those for a nonisothermal fixed-bed system, which are derived from mass and heat balances over each phase in the system. They will first be derived in fairly general form and will be followed by a discussion of their implicit assumptions.

Disregarding any radial gradients in velocity, concentration, or heat, the balances over an axial differential section of a packed column of cross-sectional area S through which a fluid is flowing are the following. (See the Nomenclature section for the complete definition and units of the terms.)

Mass balance over both fluid and solid phases:

$$S G\, dc\, dt' + \alpha S\, dc\, dz' + (1-\alpha)(1-\varepsilon)\, S\, \rho_s\, dq'\, dz' + (1-\alpha)\,\varepsilon\, S\, dc^*\, dz' + S\,\alpha\, dN_M\, dt' = 0$$

Heat balance over both fluid and solid phases:

$$S G \rho_f C_f\, dT\, dt' + \alpha S \rho_f C_f\, dT\, dz' + (1-\alpha) S \left(\rho_s C_s (1-\varepsilon) + \rho_f C_f \varepsilon\right) dT_s\, dz' + S\,\alpha\, dN_T\, dt' = a_w h_w (T_{air} - T)\, dt'\, dz'$$

Dispersive and diffusive mass- and heat-flux balances:

$$N_M = -(E_D + D_M)\frac{dc}{dz},$$

$$\frac{N_T}{C_f \rho_f} = - (E_D + D_T) \frac{dT}{dz'}$$

Mass balance over the solid phase:

$$S\ (1-\alpha)(1-\varepsilon)\ \rho_s\ dq'\ dz' + (1-\alpha)\ \varepsilon\ dc^*\ dz'$$
$$= - S\ k_M\ a_p\ (c^* - c)\ dt'\ dz'$$

Heat balance over the solid phase:

$$S\ (1-\alpha) \left(\rho_s C_s\ (1-\varepsilon) + \rho_f C_f\ \varepsilon\right) dT_s\ dz'$$
$$= - S\, h_p\, a_p\, (T_s - T)\ dt'\ dz' + (1-\alpha)(1-\varepsilon)$$
$$S\ \Delta H_{ads}\, \rho_s\ dq'\ dz'$$

Note that in the mass balances, the solid is treated in two parts, as a $(1-\varepsilon)$ solid fraction of density ρ_s and concentration q' in equilibrium with an immobile fluid fraction ε of concentration therefore of c^*. In the heat balances the solid and the immobile fluid are also assumed to be in thermal equilibrium, that is, at the same temperature. Dividing through by the differential elements and taking limits results in the following partial differential equations:

$$\frac{\partial c}{\partial t'} + \frac{(1-\alpha)\,\varepsilon}{\alpha} \frac{\partial c^*}{\partial t'} + \rho_s \frac{(1-\alpha)(1-\varepsilon)}{\alpha} \frac{\partial q'}{\partial t'} + v \frac{\partial c}{\partial z'}$$
$$- (E_D + D_M) \frac{\partial^2 c}{\partial z'^2} = 0 \qquad (2\text{-}1)$$

$$\frac{\partial T}{\partial t'} + \frac{\rho_s C_s (1-\varepsilon) + \rho_f C_f \varepsilon}{\rho_f C_f \alpha} (1-\alpha) \frac{\partial T_s}{\partial t'} + v \frac{\partial T}{\partial z'} -$$
$$- (E_D + D_T) \frac{\partial^2 T}{\partial z'^2} = \frac{h_w a_w}{\rho_f C_f \alpha} (T_{air} - T) \qquad (2\text{-}2)$$

$$\frac{\partial q'}{\partial t'} + \frac{\varepsilon}{\rho_s(1-\varepsilon)} \frac{\partial c^*}{\partial t'} = - \frac{k_M a_p}{\rho_s(1-\varepsilon)(1-\alpha)} (c^* - c) \qquad (2\text{-}3)$$

$$\frac{\partial T_s}{\partial t'} = - \frac{h_p a_p}{(\rho_s C_s(1-\varepsilon) + \rho_f C_f \varepsilon)(1-\alpha)} (T_s - T)$$

$$+ \frac{(1-\varepsilon)\ \rho_s\ \Delta H_{ads}}{\rho_s C_s(1-\varepsilon) + \rho_f C_f \varepsilon} \frac{\partial q'}{\partial t'} \qquad (2\text{-}4)$$

The interface between the surface of the solid and the fluid is considered to be at equilibrium and is represented by an expression of the type

$$q' = f(T_s,\ c^*) \qquad (2\text{-}5)$$

Inherent in these equations is the assumption that the densities, heat capacities, heat of adsorption, and transfer coefficients are not functions of temperature or concentration; these effects could be included in a computer solution. The most important assumption is that the mass and heat transfer can be lumped into over-all linear driving-force relationships. For heat transfer, this is a very good assumption since intraparticle heat transfer is good. But as discussed by Sweed and Wilhelm (1969) for a similar system, this is only very approximate in the case of mass transfer, since these processes are particle-diffusion controlled. For an accurate simulation, these authors recommend including the radial particle profile equations. They report that this takes an order of magnitude more computer time, however. The above equations are written for a system in which only one component is

adsorbed from the liquid mixture. In the multicomponent case, there is one mass balance equation for each component for each phase.

A discussion of the adsorption equilibrium distribution relationships can be found in Ross and Oliver (1964) for gas-solid systems and in Kipling (1965) for liquid-solid systems. The three main types are:

$$q' = A c^* \qquad \text{(Linear)} \qquad (2\text{-}6a)$$

$$q' = A (c^*)^k \qquad k < 1 \quad \text{(Freundlich)} \qquad (2\text{-}6b)$$

$$q' = \frac{A c^*}{1 + A c^*} \qquad \text{(Langmuir)} \qquad (2\text{-}6c)$$

(A, k are functions of T_s)

The Freundlich isotherm was found to fit the experimental data for the HAc-water-activated carbon system best.

Analytical solutions of this general set of equations are not known, so that one might use a computer computation similar to those reported by Wilhelm et al. (1968), Sweed and Wilhelm (1969), and Rolke and Wilhelm (1969) for parametric pumping. This was tried during the initial stage of this investigation, but was found to be an inefficient approach at this early stage of process idea generation. The reason for this is that these unsteady-state computations consume quite a lot of computer time, and thus the simulation of each new column arrangement is rather expensive. It is also difficult to reveal the over-all relationships between various possible column arrangements or other variables by computer computation. A more

successful approach for this problem is outlined below. Before dropping the idea of computer simulation, however, it should be said that when the qualitative and semiquantitative aspects of cycling-zone adsorption are well understood, one can return to it to optimize the process.

Equilibrium-Theory Equations

Since the separation effect in cycling zone adsorption depends on a cyclic alteration in the phase equilibrium rather than on any rate differences, it seems reasonable first to design a good equilibrium process on the assumption that rates of exchange are very great, and then to develop the mass- and heat-transfer relationships for the general case in which rates may be important. One analogy would be the example of distillation calculations, in which the design is first made on the assumption of theoretical equilibrium plates and then is modified by the incorporation of plate-efficiency calculations.

For these processes, equilibrium means local equilibrium, the assumption that at a particular point in the column the stationary phase is in equilibrium with the mobile phase. Thus the linear driving-force terms are dropped from the equations because

$$c = c^* \tag{2-7}$$

$$T = T_s \tag{2-8}$$

when local equilibrium exists. One way of approaching this condition, assuming constant transfer coefficients, is to decrease the flow rate through the column. This in turn

tends to increase the effect of the axial dispersive (second derivative) terms, especially if the boundary conditions generate regions of steep temperature or concentration gradients. As pointed out by Lapidus and Amundson (1952) for the case of ion exchange which is similar, there is a conflict, and either the interphase transfer or the axial dispersive terms determine the exact solution of the physical system. However, it is quite common in ion-exchange and chromatographic work to neglect these terms as a first approximation, and as will be shown, this leads to an adequate approximation in the present experimental case.

Since it is shown in Appendix A that the term containing the heat of adsorption in the heat-balance equation, 2-4, is negligible, the thermal equations, 2-2 and 2-4, can be solved independently of the mass-balance equations. Because 2-2 and 2-4 are linear, these have an analytical solution in their general form which was obtained by Lapidus and Amundson (1952). For the experimental system, the interphase mass transfer is poor relative to the interphase heat transfer; therefore when the column is operated at conditions approaching local mass equilibrium, the axial thermal-dispersion terms are controlling in the thermal equations, as shown in Appendix A. However, the effect is minor except in the interstage heat regenerator; its inclusion for that case is shown in Appendix B. The effect does not need to be included in the adsorption-column calculations, as shown in Chapter 5. Again in Appendix A, it is demonstrated that axial mass-transfer effects are negligible in the experiments,

or rather that these systems are in the intraparticle diffusion-controlled regime as mentioned before. The extent to which the local equilibrium approximation is valid here is shown in the Experimental Results section.

To derive the equilibrium theory equations, the terms for interphase transfer heat loss, axial dispersion, and heat of adsorption are neglected in Equations 2-1, 2-2, 2-3, and 2-4, and Equations 2-6b, 2-7, and 2-8 are substituted into 2-1, 2-2, 2-3, and 2-4. Then using the following dimensionless variables,

$y = c/c_o$ (concentration in units of feed concentration)

$z = z'/z$ (axial length in units of column length)

$t = t'v/z$ (time in units of fluid residence time)

$\theta = \dfrac{T - T_o}{T_H - T_o}$ (temperature in units of amplitude; $T_o = (T_H + T_C)/2$)

the resulting equations are:

$$\left(1 + \frac{1}{E}\right)\frac{\partial y}{\partial t} + \frac{\partial}{\partial t}\left(\frac{1}{D}\, y^k\right) + \frac{\partial y}{\partial z} = 0 \qquad (2\text{-}9)$$

$$\frac{\partial \theta}{\partial t} + \frac{1}{u_{th}}\frac{\partial \theta}{\partial z} = 0 \qquad (2\text{-}10)$$

The resulting dimensionless groups are:

$E = \dfrac{\alpha}{(1-\alpha)\varepsilon}$, immobile fluid capacity ratio

$D = \dfrac{\alpha}{(1-\alpha)(1-\varepsilon)\rho_s} A\, c_o^{k-1}$, solid equilibrium capacity ratio

$$u_{th} = \frac{\rho_f C_f \alpha}{\rho_s C_s (1-\varepsilon)(1-\alpha) + \rho_f C_f \varepsilon (1-\alpha) + \rho_f C_f \alpha} ,$$

thermal wave velocity (see Appendix C for expression when wall capacitance is important).

Note that the equilibrium constants A, k, and, therefore, D are functions of θ.

If it is assumed that the temperature of the column is changed by changing the temperature of the inlet feed stream, the boundary conditions are

$$y = y_o = 1 \qquad z = 0 \qquad t > 0$$

$$\theta = \mathrm{per}(\omega t) \qquad z = 0 \qquad t > 0$$

where per(ωt) is a notation for a general time-periodic function of dimensionless frequency ω. By a straightforward application of the Laplace transform, the solution of Equation 2-10 is:

$$\theta = \mathrm{per}\left(\omega(t - z/u_{th})\right) \tag{2-11}$$

which means the output temperature is simply delayed by the time it takes the temperature wave to travel through the column. This travelling-wave case reduces the standing-wave case for $u_{th} = \infty$, for then

$$\theta = \mathrm{per}(\omega t) \ . \tag{2-12}$$

Equation 2-11 approximates the experimental travelling-wave situation. Since u_{th} is not very large in practice, the standing-wave case can not be approximated by input forcing. Rather, it is produced by a jacketed column of small enough diameter that the radial thermal gradients are negligible, with heat transferred through the walls of the column well enough to overcome the

natural thermal dynamics of the column.

Because θ is a periodic function of t and z, the parameters D and k in Equation 2-9 are periodic functions of these variables. The solution of Equation 2-9 is now outlined. The occurrence of the independent variables in the combination $t - z/u_{th}$ in Equation 2-10 suggests a change to the variables

$$\tau = t - z/u_{th}$$
$$\zeta = z$$

Thus θ = per (τ), making D and k functions of τ only and not of ζ. Equation 2-9 is transformed into the new coordinate system using the following relationships:

$$\frac{\partial}{\partial t} = \frac{\partial}{\partial \tau}\frac{\partial \tau}{\partial t} + \frac{\partial}{\partial \zeta}\frac{\partial \zeta}{\partial \tau} = \frac{\partial}{\partial z}$$

$$\frac{\partial}{\partial z} = \frac{\partial}{\partial \tau}\frac{\partial \tau}{\partial z} + \frac{\partial}{\partial \zeta}\frac{\partial \zeta}{\partial z} = -\frac{1}{u_{th}}\frac{\partial}{\partial \tau} + \frac{\partial}{\partial \zeta}$$

$$\frac{d\tau}{d\zeta} = \frac{dt}{dz} - \frac{1}{u_{th}}$$

Equation 2-9 becomes

$$\left(1 + \frac{1}{E} - \frac{1}{u_{th}} + \frac{ky^{k-1}}{D}\right)\frac{\partial y}{\partial \tau} + \frac{\partial y}{\partial \zeta}$$
$$= y^k\left(\frac{dD^{-1}}{d\tau} + \frac{1}{D}\frac{dk}{d\tau}\ \ln y\right) \qquad (2\text{-}13)$$

with the boundary condition

$$y = y_o \qquad \zeta = 0 \qquad \tau > 0$$

The Equilibrium-Theory Solution

This first-order hyperbolic equation can be solved by the method of characteristics, a technique which is discussed in numerous texts such as Sneddon (1957). Equation 2-13 is equivalent to the following set of ordinary differential equations:

$$\frac{d\zeta}{1} = \frac{d\tau}{\left(1 + \frac{1}{E} - \frac{1}{u_{th}} + \frac{ky^{k-1}}{D}\right)} = - \frac{dy}{y^k\left(\frac{dD^{-1}}{d\tau} + \frac{1}{D}\frac{dk}{d\tau}\ln y\right)} \qquad \text{(2-14a, 2-14b)}$$

Solutions of Equation 2-14a are known as the $\tau - \zeta$ characteristics; solutions of 2-14b, which determine the concentration, y, as a function of τ, are only valid along these characteristics.

Equation 2-14b can be written

$$y^k\, dD^{-1} + \frac{y^k}{D}\ln y\, dk + \left(1 + \frac{1}{E} - \frac{1}{u_{th}} + \frac{ky^{k-1}}{D}\right) dy = 0 .$$

If it can be shown that there is a function, f, such that

$$\frac{\partial f}{\partial D^{-1}} = y^k \qquad \text{(A)}$$

$$\frac{\partial f}{\partial k} = \frac{y^k}{D}\ln y \qquad \text{(B)}$$

$$\frac{\partial f}{\partial y} = 1 + \frac{1}{E} - \frac{1}{u_{th}} + \frac{ky^{k-1}}{D} \qquad \text{(C)}$$

then the left-hand side of Equation 2-14b is an exact differential of f because of the relationship

$$df = \frac{\partial f}{\partial D^{-1}} dD^{-1} + \frac{\partial f}{\partial k} dk + \frac{\partial f}{\partial y} dy \ .$$

The solution to df = 0 is, obviously, f = constant. The function, which is determined by integrating the Equations A, B, and C, is

$$f = \frac{y^k}{D} + \left(1 + \frac{1}{E} - \frac{1}{u_{th}}\right) y$$

so that the solution to Equation 2-14b is

$$\frac{y^k}{D} + \left(1 + \frac{1}{E} - \frac{1}{u_{th}}\right) y = C_1 \qquad (2\text{-}15)$$

$$(C_1 = \text{constant})$$

It was not necessary to specify the wave form of the travelling temperature wave to solve Equation 2-14b. It is now necessary to do so to solve Equation 2-14a for the characteristics. The experimental temperature cycling, discussed in Chapter 5, can be approximated by an ideal square wave. The temperature switches instantaneously from a fixed hot temperature to a fixed cold temperature at even multiples of π/ω and switches from the cold temperature to the hot temperature at odd multiples of π/ω. This means that $D(\tau)$ and $k(\tau)$ also cycle in a square wave of frequency ω. Equation 2-15 indicates that y remains constant along a characteristic except when D and k change. Therefore, y remains constant except at the switch times, where Equation 2-15 indicates that it changes in accordance with the relationship

$$\frac{y_i^{k_i}}{D_i} + 1 + \frac{1}{E} - \frac{1}{u_{th}} y_i = \frac{y_{i-1}^{k_{i-1}}}{D_{i-1}} + \left(1 + \frac{1}{E} - \frac{1}{u_{th}}\right) y_{i-1} \qquad (2\text{-}16)$$

where i - 1 refers to conditions before the switch and i to conditions afterward. These results are depicted graphically in the next section.

Linear Isotherm

One notes that if k = 1, the linear isotherm is recovered and then Equation 2-14a no longer depends on the concentration; that is, the characteristics are not concentration dependent. This is a restrictive but useful approximation with which to first examine cycling zone adsorption.

Defining the concentration-wave velocity, u_c, to be the following function of D, and therefore of θ, and defining β to represent the change in u_c during the hot and cold portions of the square-wave cycle,

$$u_c(\theta) = \frac{1}{1 + \frac{1}{E} + \frac{1}{D(\theta)}}$$

then

$$u_c = u_o + \beta \text{ when } \theta = sq(\omega\tau) = +1 \quad \text{(Hot half cycle)}$$
$$= u_o - \beta \text{ when } \theta \quad \text{"} \quad = -1 \quad \text{(Cold half cycle)}$$

Since Equation 2-14a reduces to

$$\frac{d\zeta}{d\tau} = \frac{u_{th}\, u_c}{u_{th} - u_c} \qquad (2\text{-}17)$$

the characteristics are straight lines having slopes of $(u_o + \beta)u_{th} / (u_{th} - u_o - \beta)$ in the hot half cycle and $(u_o - \beta)u_{th} / (u_{th} - u_o + \beta)$ in the cold half cycle.

Equation 2-15 becomes:

$$y(u_{th} - u_c) = u_c\, u_{th}\, C_2 \qquad (2\text{-}18)$$

$(C_2$, constant)

Figure 2-1 is a plot of the characteristics where it has been assumed that $u_{th} > u_c$. When a characteristic passes from a hot region into a cold region, Equation 2-18 shows that the concentration along it shifts to a lower value determined by the ratio

$$q = \frac{u_{th} - (u_o + \beta)}{u_{th} - (u_o - \beta)} \cdot \frac{u_o - \beta}{u_o + \beta} \qquad (2\text{-}19)$$

when it passes from a cold into a hot region, the concentration shifts to a higher value determined by the ratio $1/q$. In Figure 2-1, the period of the cycle $2\pi/\omega$ is chosen for illustration to have

$$\frac{u_{th} - (u_o - \beta)}{u_{th}\,(u_o - \beta)} \geq \frac{\pi}{\omega} > \frac{u_{th} - (u_o + \beta)}{u_{th}\,(u_o + \beta)} \qquad (2\text{-}20a)$$

although this need not always be true. Since a characteristic in the cold period travels at a slower velocity than in the hot period, some characteristics undergo two temperature changes and finally leave the column at the start of the hot period at their original concentration, y_o. Some characteristics, entering the bottom of the column during the hot period, also leave the top at the end of this period at their original concentration, y_o. However, the rest of the characteristics which undergo one and only one temperature change, emerge with their concentration changed. Also note that after the characteristics originating along the ζ-axis at time $\tau = 0$ are swept out of the column, the initial condition of the column is no longer important. Thus a cyclic steady state has been obtained.

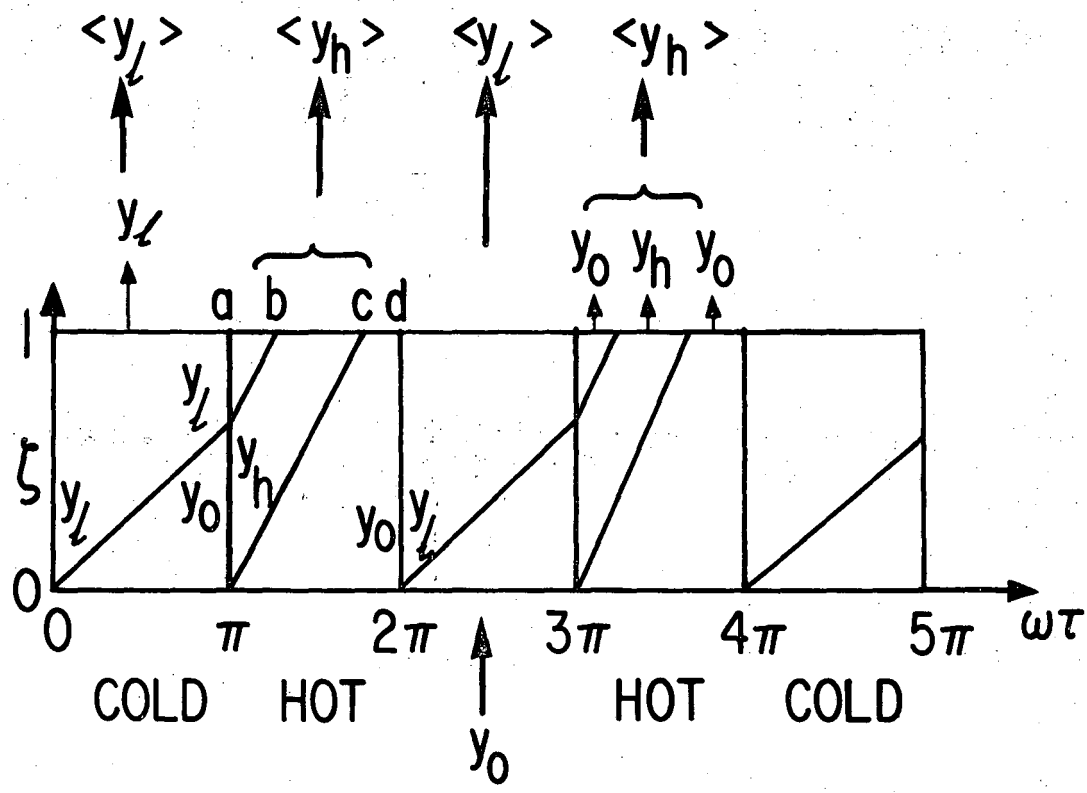

XBL 697-937

Figure 2-1. Characteristic lines used in equilibrium theory for linear isotherms - single-zone square-wave cycling.

Optimum Cycling Frequency

It is now necessary to find the optimum cycle frequency for the column, that is, to minimize the portion of the cycle for which the effluent has concentration y_o, as this portion represents no separation. One way to do this would be to have unequal heating and cooling periods. Only in this way can there be all high-concentration effluent in the heating period and low-concentration effluent in the cooling period. For reasons that will be evident later, it is preferable to have equal periods of heating and cooling, at least for the multiple-column arrangement. There is clearly no point in making π/ω greater than $\left(u_{th} - (u_o - \beta)\right)/u_{th}(u_o - \beta)$ since y_o would break through from the bottom in both half cycles. Nor should it be less than $\left(u_{th} - (u_o + \beta)\right)/u_{th}(u_o + \beta)$ since some of the characteristics starting in both half cycles would undergo two temperature changes and emerge with concentration y_o. It is shown in the next chapter, for the case when $u_o + \beta \simeq u_o - \beta = u_o$, that the optimum separation is given by having

$$\frac{\pi}{\omega} = \frac{u_{th} - u_o}{u_{th}\, u_o}$$

There is still the problem of deciding, for finite values of β, where π/ω should be in the range of expression 2-20a. It is necessary to compute the average y_h concentration $\langle y_h \rangle$. The fractions (ab + cd)/ad and bc/ad must be computed from the slopes of the characteristics in Figure 2-1. These are found to be:

$$\frac{bc}{ad} = q$$

$$\frac{ab + cd}{ad} = 1 - q$$

Since this is true no matter how they are drawn, the average separation is a constant optimum in this range. The average separation factor α_{av} is given by

$$\langle y_\ell \rangle = y_o\, q$$

$$\langle y_h \rangle = y_o(1 - q) + y_o \frac{1}{q} \cdot q = y_o(2 - q)$$

$$\alpha_{av} = \frac{\langle y_h \rangle}{\langle y_\ell \rangle} = \frac{2-q}{q}$$

Also, it can be shown that

$$\alpha_{pk} = \frac{1}{q^2} \quad \text{for all } \omega.$$

Multiple-Zone Case

In the multiple column arrangement, the optimum phase lag between successive columns operating at their optimum frequency is found in a similar manner. For the approximation $u_o + \beta \simeq u_o - \beta = u_o$, the optimum is found to be exactly π radians, using the equations of the next chapter. In this more exact treatment, the average separation $\alpha_{av,n}$ is a constant optimum in the range of the phase lag, γ, given by the relationship

$$\frac{\pi}{\omega} - \frac{u_{th} - (u_o + \beta)}{u_{th}(u_o + \beta)} \geq \frac{u_{th} - (u_o - \beta)}{u_{th}(u_o - \beta)} \left(\frac{\gamma}{\pi} - 1\right) \geq \frac{\pi}{\omega} - \frac{u_{th}(u_o - \beta)}{u_{th}(u_o - \beta)} \tag{2-20b}$$

where ω is in the range of Equation 2-20a. Since $\gamma = \pi$ is

always in this range, this case will be considered in the diagrams. The peak separation $\alpha_{pk,n}$ is a constant optimum for a range equal in magnitude to 2π less the range of Equation 2-20b. The center of this range is the center of the range of Equation 2-20b.

The characteristic diagram for this case is shown in Figure 2-2, where it has been assumed that the cyclic steady state has been assumed to hold in each zone and where the cycle period has been chosen to be $\left(u_{th} - (u_o - \beta)\right)/u_{th}(u_o - \beta)$. The fractions are similar to the previous case,

$$\frac{ab}{ac} = q$$

$$\frac{bc}{ac} = 1 - q$$

This results in the difference equations

$$\langle y_h \rangle_n = \langle y_\ell \rangle_{n-1}(1 - q) + \langle y_h \rangle_{n-1} \frac{1}{q} \cdot q \qquad (2\text{-}21a)$$

$$\langle y_\ell \rangle_n = \langle y_\ell \rangle_{n-1} \cdot q \qquad (2\text{-}21b)$$

with the boundary conditions being

$$\langle y_h \rangle_o = \langle y_\ell \rangle_o = y_o \qquad (2\text{-}22)$$

The solution to Equation 2-21b is

$$\langle y_\ell \rangle = y_o \, q^n \qquad (2\text{-}23)$$

which, inserted in Equation 2-21a, results in

$$\langle y_h \rangle_n = \left[1 + (1 - q) \sum_{i=0}^{n-1} \left(\frac{1 - b}{1 + b}\right)^i\right] y_o$$

$$= y_o \left[2 - q^n\right] \qquad (2\text{-}24)$$

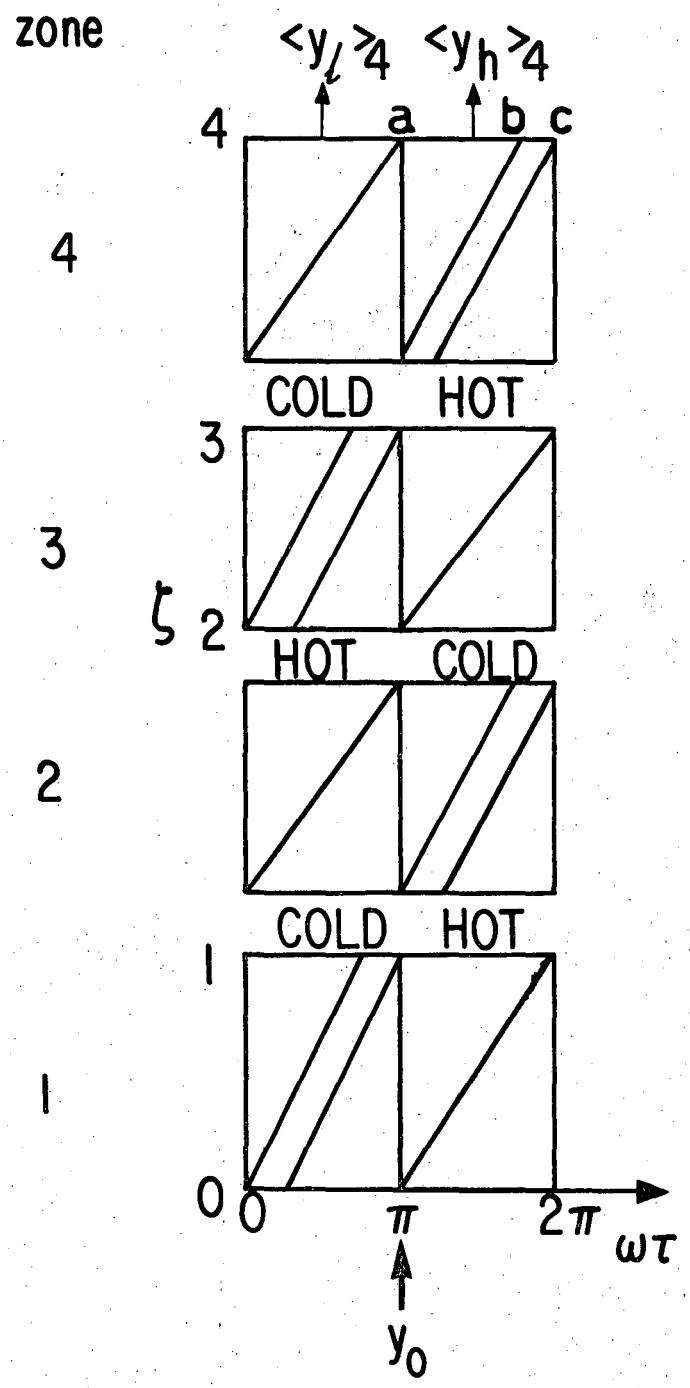

XBL 697-938

Figure 2-2. Characteristic lines used in equilibrium theory for linear isotherms - multiple-zone square-wave cycling.

and

$$\alpha_{av,n} = \frac{2 - q^n}{q^n} \tag{2-25a}$$

$$\alpha_{pk,n} = \frac{1}{q^{2n}} \tag{2-25b}$$

As $n \rightarrow \infty$, this predicts that all of the solute comes out during the hot cycle and that the effluent during the cold cycle has zero concentration. The average concentration during the hot cycle must therefore be limited to twice the feed concentration, but there is no limitation to the peak value of this concentration. This is one obvious defect of the linear-isotherm assumption. Physically, the preferential adsorption isotherm for any system must go to zero, both at zero concentration and as the concentration approaches that of pure solute, so that no isotherm can remain linear over the whole range of concentration.

For $u_{th} = \infty$, the standing-wave case, this is the same result that was obtained for the batch form of direct mode (jacketed column) parametric pumping (Pigford, Baker and Blum, 1969a) for the same cycle frequencies. For parametric pumping, n does not refer to zone number, but to the number of flow-reversal cycles over one zone. The important difference to be noted is that in cycling zone adsorption, actual production is realized, whereas in the parametric pumping experiment there was no feed and therefore no production.

Amplification by the Thermal Wave-Velocity

Before extending this treatment to the case of the nonlinear isotherm, it is of interest to examine Equation

2-19, which predicts the concentration shift when a characteristic crosses a thermal wave. Although there is a natural thermal velocity in the system as indicated by the expression for u_{th} which depends on heat capacity ratios, theoretically this velocity could be overridden with a travelling wave imposed on the system from an outside source in the same way as the standing wave was imposed. Some experimental proposals for this will be discussed in Appendix C; for the following discussion it will be assumed that a thermal wave of arbitrary velocity can be imposed on the column. Three possible cases need to be considered, and these are displayed in the original t-z coordinate system in Figure 2-3:

<u>Case 1</u>	$u_{th} > u_c^H > u_c^C$	Figure 2-3a
<u>Case 2</u>	$u_{th} < u_c^C < u_c^H$	Figure 2-3b
<u>Case 3</u>	$u_c^C < u_{th} < u_c^H$	Figure 2-3c

In Case 1, from Equation 2-19, it can be seen that

$y_i \longrightarrow 0$ $\quad$ i = cold, i - 1 = hot $\quad$ (cold thermal wave)

$y_i \longrightarrow \infty$ $\quad$ i = hot, i - 1 = cold $\quad$ (hot thermal wave)

for $u_{th} \longrightarrow u_c^H > u_c^C$

In Case 2,

$y_i \longrightarrow 0$ $\quad$ i - 1 = cold, i = hot $\quad$ (cold thermal wave)

$y_i \longrightarrow \infty$ $\quad$ i - 1 = hot, i = cold $\quad$ (hot thermal wave)

for $u_{th} \longrightarrow u_c^C < u_c^H$

One can see from Figures 2-3a and 2-3b that the predicted infinite concentration can exist for only an infinitesimal length of time, but that the zero concentration

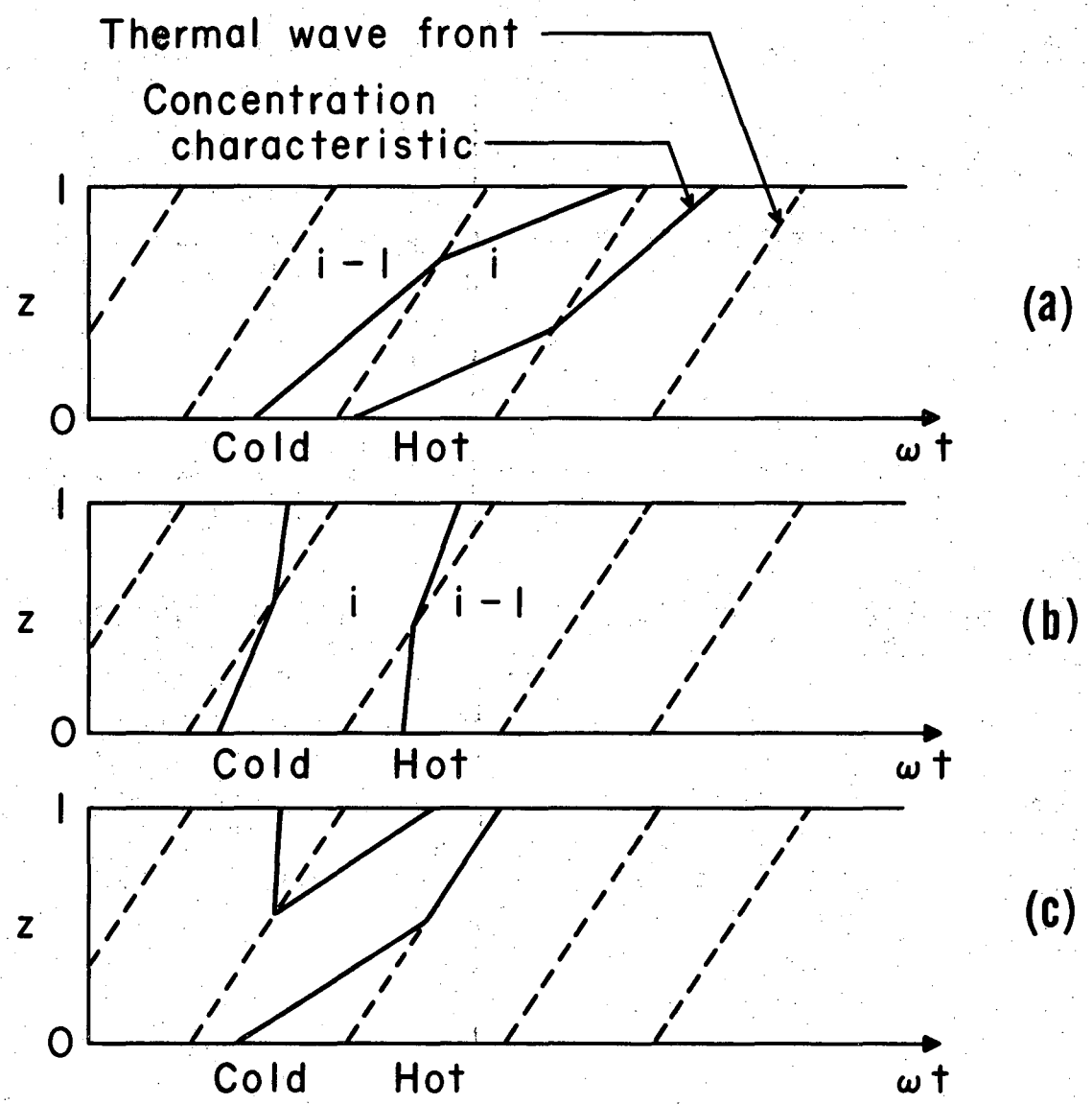

XBL 697-1049

Figure 2-3. Characteristic lines showing possible interactions between thermal waves and concentration waves - step forcing.

(a) Thermal wave faster than either concentration wave.

(b) Thermal wave slower than either concentration wave.

(c) Thermal wave of intermediate velocity.

lasts for the length of time, t_ℓ, between the emergence of the two concentration waves starting at the same point on the $z = 0$ line,

$$t_\ell = \frac{1}{u_c^C} - \frac{1}{u_c^H}$$

Although it can not be predicted from Equation 2-19 directly, it can be seen from combining the inequalities from Cases 1 and 2 that for Case 3,

$$y_i \longrightarrow 0 \qquad \text{(cold thermal wave)}$$

$$y_i \longrightarrow \infty \qquad \text{(hot thermal wave)}$$

$$\text{for } u_c^C < u_{th} < u_c^H$$

The prediction of this large amplification in the separation effect caused by the interaction of the travelling thermal and concentration waves, as their velocities approach the same value, indicates that some experimentation should be done along these lines. Experimental proposals will be discussed in a later chapter.

As before, the prediction of an infinite concentration is a defect of the linear-isotherm assumption. It can be shown in a similar manner that Equation 2-19 predicts that the concentration shift smoothly approaches unity as $u_c^C > u_{th} \longrightarrow 0$ and smoothly approaches the standing-wave value for $0 \geq u_{th} \longrightarrow -\infty$ (indicating a disadvantage in using thermal waves emanating at the exit of the column and propagating backward through the column) and for $u_c^H < u_{th} \longrightarrow \infty$.

Nonlinear Isotherm

As mentioned before, for square-wave forcing, Equation 2-15 indicates that y remains constant except for discontinuity at the instants of temperature change. This in turn implies that the characteristics, given by the solution of Equation 2-14a, are straight except for the discontinuity where they cross a thermal wave. Thus the solution in the periods between temperature switches reduces to the isothermal problem with initial conditions given by the solution of Equation 2-16 at multiples of $\tau = \pi/\omega$ along the ζ-coordinate. The boundary condition again is $y = y_o$ at $\zeta = 0$.

Equation 2-16 can be solved by conventional non-linear algebraic root-finding techniques such as Newton's method. The isothermal equation now to be solved for a single period is

$$\frac{\partial y}{\partial \zeta} + \left(1 + \frac{1}{E} - \frac{1}{u_{th}} + \frac{k_i}{D_i} \; y^{k_i - 1} \frac{\partial y}{\partial \tau}\right) = 0 \qquad (2\text{-}26)$$

with

$$y = y_o = 1 \qquad \zeta = 0 \qquad \tau > 0$$
$$y = y_i \qquad \zeta > 0 \qquad \tau = 0$$

Note that D_i and k_i are now constants. This is similar to the standard ion-exchange problem treated by Goldstein (1953). Using the notation,

$$g(y) = \left(1 + \frac{1}{E} - \frac{1}{u_{th}}\right) y + \frac{y^{k_i}}{D_i} \qquad (2\text{-}27)$$

then Equation 2-26 is $\qquad (g'(y) = dg/dy)$

$$g'(y)\frac{\partial y}{\partial \tau} + \frac{\partial y}{\partial \zeta} = 0 \qquad (2\text{-}28)$$

This is equivalent, according to the method of characteristics, to

$$\frac{d\zeta}{1} = \frac{d\tau}{g'(y)} = \frac{dy}{0} \qquad (2\text{-}29a,\ 2\text{-}29b)$$

for which the solution is

$$g'(y)\,\zeta = \tau + C_3 \qquad (2\text{-}30)$$

$$y = C_4 \qquad (2\text{-}31)$$

$$(C_3, C_4 \text{ constants})$$

Thus $1/g'(y)$ is the concentration wave velocity, which is dependent on y. The characteristics emanating from boundary conditions of differing values of y will have different slopes, but as shown by Equations 2-30 and 2-31, they are straight and y is constant along them. The general solution of Equation 2-28 is then

$$y = f(\tau - g'(y)\,\zeta) \qquad (2\text{-}32)$$

Consider the case in which $y_i > 1$ shown in Figure 2-4a. Since $g'(y_i) < g'(1)$, the characteristics diverge at the origin. The fan-shaped region between the two boundary value characteristics is called a "simple" wave region. When

$$\zeta > \frac{\tau}{g'(y_i)}, \quad y = y_i$$

$$\zeta < \frac{\tau}{g'(1)}, \quad y = 1$$

In the simple wave region,

Figure 2-4. Equilibrium theory solution for nonlinear isotherms - single-zone step forcing: simple-wave case.

(a) Characteristics.

(b) Effluent concentration profile.

Figure 2-5. Equilibrium-theory solution for nonlinear isotherms - single-zone step forcing: shock-wave case.

(a) Characteristics.

(b) Effluent-concentration profile.

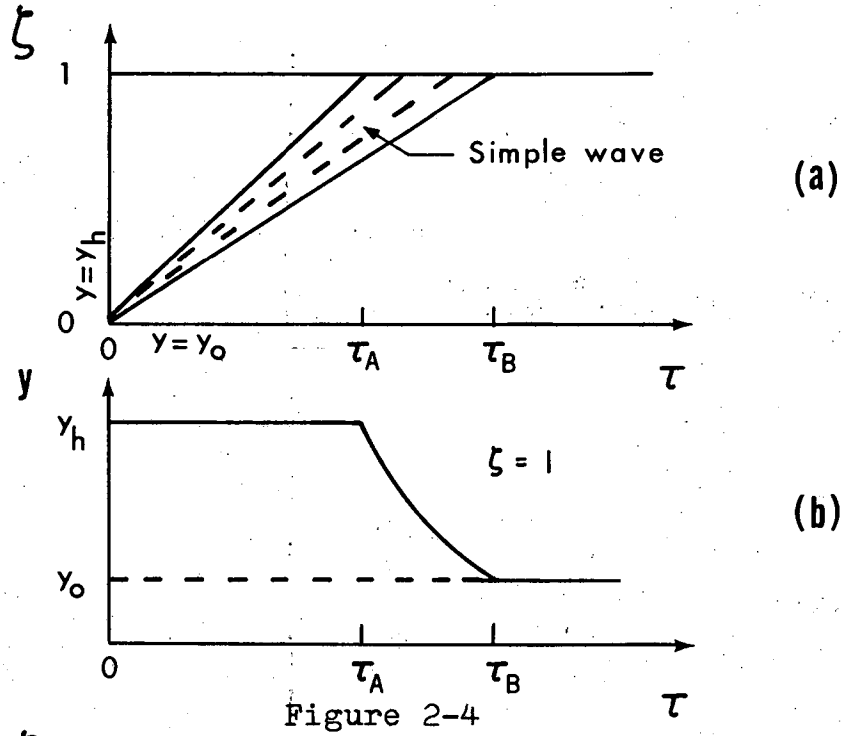

Figure 2-4

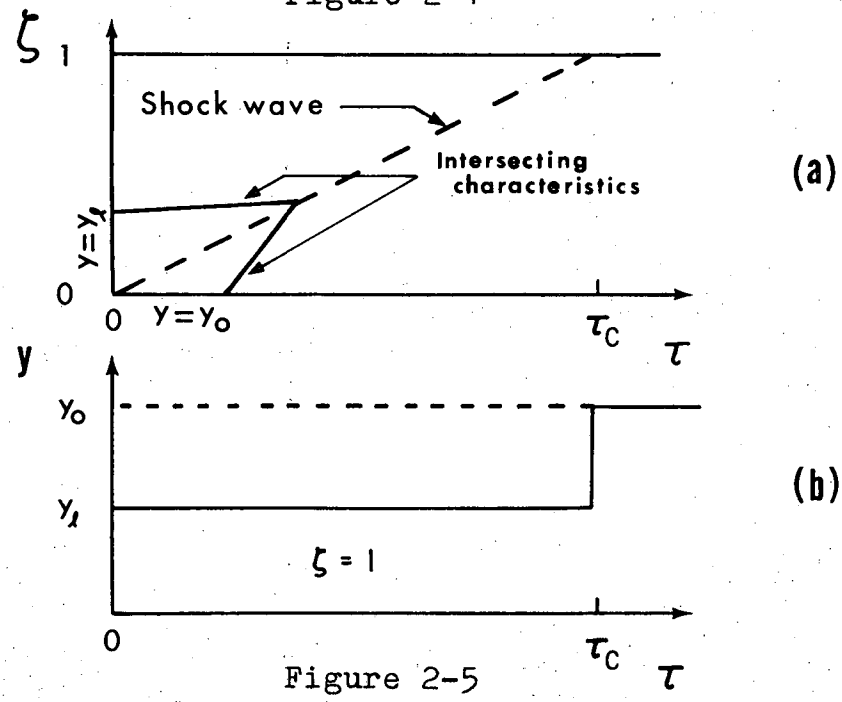

Figure 2-5

XBL 697-975

$$\frac{\zeta}{g'(1)} < \zeta < \frac{\tau}{g'(y_i)}$$

the slopes emanate from the origin so that

$$\tau - g'(y)\,\zeta = 0 \tag{2-33}$$

and the slopes vary continuously. The values of y in this region are found by solving Equation 2-33,

$$y = g'^{-1}\left(\frac{\tau}{\zeta}\right) = \left[\frac{D_i}{k_i}\left(\frac{\tau}{\zeta} - \left(1 + \frac{1}{E} - \frac{1}{u_{th}}\right)\right)\right]^{\frac{1}{k_i - 1}} \tag{2-34}$$

and are shown in Figure 2-4b.

For the case in which $y_i < 1$ shown in Figure 2-5a, since $g'(y_i) > g'(1)$, the characteristics converge immediately at the origin, hence a discontinuity or "shock" wave occurs. The speed of propagation of the shock wave, u_{sh}, may be found from the fact that the discontinuity moves with a speed such that there is no accumulation of mass at the discontinuity. Letting [y] and $\left[\frac{1}{E}\,y + \frac{y^{k_i}}{D_i}\right]$ denote the magnitude of the discontinuity in the mobile and stationary phases, and using the fact that the normalized fluid-phase velocity in the τ-ζ coordinate system is $1/(1 - 1/u_{th})$, one obtains

$$\left(\frac{1}{1 - \frac{1}{u_{th}}} - u_{sh}\right)[y] = u_{sh}\left[\frac{1}{E}\,y + \frac{y^{k_i}}{D_i}\right]$$

or

$$u_{sh} = \frac{1}{1 + \frac{1}{E} - \frac{1}{u_{th}} + \frac{1}{D}\,\frac{y^{k_i} - 1}{y_i - 1}} \tag{2-35}$$

Figure 2-5b is a plot of the effluent concentration for this case.

Equations 2-34 and 2-35 are the basic equations for the nonlinear equilibrium case. Figure 2-6a depicts the characteristics for a single column with the cycle period chosen such that

$$\frac{\pi}{\omega} = \frac{u_{th} - u_{sh}}{u_{th}\ u_{sh}}$$

Figure 2-6b shows the effluent from such a column. As before, there is an optimum cycle time.

Multiple-Zone Case

In the multiple column arrangement, these long sections of lean and enriched fluid are sent through the successive zones. For the enriched section travelling through the second zone, the front remains a shock wave and the rear becomes more diffuse. Eventually, if the concentration difference between enriched and lean sections becomes great enough, the simple wave can overtake the shock wave and diminish the peak concentration. This is what keeps the concentration peak from becoming infinite as was predicted in the linear-isotherm case. This skew waveform is similar to that describing conventional nonlinear chromatographic pulses which was first worked out by Weiss (1943) and De Vault (1943).

Because the effluent from one zone containing simple wave regions becomes the boundary condition for the next zone, the development of a general expression for n zones for the nonlinear case would be difficult. However, the two-zone case will be derived for the conditions of the

Figure 2-6. Equilibrium-theory solution for nonlinear isotherms - dual-zone square-wave cycling: Zone 1 results.

(a) Characteristics.

(b) Effluent-concentration profile.

Figure 2-7. Equilibrium-theory solution for nonlinear isotherms - dual-zone square-wave cycling: Zone 2 results.

(a) Characteristics.

(b) Effluent-concentration profile.

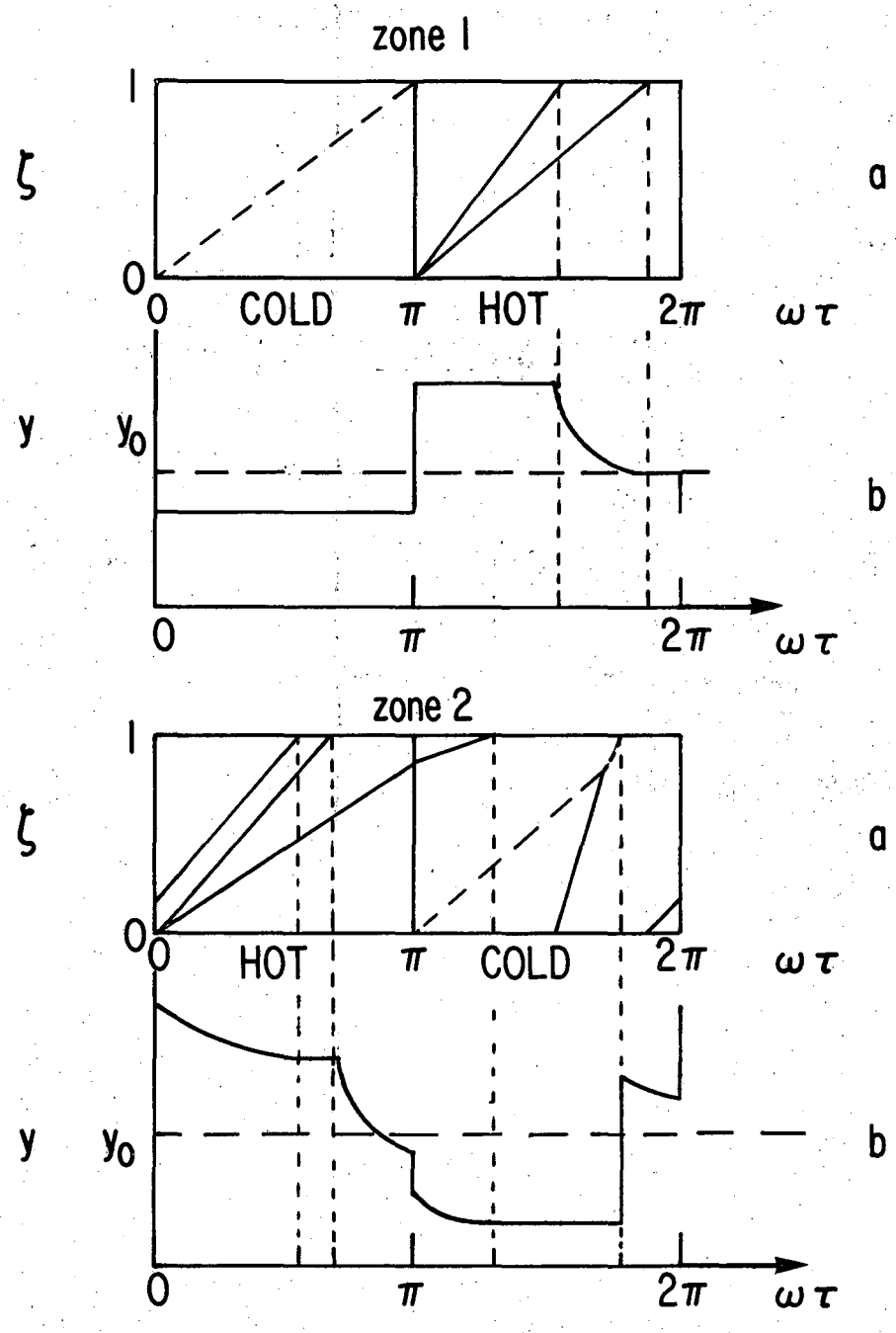
zone 1
1
ζ
0
0
COLD
π
HOT
2π
ωτ
a
y
y_0
b
0
π
2π
ωτ
zone 2
1
ζ
0
0
HOT
π
COLD
2π
ωτ
a
y
y_0
b
0
π
2π
ωτ

XBL 697-940

experiment. The cycle period was chosen to be approximately that of Figure 2-6a so that the effluent shown in Figure 2-6b was fed to the second zone. The characteristics and boundary conditions for Zone 2 are plotted in Figures 2-7a and 2-7b for each half cycle after the cyclic steady state is reached. The only region not handled directly by Equations 2-34 and 2-35 is the intersection of the shock wave and the simple wave at point I. When this happens, the maximum concentration begins to decrease from y_h and the locus of the maximum which is also the path of the shock wave is given by

$$\frac{d\tau^*}{d\zeta} = \frac{1}{u_{sh}(y_{2\ell}, y^*)} \tag{2-36}$$

where τ^* is the τ coordinate of the maximum y^*. y^* as a function of τ^* and ζ is given by the intersecting characteristics of the simple wave. The input function of the simple wave at $\zeta = 0$ to Zone 2 is the effluent simple wave from Zone 1 at $\zeta = 1$, while Zone 1 is hot. Letting the subscripts H and C indicate hot and cold, it is given by Equation 2-34, so that

$$\tau = g'_H(y) \qquad \zeta = 0 \tag{2-37}$$

When $\zeta > 0$, the equation for the simple wave characteristics in zone 2 are

$$\tau = g'_H(y) + g'_c(y)\zeta = h(y, \zeta) \tag{2-38}$$

Thus

$$\tau^* = h(y^*, \zeta) \tag{2-39}$$

so that

$$y^* = h^{-1}(\tau^*, \zeta) \tag{2-40}$$

The equation to be solved is then

$$\frac{d\tau^*}{d\zeta} = \frac{1}{u_{sh}\left(y_{2\ell}, h^{-1}(\tau^*, \zeta)\right)} \tag{2-41}$$

The initial conditions for Equation 2-41 are the coordinates of the initial intersection, point I. There

$$\tau_o^* = \frac{\zeta}{u_{sh}(y_{2\ell}, y_h)} = g'_H(y_h) + g'_c(y_h)\,\zeta$$

so that

$$\zeta_o = \frac{g_h^{-1}(y_h)\, u_{sh}(y_{2\ell}, y_h)}{1 - g'_c(y_h)\, u_{sh}(y_{2\ell}, y_h)} \tag{2-42}$$

$$\tau_o^* = \frac{g_H^{-1}(y_h)}{1 - g'_c(y_h)\, u_{sh}(y_{2\ell}, y_h)} \tag{2-43}$$

After solving Equation 2-41 with 2-42 and 2-43, y^* is found from Equation 2-40.

<u>Amplification by the Thermal Wave-Velocity</u>

This case will not be developed in detail since the same equations as in the previous section are used. Again, however, one finds that there is no longer a prediction of an infinite concentration, since the simple wave region overtakes the shock wave and diminishes the maximum.

Comparison of Multiple-Zone and Travelling-Wave Cases

Before closing this chapter, there is one more point to be made. The multiple-zone system can be viewed as an approximation of one column with a travelling thermal wave of a velocity equal to that of the concentration wave. Since in the former case, each zone is π radians out of phase with the preceding zone, the effect is to produce a stairstep wave which moves through the zones. For a constant over-all length, as the length of the individual zones decreases, the number of zones increases. Thus the stairstep wave becomes an increasingly better approximation to a smooth travelling wave.

On this generalization, one can say that it is the occurrence of the amplification by the thermal wave propagation that one would like to utilize. Although superficially the multiple-zone effect seems quite different from this travelling-wave effect, it is in reality a physically practical way of implementing it. Other ways will be suggested later.

CHAPTER 3

THE PERTURBATION SOLUTION OF THE GENERAL EQUATIONS OF CYCLING ZONE ADSORPTION

Since the equilibrium theory has indicated that a considerable separation effect is possible utilizing cycling zone adsorption, one would next like to examine the effect of finite rates of transfer. It has already been mentioned that, at least for liquid-solid systems, heat transfer will not be a problem if the natural thermal velocity is acceptable. There will still be difficulties in imposing an arbitrary thermal velocity; this is treated in Appendix C. However, the prime transfer question seems to be whether the low intraparticle mass-transfer rates will allow throughputs large enough to make the process commercially interesting. In this chapter, a simplified approach to answering that question will be presented. The general equations will be linearized so that an analytic solution is possible; then the response to sinusoidal forcing of the temperature will be found. This linearization is only valid for small deviations in the dependent variables. Since the objective of this process is presumably to obtain large separations, the method has a restricted application, but it is useful as an initial approach to determining the mass-transfer effects.

If the axial-dispersion terms are neglected and a linear isotherm is assumed, Equations 2-1 and 2-3 become:

$$\frac{\partial c}{\partial t} + \frac{1-\alpha}{\alpha}\frac{\partial X}{\partial t} + \frac{\partial c}{\partial z} = 0 \qquad (3\text{-}1)$$

$$\frac{\partial X}{\partial t} = -\frac{Z_o}{v}\frac{k_M\, a_p}{(1-\alpha)}(c^* - c) \qquad (3\text{-}2)$$

where X is the lumped solid-phase concentration defined as

$$X = \rho_s A c^* (1-\varepsilon) + \varepsilon c^* = A' c^*$$

where

$$A' = \rho_s A (1-\varepsilon) + \varepsilon \ .$$

By assuming the thermal-equilibrium travelling-wave function, Equation 2-11, and specifying a sinusoidal periodic function, the forcing function becomes:

$$\theta = e^{i\omega(t - z/u_{th})}$$

If A is linearized,

$$A = A(T) = A_o\, e^{\frac{\Delta H_{ads}}{R}\left(\frac{1}{T} - \frac{1}{T_o}\right)}$$

$$\sim A_o\left(1 - \frac{\Delta H_{ads}}{R\, T_o^{\,2}}(T - T_o)\right)$$

and the following deviation variables are defined:

$$\chi = \frac{1}{c_o}\left(\frac{X}{A_o'} - c_o\right)$$

$$\varphi = \frac{1}{c_o}(c - c_o)$$

the equations become

$$\frac{\partial \varphi}{\partial t} + m_o\frac{\partial \chi}{\partial t} + \frac{\partial \varphi}{\partial z} = 0 \qquad (3\text{-}3)$$

$$K \frac{\partial \chi}{\partial t} = \varphi - \chi - d' y_o \, e^{i\omega(t - z/u_{th})} \tag{3-4}$$

where

$$K = \frac{v}{Z_o} \frac{(1-\alpha) A_o'}{k_M a_p} = \frac{v}{Z_o} \frac{m_o}{v} \frac{\alpha v}{k_M a_p} = \frac{m_o}{NTU}$$

$$m_o = \frac{1-\alpha}{\alpha} A_o'$$

NTU = number of transfer units

$$A_o' = \rho_s A_o (1-\varepsilon) + \varepsilon$$

$$d' = \frac{A_o \rho_s (1-\varepsilon)}{A_o \rho_s (1-\varepsilon) + \varepsilon} \frac{\Delta H_{ads}}{R T_o^2} (T_H - T_o)$$

Note that the second-order deviation terms involving $d' \frac{\partial \chi}{\partial t}$ and $d'\chi$ have been neglected.

Assuming a solution of the form

$$\chi = \bar{\chi}(z) \, e^{i\omega t}$$

$$\varphi = \bar{\varphi}(z) \, e^{i\omega t}$$

with considerable algebraic manipulation one obtains:

$$\mathrm{Re}\ \varphi(1) = \frac{d'\ y_o\ m_o}{\left(m_o + 1 - \frac{1}{u_{th}}\right)^2 + \Omega^2\left(1 - \frac{1}{u_{th}}\right)^2} \left\{\left(m_o + 1 - \frac{1}{u_{th}}\right)\right.$$

$$\left[\cos\left(\frac{\omega}{u_{th}}\right) - \exp\left(-\frac{m_o\ \Omega}{1+\Omega^2}\ \omega\right)\cos\left(\left(1 + \frac{m_o}{1+\Omega^2}\right)\omega\right)\right]$$

$$-\ \Omega\left(1 - \frac{1}{u_{th}}\right)\left[\sin\left(\frac{\omega}{u_{th}}\right) - \exp\left(-\frac{m_o\ \Omega}{1+\Omega^2}\ \omega\right)\right.$$

$$\left.\left.\sin\left(\left(1 + \frac{m_o}{1+\Omega^2}\right)\omega\right)\right]\right\} \tag{3-5}$$

$$\mathrm{Im}\ \varphi(1) = \frac{-d'\ y_o\ m_o}{\left(m_o + 1 - \frac{1}{u_{th}}\right)^2 + \Omega^2\left(1 - \frac{1}{u_{th}}\right)^2} \left\{\left(m_o + 1 - \frac{1}{u_{th}}\right)\right.$$

$$\left[\sin\left(\frac{\omega}{u_{th}}\right) - \exp\left(-\frac{m_o\ \Omega}{1+\Omega^2}\right)\omega\ \sin\left(\left(1 + \frac{m_o}{1+\Omega^2}\right)\omega\right)\right]$$

$$+\ \Omega\left(1 - \frac{1}{u_{th}}\right)\ \cos\left(\frac{\omega}{u_{th}}\right)\exp\left(-\frac{m_o\ \Omega}{1+\Omega^2}\right)\omega$$

$$\left.\left.\cos\left(\left(1 + \frac{m_o}{1+\Omega^2}\right)\omega\right)\right]\right\} \tag{3-6}$$

where $\Omega = \omega K$.

Since the amplitude of the deviation is found from

$$|\bar{\varphi}(1)| = \left(\mathrm{Im}^2\ \bar{\varphi}(1) + \mathrm{Re}^2\ \bar{\varphi}(1)\right)^{1/2} \qquad (3\text{-}7)$$

the maximum amplitudes for various values of u_{th} and K are found by maximizing Equation 3-7 by searching along ω. Although the function is not unimodal, the absolute maximum was found to be the local maximum for which ω is smallest. Thus one starts with $\omega = 0$ and proceeds to increase ω until Equation 3-7 starts to decrease.

For the special case of $\Omega = 0$, Equation 3-7 reduces to the local equilibrium case, differing only from the linear case of Chapter 2 in that the concentration velocities during the hot and cold periods are approximated by the mean value

$$u_c = u_o = 1/(1 + m_o)$$

and the optimum amplitude is found to be

$$\frac{2\ d'\ y_o}{1 + \frac{\pi}{\omega}} \quad \text{for} \quad \omega = \frac{u_{th}\ u_o}{u_{th} - u_o}\pi \quad \text{for} \quad u_{th} \neq u_o$$

$$m_o d' y_o \omega \longrightarrow \infty \quad \text{for} \quad \omega \longrightarrow \infty \qquad \text{for } u_{th} = u_o$$

As expected in the interphase mass-transfer case ($\Omega \neq 0$) the amplitude is less than the equilibrium case, as shown in Figure 3-1 where $m_o = 7.75$ results from a linear approximation to the experimental isotherms presented in Chapter 4. In Figure 3-2, the effect of mass transfer on the amplitude at the optimum frequency is shown. Predicted

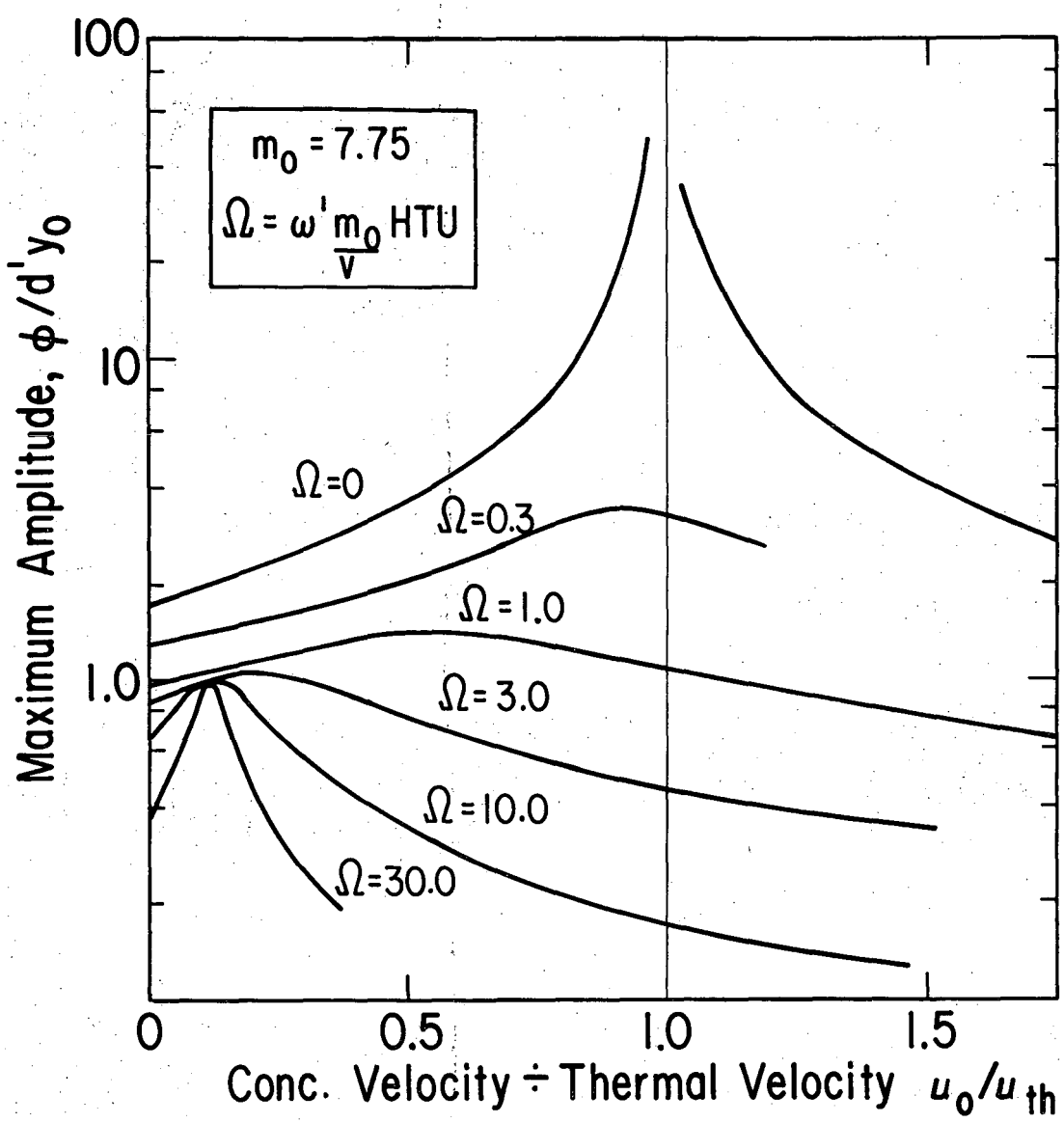

XBL 697-939

Figure 3-1. Effect of the thermal-wave velocity and the frequency-mass transfer parameter on the optimum amplitude of the cycling zone adsorption separation: linearized solution.

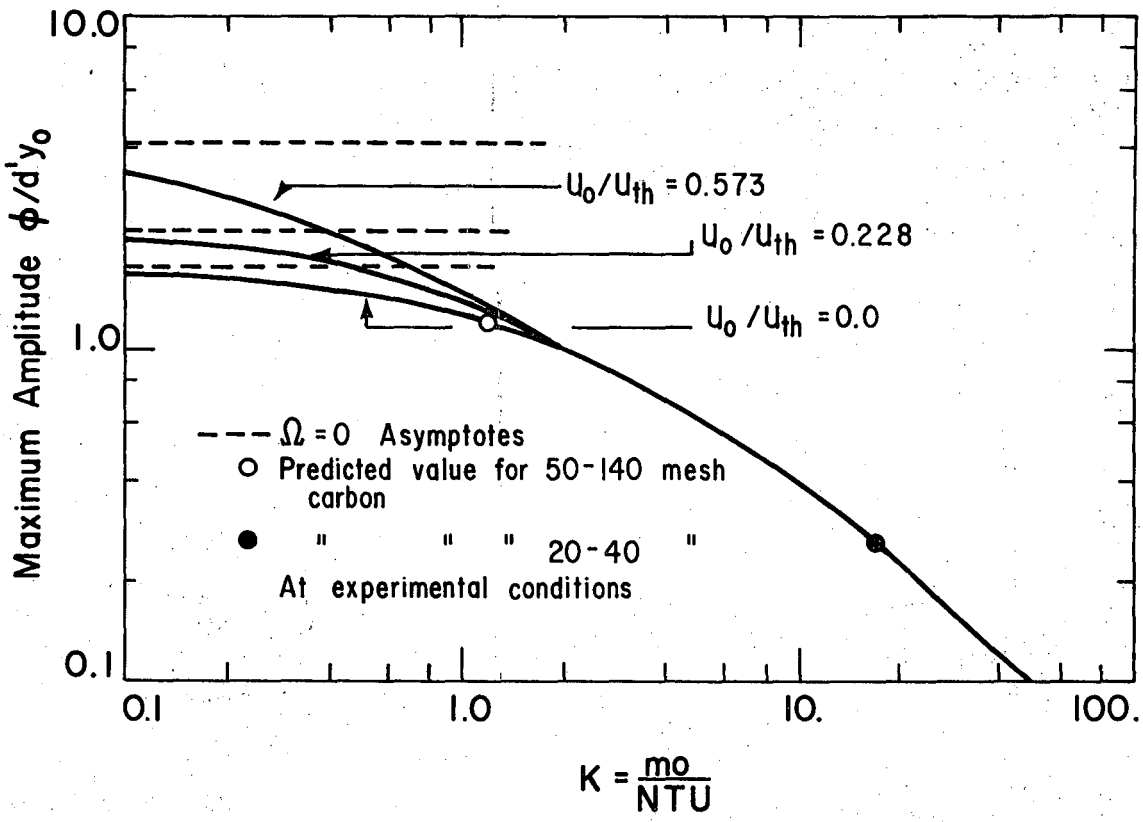

XBL 697-957

Figure 3-2. Effect of the mass transfer and the thermal-wave velocity on the amplitude of the cycling zone adsorption separation at optimum frequency: linearized solution.

values for the experimental system are shown, using the calculations in Appendix A. Although the experimental study presented in Chapters 4 and 5 contained no experiments specifically designed to examine mass-transfer effects, some mass-transfer rate effects are contained in the cycling frequency study (Figure 5-7). In order to compare the results from the experiment, in which the forcing was square-wave, with the sinusoidal response theory just presented, the following reasoning was used.

It can be shown that, for $\Omega = 0$ and square-wave forcing, the cycle-averaged amplitude is the same as the amplitude obtained with sinusoidal forcing. Therefore to make a rough comparison with the theory above, the experimental cycle-averaged results in Figure 5-7 for 50-140 mesh carbon for the cold half cycle (since the nonlinear-equilibrium theory predicts an exact square-wave response only for this half cycle) are compared with the predicted amplitude of Figure 3-2.

Table 3-1. Optimum Frequency Response for Single-Zone Standing-Wave Frequency

	Optimum frequency, cycles/min.	Optimum amplitude ÷ optimum amplitude at $\Omega = 0$
Predicted (Figure 3-2)	.042	0.715
Experimental (Figure 5-7)	.050	0.836

Note that as indicated in Figure 3-2, the curves for various thermal-wave velocities merge into the same envelope as the number of transfer units decreases and that the advantage of travelling-wave forcing only occurs for systems having a relatively large number of transfer units. For a given system, the number of transfer units can be increased (at constant throughput) by lengthening the column. However, economic considerations such as equipment size and pressure drop restrict the practical length for a column.

CHAPTER 4

SEPARATION OF ACETIC ACID AND WATER WITH ACTIVATED CARBON BY CYCLING ZONE ADSORPTION - THE EXPERIMENTS

The acetic acid-water-carbon system was chosen after some preliminary screening experiments mainly for the following two reasons: (1) There is a reasonably large temperature effect on the equilibrium distribution coefficient, and (2) effluent concentrations can be determined continuously using an electrical conductivity cell and intermittently by aqueous-phase acid-base titrations. Although there is little economic incentive for the separation of this particular system, it is similar to aqueous systems containing small amounts of organic pollutants, such as phenol, which do present a purification problem. At the same time, although the experiments were limited to a dilute system, it is felt that the concepts are applicable to a wide class of systems over the whole range of concentration, provided only that there is a temperature effect on the equilibrium coefficient.

The Experimental System

Reagent-grade acetic acid (HAc) was used without further purification and was diluted with distilled water. Pittsburgh Activated Carbon Company supplied the samples of CAL type activated carbon, 12 to 40 mesh. The 20-to-40 mesh carbon was obtained by screening the original carbon.

The 50-to-140 mesh size was obtained by grinding the original carbon with a mortar and pestle and then screening.

Equilibrium-distribution isotherms for the 50-to-140 mesh carbon were determined in batch experiments in the following way. For each point, a measured amount of carbon was weighed into a plastic bottle to which was added a measured volume of HAc of known concentration. The bottle was sealed and the system equilibrated by tumbling in a constant-temperature bath for three hours. Then a sample of the solution was quickly separated from the carbon and titrated. The amount adsorbed was determined by difference; hence the preferential adsorption isotherm was determined, rather than the individual-component isotherms. The preferential adsorption, q is determined by the relation

$$q = \frac{V_o}{W_o} (c_o - c)$$

where V_o is the volume of HAc solution of normality c_o originally added and W_o is the original weight of the carbon added. The final concentration, c, is the concentration in equilibrium with q at the constant temperature.

The results are shown in Figure 4-1. The coefficients for the least-squares fit of the data to the Freundlich isotherm

$$\ln q = \ln A(T) + k(T) \ln c$$

are shown in Table 4-1.

The necessary carbon parameters, shown in Table 4-2, were determined as follows. The particle density,

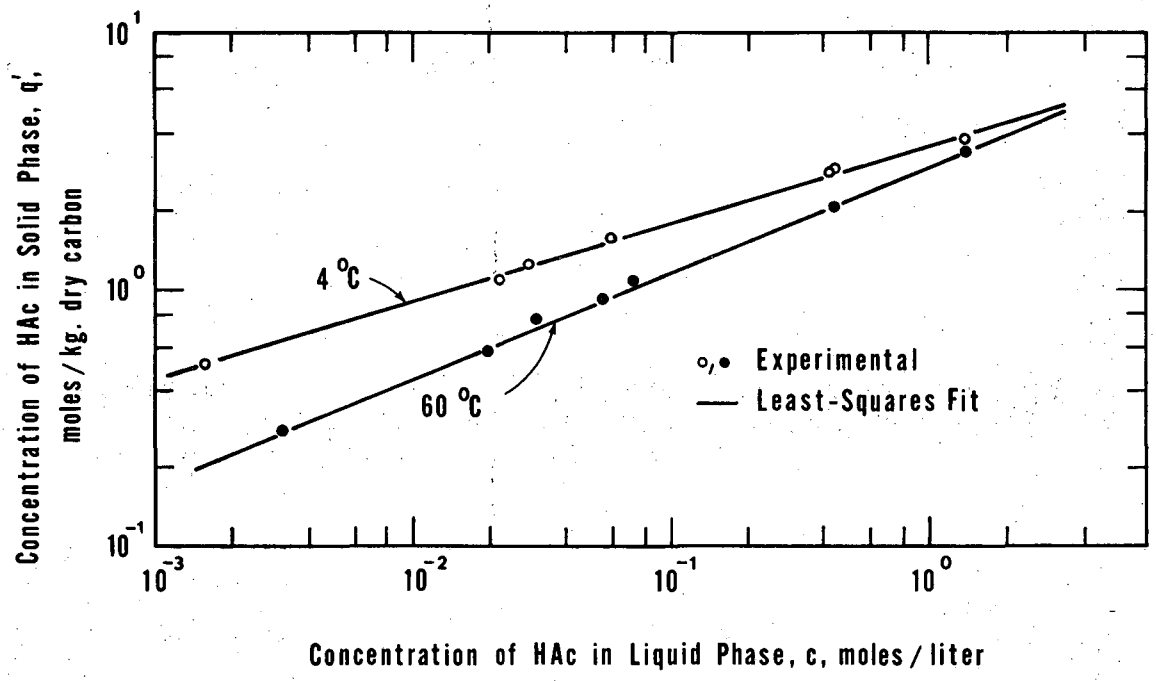

XBL 697-958

Figure 4-1. Preferential equilibrium adsorption isotherms for aqueous HAc on Pittsburgh activated carbon, CAL type, 50-140 mesh.

Table 4-1. Freundlich Equilibrium Distribution Parameters[a]

Temperature, °C	A	k
4	3.646	0.3052
60	3.019	0.4119

[a]The units of A are (moles/liter dry carbon)·(liters/mole)^k.

Table 4- 2. Activated Carbon Physical Parameters

	Mesh size		
	20-40	50-140	Units
Structural density, ρ_s	1.728	1.820	g/cm^3
Particle density, ρ_p	0.8018	0.7822	g/cm^3
Intraparticle void fraction, ε	0.5360	0.5702	-
Interparticle[a] void fraction, α	.438-.473	.426-.443	-
Particle diameter, d_p	.420-.841	.105-.297	mm
Heat capacity,[b] C_s	0.25	0.25	cal/g-°C

[a]Depending on particular experiment.

[b]Supplied by manufacturer.

ρ_c, was determined by evacuating a small container of carbon particles and then allowing mercury to enter the container at atmospheric pressure. The mercury was assumed to be unable to enter the pores. The structural density, ρ_s, was determined in the same way, but using water, which was assumed to enter the pores. This procedure results in a lower structural density than using helium, since water can not enter the very fine pores that helium can penetrate, but it was felt that this allowed one to obtain a more realistic measure of the intraparticle void fraction, ε, available to the aqueous experimental system. The intraparticle void fraction was calculated using the relation

$$\varepsilon = 1 - \rho_p/\rho_s$$

The interparticle void fraction, α, which depends on the manner in which the column is packed, was calculated from the relation

$$\alpha = 1 - \frac{W_o}{\rho_p V_T}$$

where W_o is the weight of carbon in the column and V_T is the volume of the column when empty.

<u>The Experimental Apparatus</u>

The experimental apparatus is shown in Figure 4-2 and schematically in Figure 4-3. The heart of the system is the column section, shown in Figure 4-4, which will be discussed first.

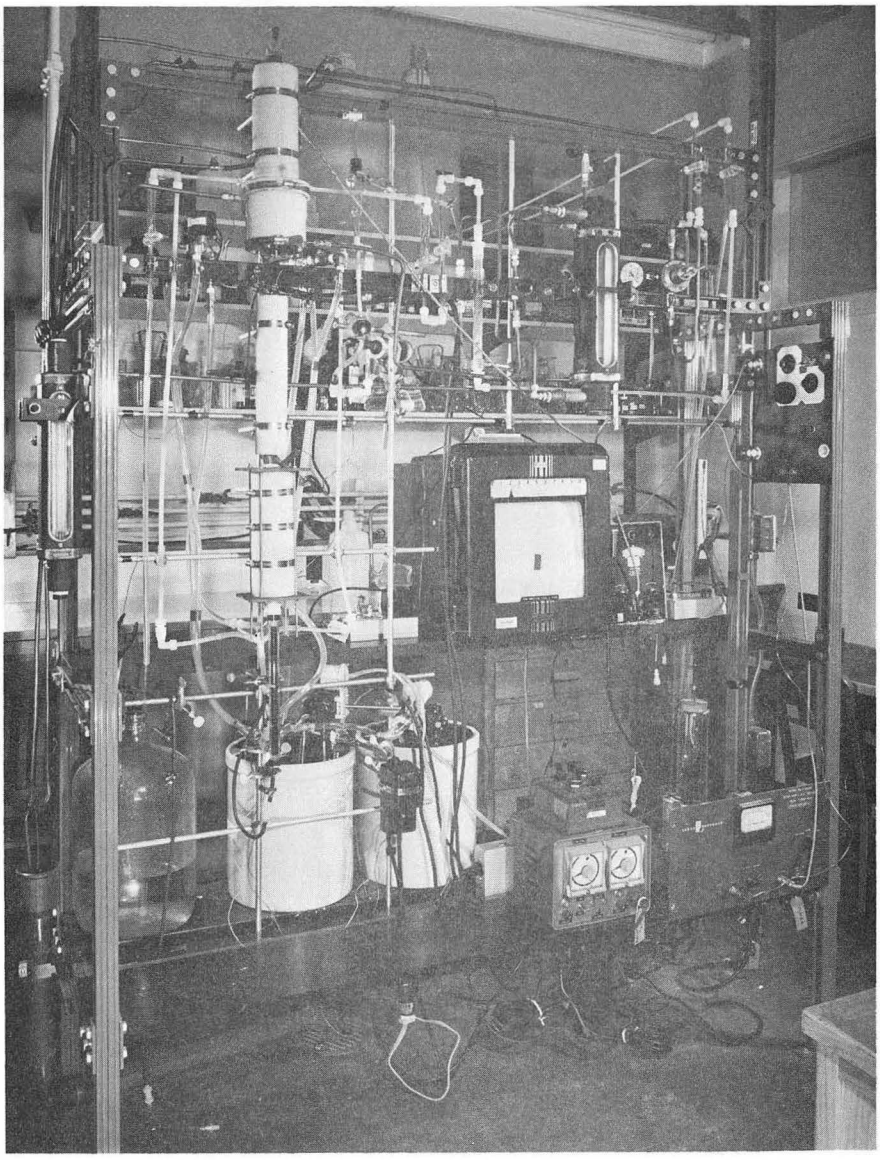

XBB 692-1395

Figure 4-2. Experimental apparatus for cycling zone adsorption.

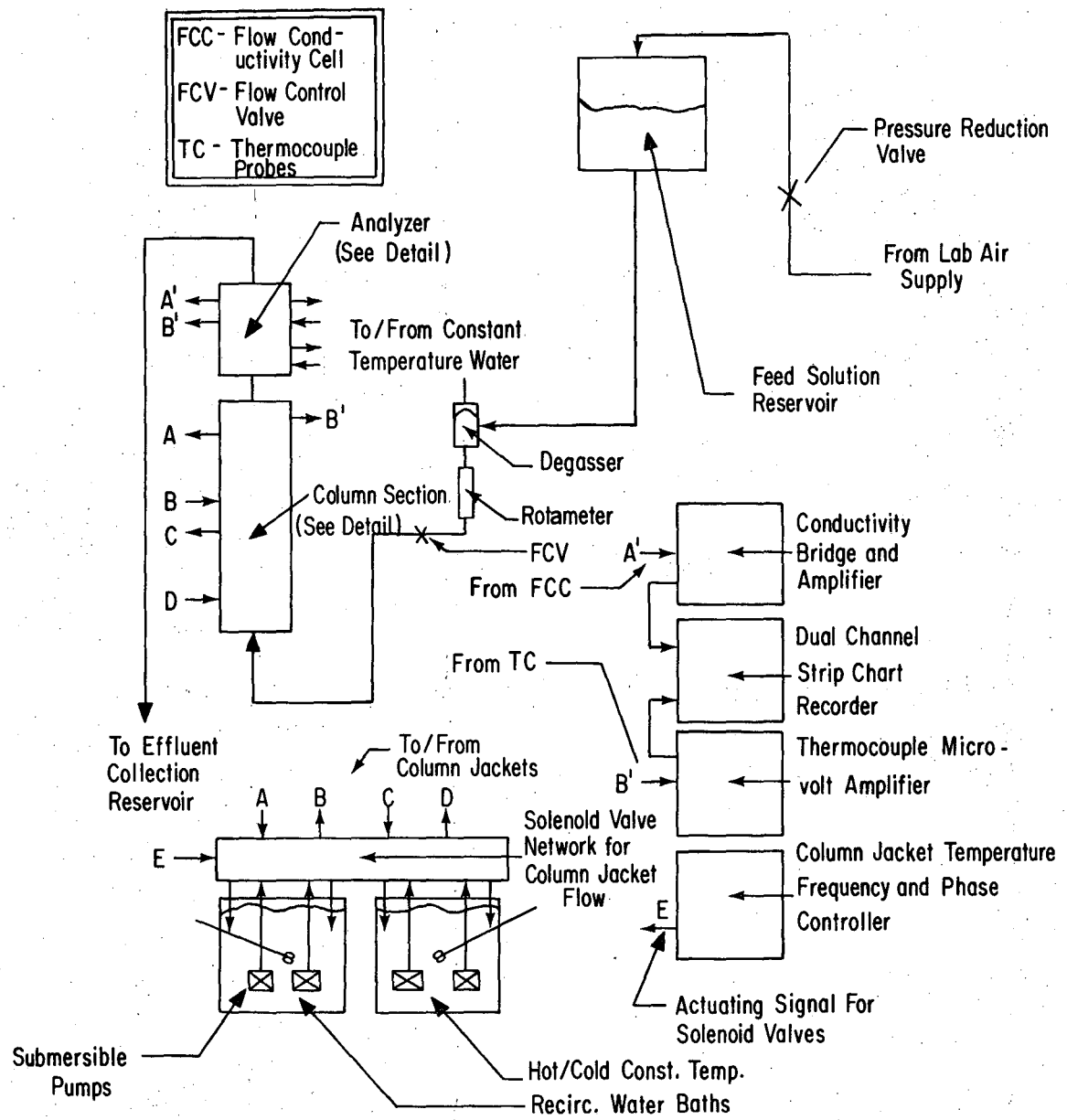

XBL 697-1053

Figure 4-3. Schematic of experimental apparatus for cycling zone adsorption.

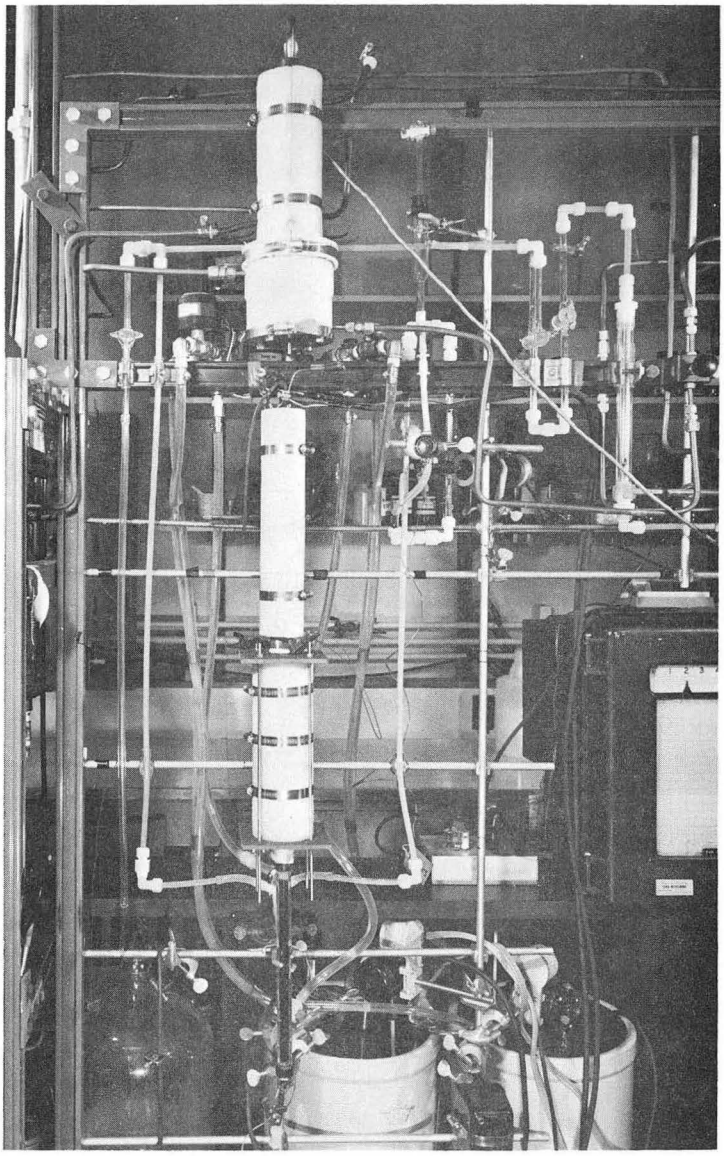

XBB 692-1394

Figure 4-4. Column and analyzer section of experimental apparatus containing (bottom) jacketed adsorption column, heat regenerator, insulated adsorption column, and (top) concentration analyzer.

Column Section

Various arrangements were used for this section to test several process ideas. The set-up in the figure consists of (from the bottom) a jacketed column, an insulated heat regenerator, and an insulated column, but this was only one of several arrangements. Also shown at the top of the figure is the analyzer, which will be discussed later. All the components of the column section used in any of the experiments are shown in Figure 4-5.

The adsorptive columns themselves were packed with glass spheres at both ends for flow distribution. The carbon particles were introduced in a water slurry. The walls of the column were tapped as the particles settled to eliminate air bubbles and insure a uniform packing. The glass wool was used to keep the carbon in place.

The polyurethane foam insulation has a heat conductivity of 1.9×10^{-2} Btu/hr-ft-°F; the one-inch thickness restricted the heat loss over the length of the columns at the experimental flow rates to only 10% (see Appendix B). The column jackets were standard glass laboratory condenser jackets. The heat regenerator was made of phenolic plastic to minimize longitudinal heat conduction along the walls and was filled with particles having heat capacity but no mass adsorptive capacity, such as glass spheres or stainless steel granules. Its operation is more fully discussed in Appendix B. As is evident from the figure, the pre-exchangers are similar to the adsorptive columns, but

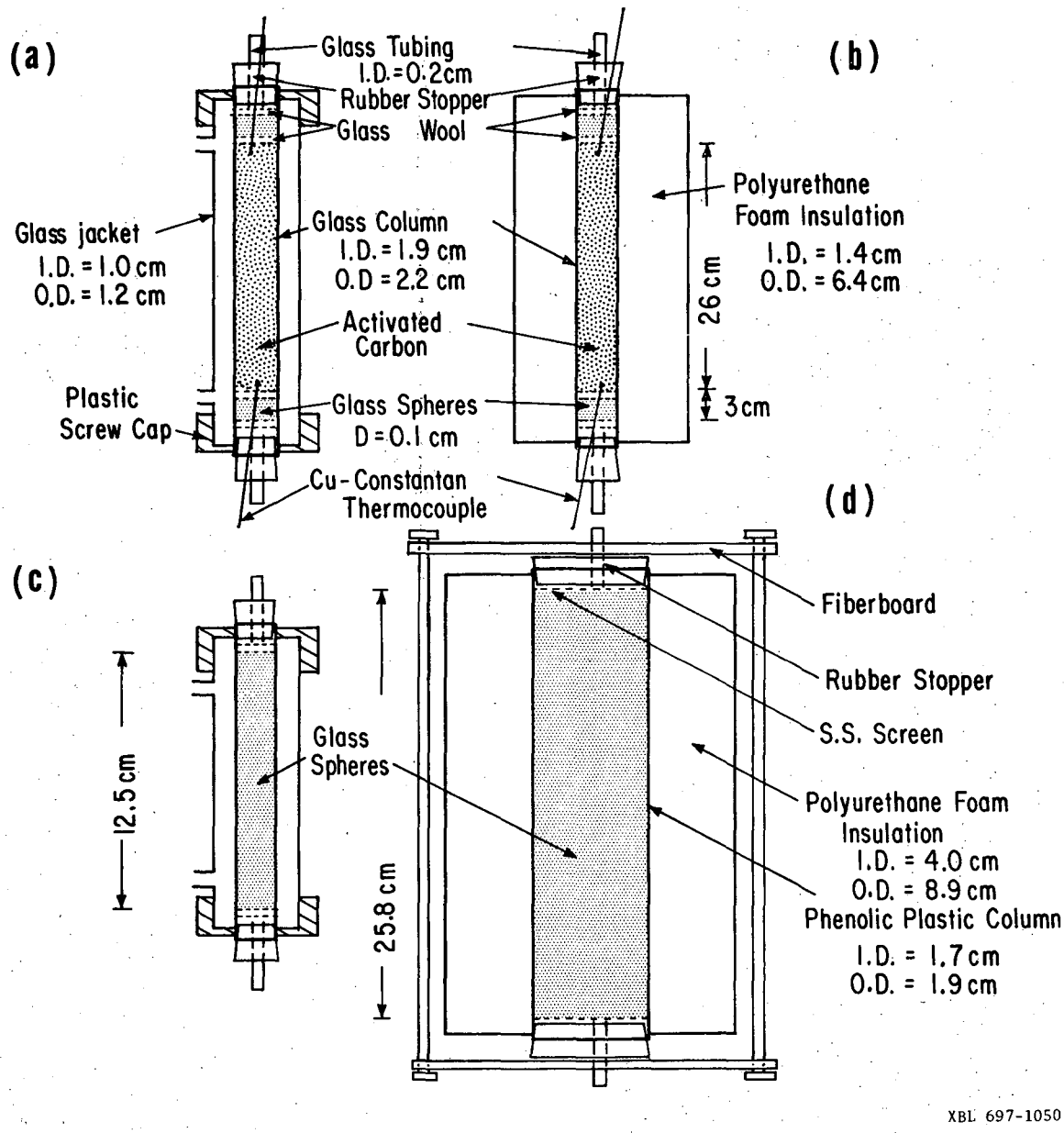

Figure 4-5. Detail of column-section components.

are packed with glass particles. These act as simple heat exchangers.

The components of this section were simply linked together by short lengths of neoprene tubing.

Peripheral Equipment

Except for the column section, the equipment remained the same for all the experiments and consisted of the following systems.

Feed Supply and Effluent-Removal System. The reservoir was a 13-gallon Nalgene plastic bottle with a 3-inch hole cut in the screw cap to allow glass tubing to extend through it after screwing it down on a rubber stopper inserted in the bottle. The lines carrying HAc solution were 0.375-inch Eastman nylon to eliminate corrosion. A rotameter was used to measure the solution flow which was directed by glass stopcocks and controlled by a 0.125-inch stainless-steel needle valve. When gravity feed did not provide sufficient flow, an air pressure system was used, employing the laboratory air supply with a pressure reduction valve. The pressure was never allowed to exceed 10 psig in order not to burst the Nalgene plastic reservoir bottle. The effluent was simply led to a 5-gallon glass bottle and was discarded.

Square-Wave Temperature-Generation System. A column was maintained at one temperature by pumping water from one of the baths through the jacket of the column.

When it was time to operate at the other temperature, flow from this bath was stopped and flow from the other bath was begun. The two constant-temperature baths were used. Each contained two submersible pumps which recirculated cooling and heating water at 1.0 liter per minute through the jackets of the columns by way of 0.375-inch Tygon tubing. The water flows were directed by means of 0.375-inch solenoid valves; the temperatures of the two zones (columns) could be forced independently of each other. The valves were switched either manually or automatically using a specially constructed repeat-cycle timer with independently adjustable on/off cycles. Ordinary temperature-controller relays were modified by increasing the capacitance in their time delay circuits to delay the exit solenoid switching by about 15 seconds because of the time delay caused by the hold-up of hot and cold water in the jackets and Tygon lines. This was simply to avoid returning hot water to the cold bath and vice versa. The hot reservoir was controlled by a mercury temperature relay and three 500-watt knife heaters. The cold bath was maintained with ice. Both were stirred. The degree of success in producing a theoretically square wave can be seen in Figure 5-8 in the Results chapter.

Measurement Systems. Temperatures and concentration signals were recorded on a Speedomax G dual-channel strip-chart recorder with a chart speed of 15 inches per hour.

Temperature. Copper-constantan thermocouples of Omega type had the thermocouple wires embedded in ceramic and encased in a thin stainless-steel jacket of 0.125 inch outside diameter. The wires themselves were fine (30-gauge) and the junction sphere was less than .063 inch in diameter so that the time lag of the thermocouple was negligible. Each hot junction had an independent ice junction. The millivolt thermocouple signal was amplified by a dc microvolt amplifier with a zero suppression circuit and led to the recorder. The accuracy of the recorder was checked with a potentiometer. Standard thermocouple tables were used to convert the readings to temperatures.

Concentration. The electrical resistance of the effluent solution was measured continuously using a Beckman flow conductivity cell (Figure 4-6) of cell constant 1.0. As shown in Figure 4-7, the concentration is a function of the resistance. Since the resistance is also a fairly strong function of temperature, as shown in Figure 4-7, the effluent had to be returned to a constant temperature before entering the cell. This was accomplished by the heat exchanger of Figure 4-6. Constant-temperature water was used in the baffled jacket at the rate of 4.5 liters per minute. The porous plug was found to give very high heat-exchange rates. At a solution flow rate of 6.90 ml/min, the effluent sample stream required 3 minutes to pass through this heat exchanger. There was also a flow of constant-temperature water of 0.75 liters per minute around the

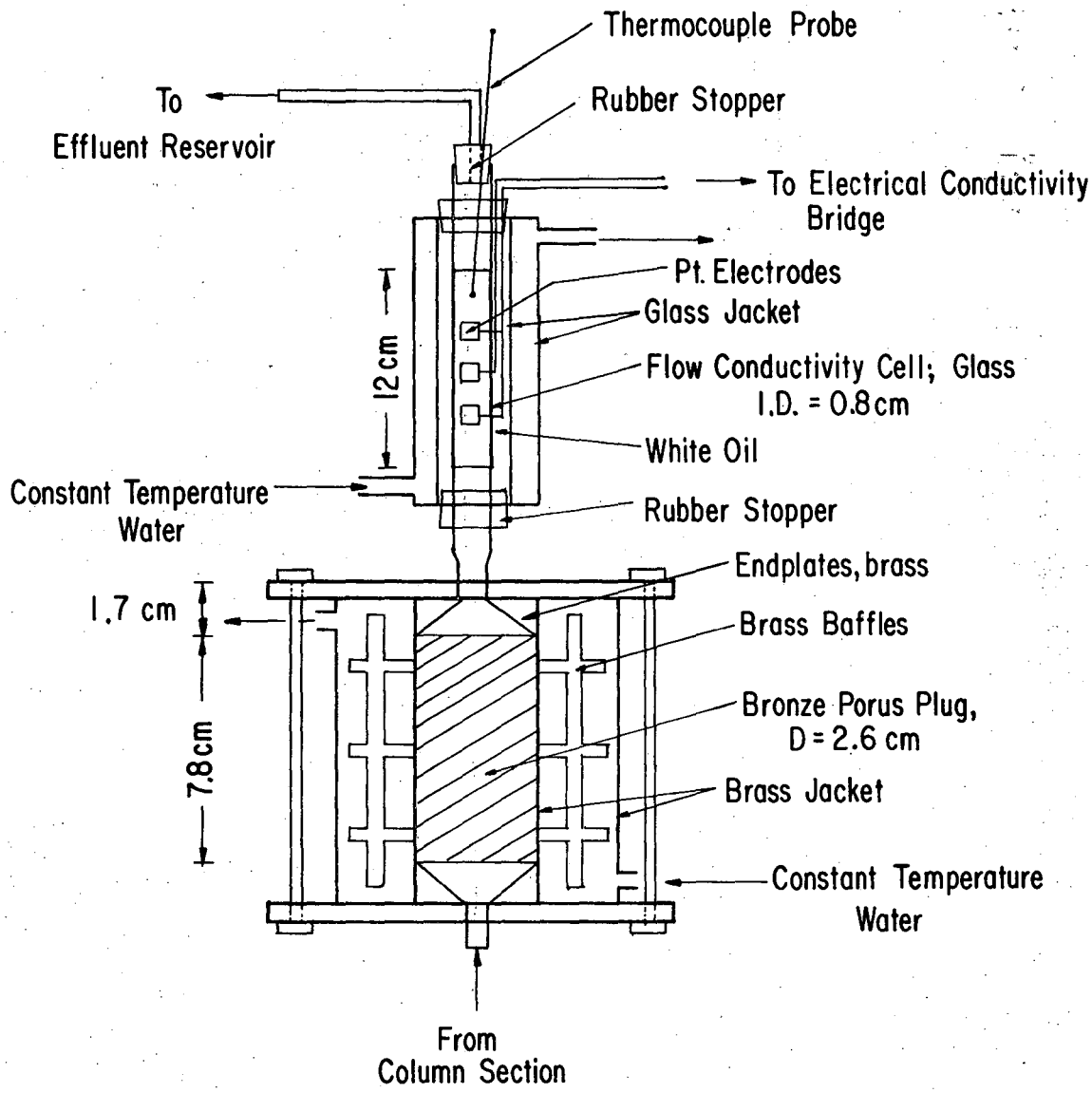

XBL 697-1054

Figure 4-6. Detail of analyzer-section components.

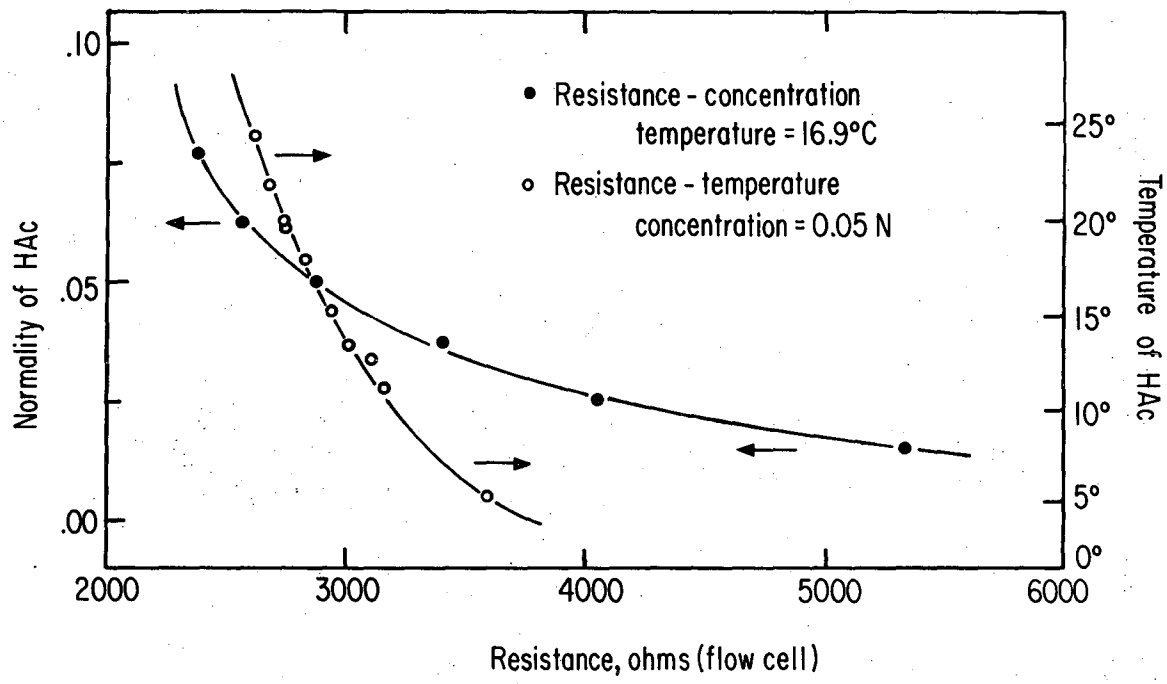

XBL 697-941

Figure 4-7. Effect of concentration and temperature on the electrical resistance of aqueous HAc solution.

flow cell itself. The temperature in the flow cell deviated less than 0.2°C for 60°C column temperature cycles; this was found to be adequate.

The resistance was determined with an Industrial Instruments electrical conductivity bridge, which was modified by adding an amplifier and rectification circuit to rectify the 1000 cycle/second output from the bridge when it was slightly off balance. This signal was demonstrated to be linearly proportional to the difference between the resistance being measured and that of the bridge setting over the recorder range.

Although the continuous conductivity recording was very helpful for determining when the cyclic steady state had been obtained, for determining when to sample, and for rapid qualitative comparisons between experiments, intermittent effluent sampling, followed by sample titration, was used to obtain quantitative results. The two reasons for this were that the nonlinear resistance-concentration and temperature-concentration functionalities made data reduction very time consuming, and that step-concentration experiments showed a considerable amount of backmixing in the heat exchanger at the low experimental flow rates so that sharp gradients in the true effluent concentrations were somewhat smoothed. The intermittent sampling was performed by sampling from an outlet immediately after the last column for 30-second periods at appropriate intervals, such as every 50, 100, or 200 seconds, depending on the

experiment. Thus about 3 milliliters were collected in each sample bottle, of which two were used in the titration. Either 0.10, 0.01, or 0.001 N NaOH solution was used as titrant, depending on the expected concentration range of the sample.

Data Reduction

After determining the sample concentrations, these were plotted and a line drawn through the points, consistent with additional information from the continuous recording. Cycle-averaged concentrations and cycle-averated separation factors were determined by planimeter integration of these plots. For this purpose, the cycle is defined as the period of positive (or negative) deviation from the feed composition, not necessarily the period of heating (or cooling.

Original data is in laboratory notebooks on file in Professor R. L. Pigford's office, 125B Lewis Hall, University of California, Berkeley, California, 94720.

CHAPTER 5

SEPARATION OF ACETIC ACID AND WATER WITH ACTIVATED CARBON BY CYCLING ZONE ADSORPTION - THE RESULTS AND COMPARISON WITH THEORY

This chapter will show the feasibility of cycling zone adsorption and the enhanced separation gained by using multiple zones. The nonlinear-equilibrium theory will be applied to the experiments with 50-140 mesh carbon to find out how well the observed wave distortion can be accounted for under this assumption.

The experimental arrangement in the column section of the apparatus is shown in Figures 5-1a, 5-1b, 5-2a, and 5-2b for the various experiments. The rest of the figures report temperature and concentration profiles from the experimental runs. The theoretical lines are the equilibrium-theory calculations assuming an ideal square wave of temperature and the isotherms of Figure 4-1.

Details of the experimental conditions not mentioned on the figures are included in the appendix to this chapter.

Applicability of Equilibrium Theory

Figure 5-3 is the base experiment to which the equilibrium theory is applied. The theory is seen to give adequate results, although it somewhat overestimates the peak values obtained experimentally. This may be due to deactivation of the carbon after repeated cycling. It

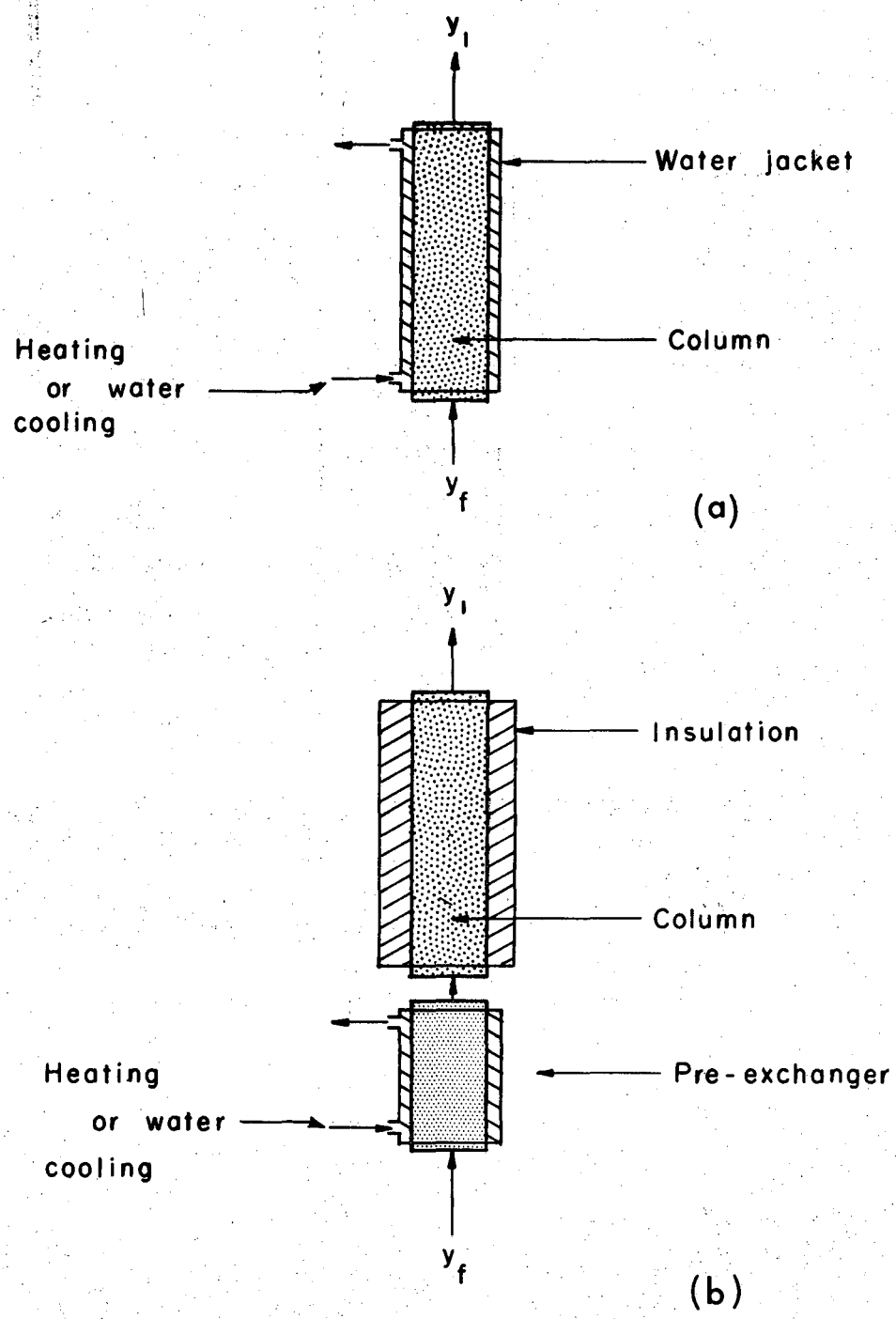

Figure 5-1a. Column-section arrangement for single-zone standing-wave experiment.

Figure 5-1b. Column-section arrangement for travelling-wave experiment.

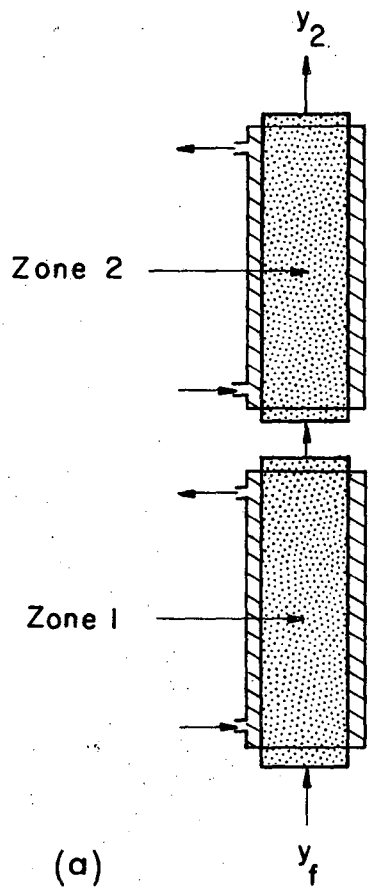

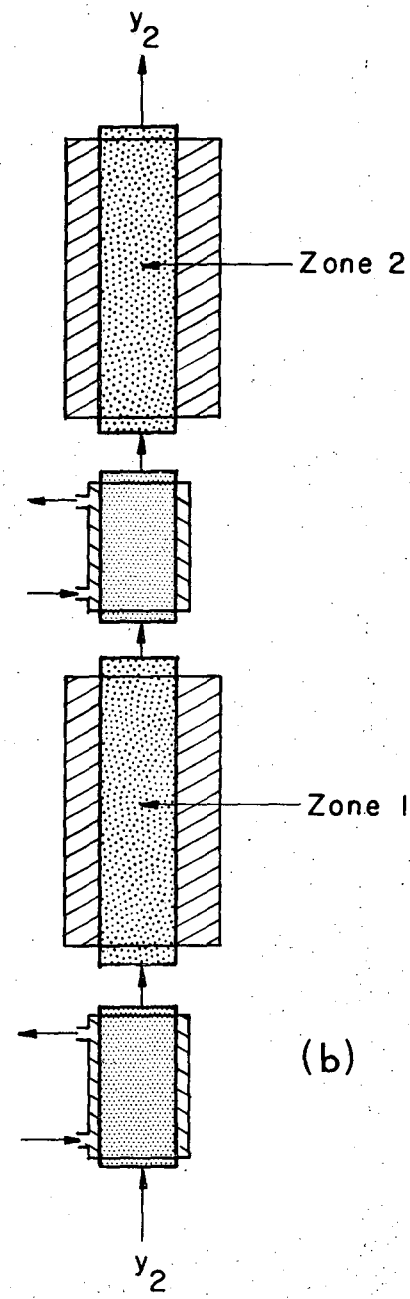

Figure 5-2a. Column-section arrangement for dual-zone standing-wave experiment.

Figure 5-2b. Column-section arrangement for dual-zone travelling-wave experiment.

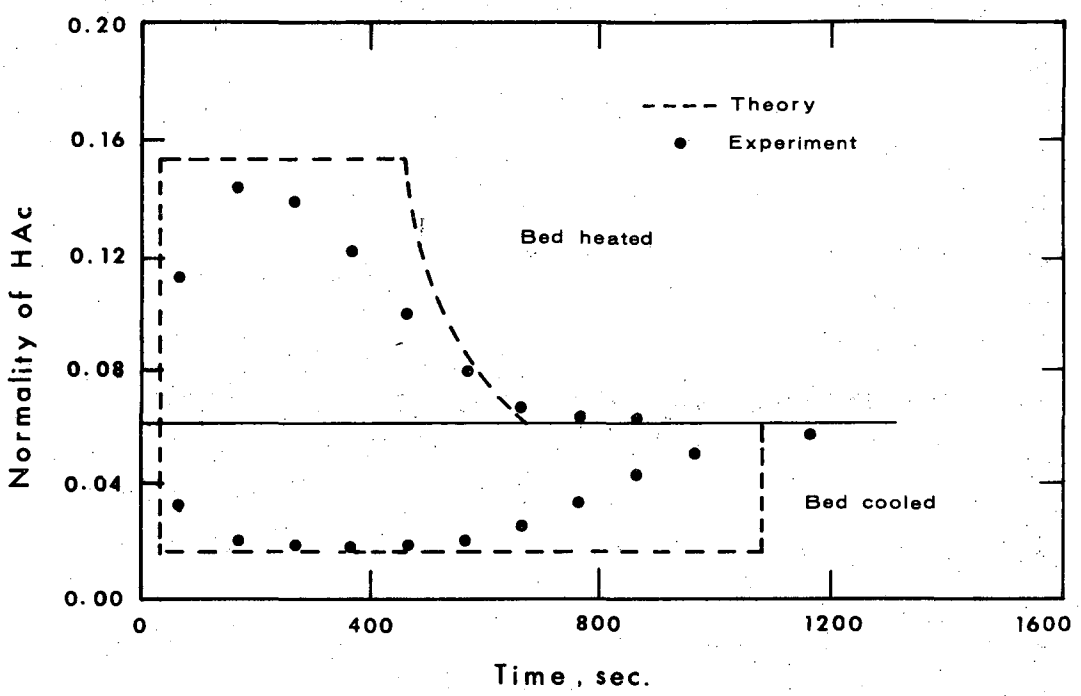

XBL 697-962

Figure 5-3. Effluent-concentration profile for single-zone standing-wave step forcing.

would probably have been better to obtain isotherm data on carbon that had undergone cycling. Also, there is some mass transfer dispersion present at those operating conditions. Figure 5-4 shows how this mass-transfer effect increases with particle size, causing the expected spreading out of the tail of the effluent concentration profile.

Single-Zone Standing-Wave Experiments - Figure 5-1a

For Figure 5-5, a linear interpolation was made in the isotherm parameters, A and k, in order to obtain parameters at the intermediate temperature, for the theoretical calculation. The two smaller thermal amplitudes were chosen equal but at a high and a low base temperature. The fact that the separation in each case was nearly the same is a particular result for this system. One notes a slight improvement in the mass transfer in the high-temperature range; this is expected because the HAc-water diffusion coefficient increases with temperature (Appendix A).

The results in Figure 5-6 illustrate two very important considerations in the design of a cycling zone adsorption process.

(1) In this example of a highly nonlinear system, the wave velocities are very different in the three concentration ranges. Thus the more separation one is able to obtain in this system -- in other words, the greater the difference between the high and low concentrations -- the larger will be the difference in the concentration

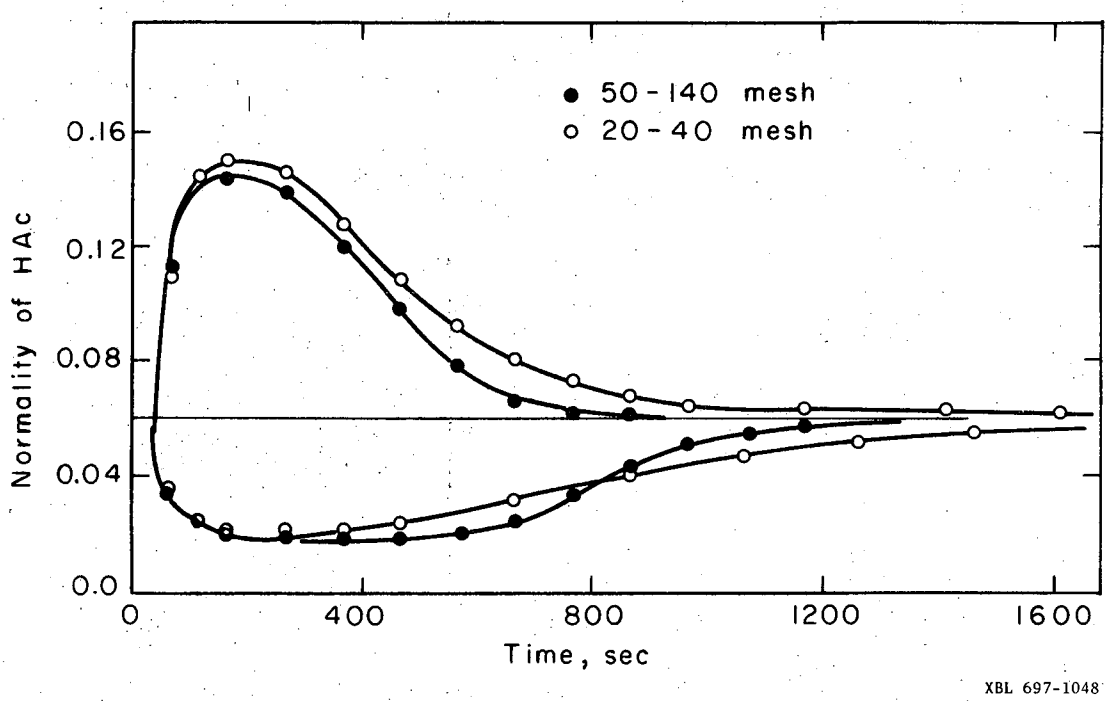

Figure 5-4. Effluent-concentration profile for a single-zone standing-wave step forcing - effect of particle size.

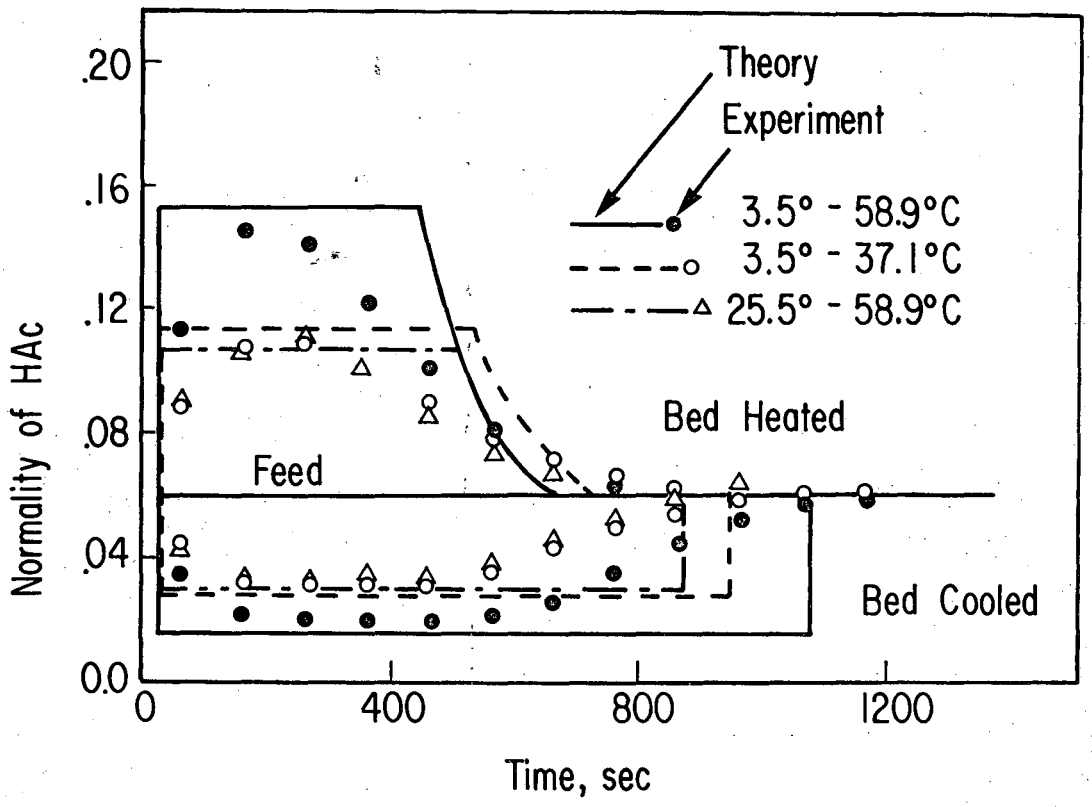

XBL 697-1055

Figure 5-5. Effluent-concentration profile for single-zone standing-wave step forcing - effect of temperature.

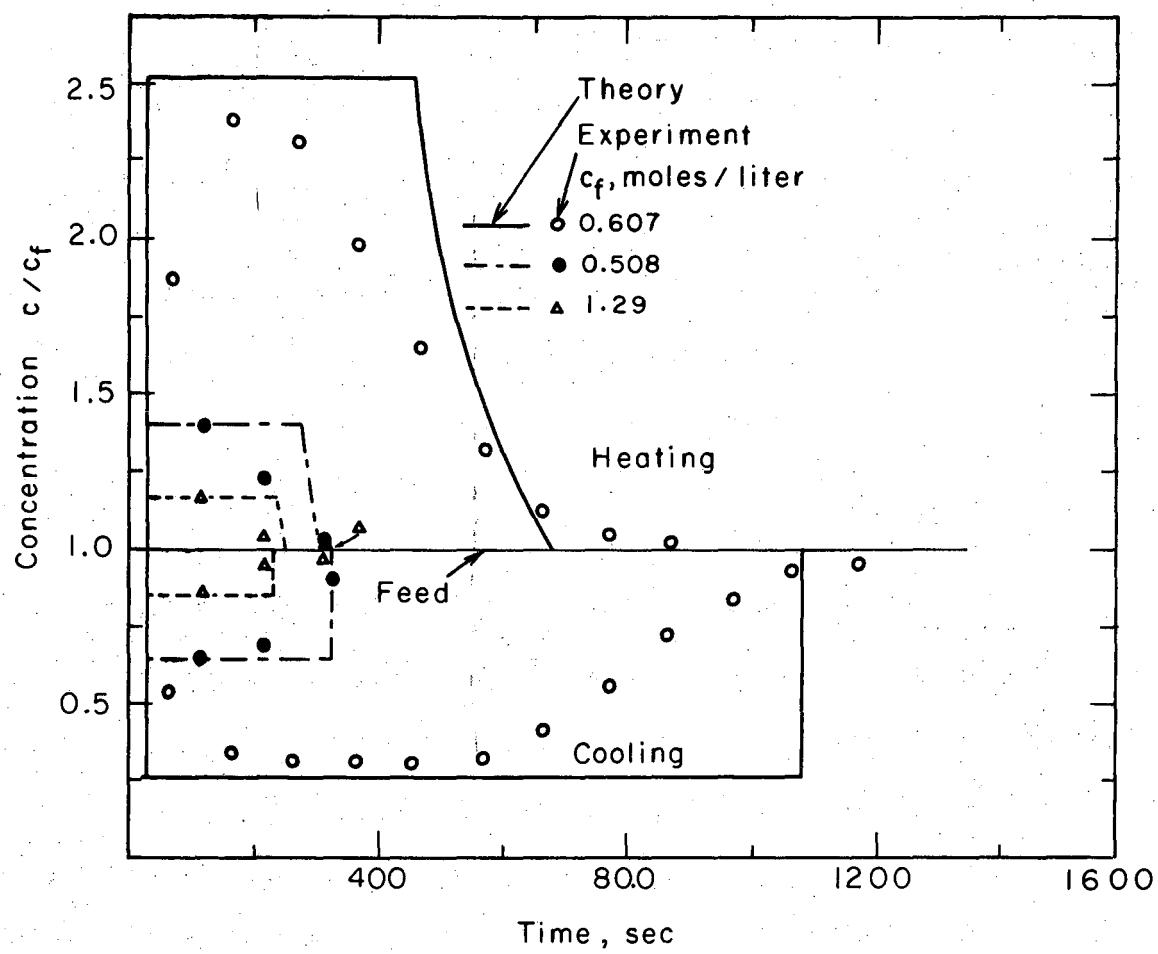

XBL 697-973

Figure 5-6. Effluent-concentration profile for single-zone standing-wave step forcing - effect of feed concentration.

velocities during each half cycle. This suggests that some recycle arrangement may be necessary in these cases.

(2) In this system, the isotherms at these upper and lower temperatures intersect at about 5 N (Figure 4-1). One observes that the separation decreases rapidly as the feed approaches this concentration. This is analogous to an azeotrope in distillation and places an upper limit on the concentration that can be achieved using this system.

The results in Figure 5-7 substantiate the theoretical prediction that there is an optimal cycle frequency giving a maximum in the average separation factor. In the presence of finite rates of mass transfer, the frequency variation has an additional effect on the separation as shown in Chapter 3. This is a monotonically increasing attenuation as the frequency is increased. Thus the peak separation factor does not remain constant with frequency as predicted by equilibrium theory. The column can not switch between equilibrium values instantaneously, and at high frequencies it does not have time to respond to one switch after the temperature is changed before the temperature is changed again. Also, at very high frequencies, the distortion of the temperature square wave contributes to this effect.

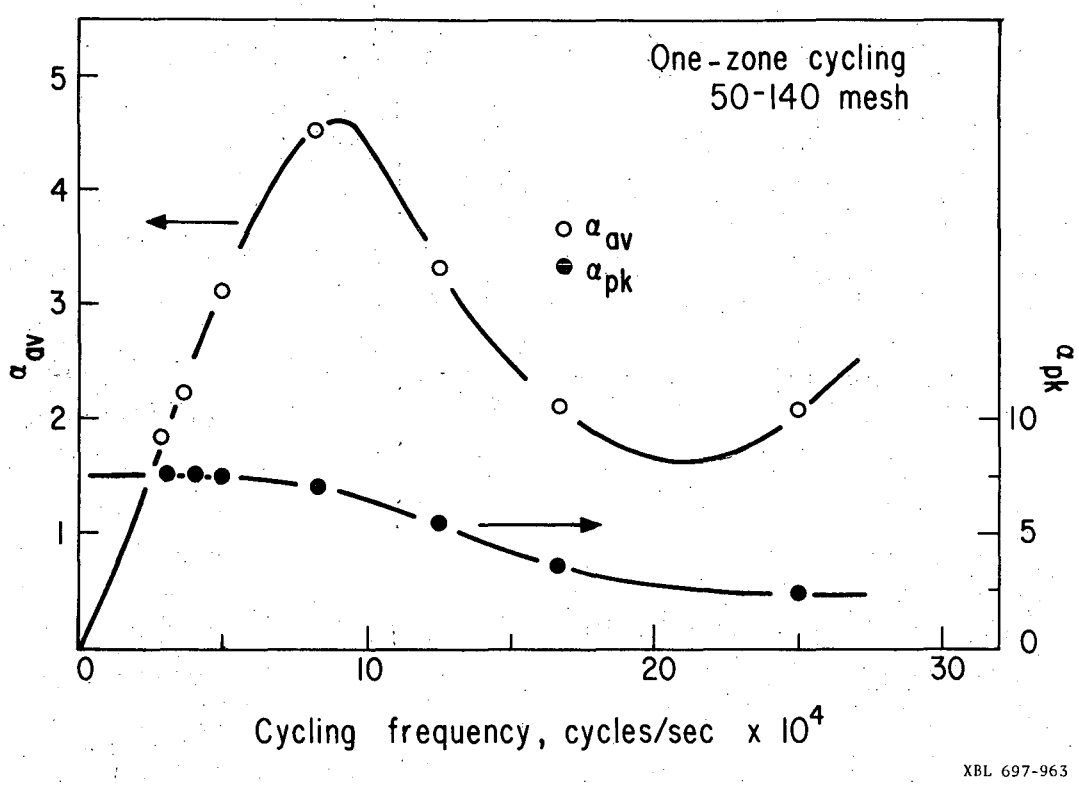

Figure 5-7. Separation factors for single-zone standing square-wave cycling - effect of frequency.

Single-Zone Travelling-Wave
Experiment - Figure 5-1b

The comparison of temperature responses for the standing- and travelling-wave experiments is shown in Figure 5-8a. The theoretical curves are plotted from Equation 2-11 of Chapter 2 with an estimate of u_{th} for the travelling-wave case calculated from heat capacity and density data and the measured void fraction. Equation C-1, including the wall capacitance, was used. Note that the curvature in the experimental outlet thermal response is almost entirely due to the nonideal square inlet temperature function. Thus Equation 2-11 is a very good approximation for this system. Note that there is an attenuation in the amplitude of the travelling thermal wave between inlet and outlet of approximately 10 percent due to the heat loss through the insulation of the column (Appendix B).

Figure 5-8b shows the comparison between the effluent concentration for the two cases. As predicted from theory, there is a slight amplification in the high and low peak values for the travelling-wave case, although, since the thermal-wave velocity is still much larger than the concentration velocities, the effect is minor. Since the concentration velocity during the heating period is larger than during the cooling period, the effect of the travelling wave is greater. The larger discrepancy between the theory and the data during the heating period than in the standing-wave case occurs because the mass-transfer dispersion has more effect on this narrow peak.

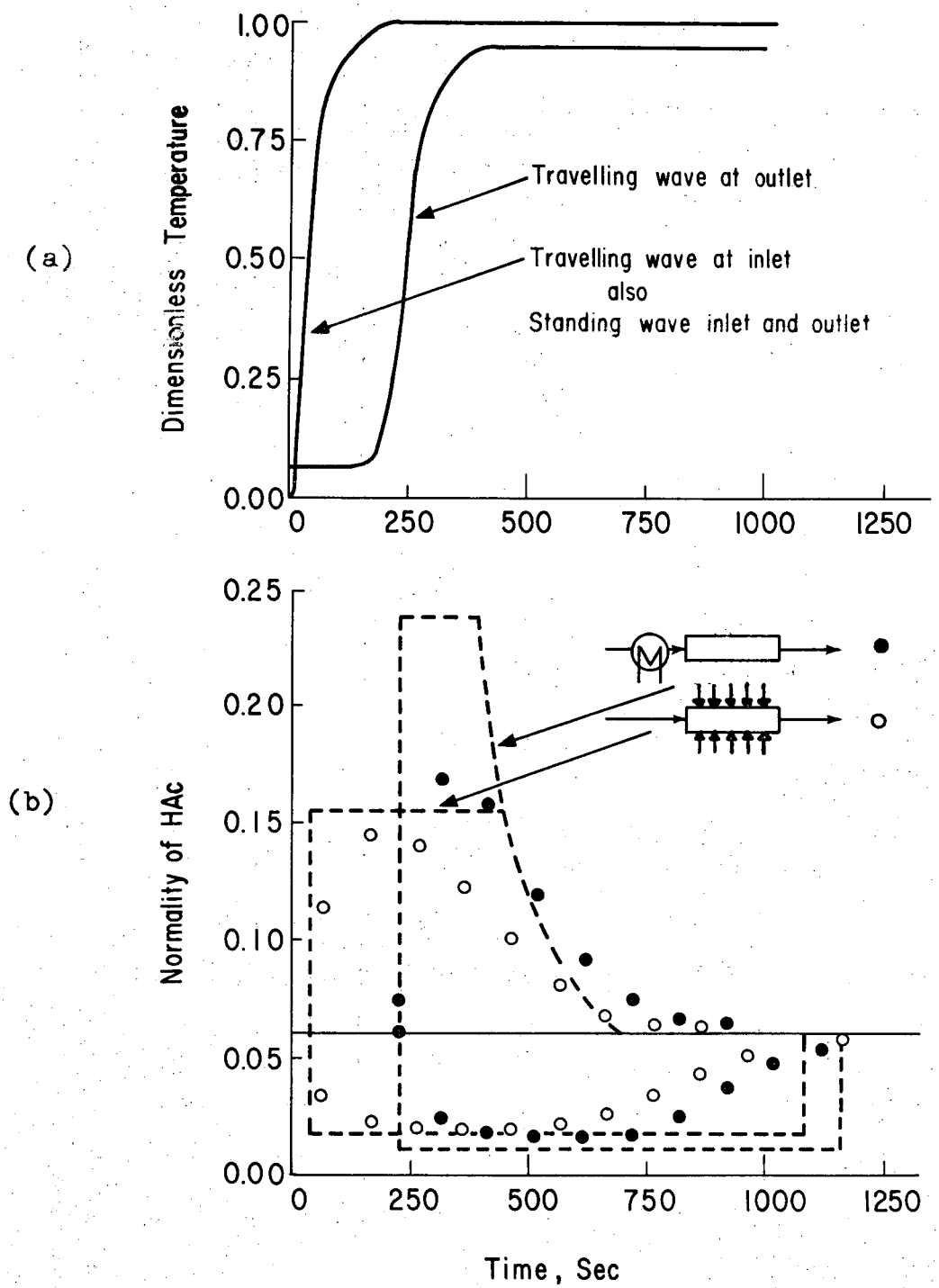

XBL 697-964

Figure 5-8. Comparison of standing- and travelling-wave step forcing on single-zone system.

(a) Temperature profiles.

(b) Effluent-concentration profiles.

Double-Zone Standing-Wave
Experiments - Figure 5-2a

The comparison between the one-zone and the two-zone experiments is shown in Figure 5-9b with the temperature forcing shown in Figure 5-9a. As can be seen from the separation factors and the curves, the second zone provides a considerable enhancement in the separation. The correct low concentration is predicted from equilibrium theory, but the high-concentration peak is narrow enough to have been considerably modified by the mass-transfer dispersion. Also, it is evident that the fact that the isotherms are nonlinear, causing the concentration-wave velocities to be concentration dependent, is important in this case. Figures 2-6 and 2-7 are helpful in understanding these results. Because the high concentration peak travels faster than, for example, the feed concentration, this peak can pass through the second zone and out before the zone is made hot. Thus it never gets shifted to an even higher concentration. To obtain this shift, one would have to make the cycle frequency for the second zone higher than that of the first.

Figures 5-10 and 5-11 show the results of varying the cycle frequency and the forcing-temperature phase relationship for the two-zone system. Larger mesh size particles were used in this study, because after extensive cycling, the smaller particles packed together so tightly that the pressure drop across the two columns exceeded the design pressure of the apparatus. The decrease in mass-

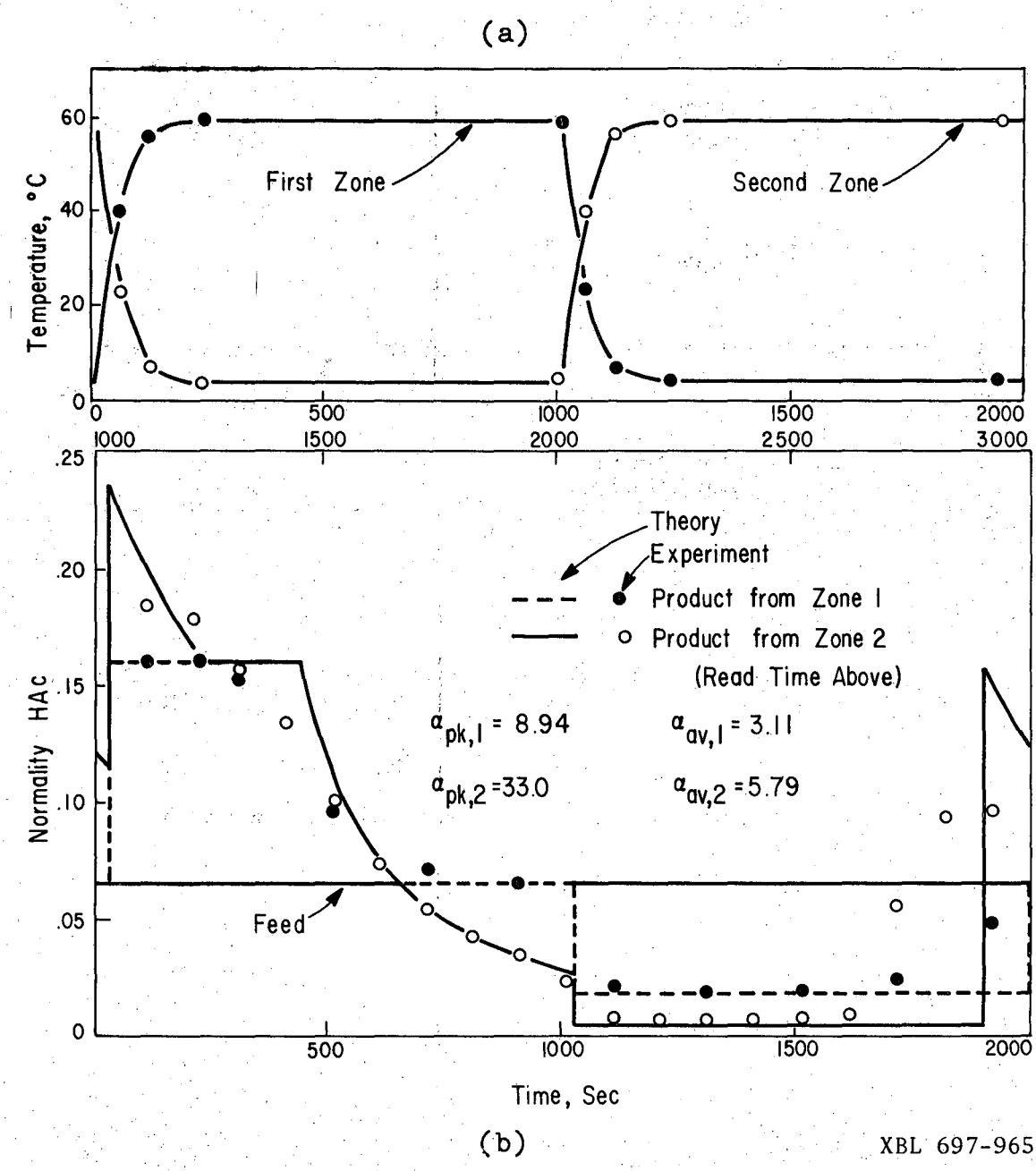

XBL 697-965

Figure 5-9. Comparison of single- and dual-zone standing square-wave cycling.

(a) Temperature profiles.

(b) Effluent-concentration profiles.

transfer rate attenuated the separation effect in comparison to the results for the smaller particles, but the response was generally similar. Again the existence of an optimum cycle frequency is confirmed in Figure 5-10.

Figure 5-11 indicates that there is an optimum phase lag, as theoretically predicted. Since the cycle frequency was chosen to correspond approximately with the slower concentration velocity (that in the cold period), an examination of expression 2-20b reveals that the optimum phase lag should be in the range of approximately $\pi/2$ to π. The experimental location of the optimum corresponds to this prediction.

Double-Zone Travelling-Wave Experiment - Figure 5-2b

Figure 5-12 illustrates the feasibility of using interstage exchangers and the resulting travelling waves in the multiple-zone arrangement. There is a slight improvement in the travelling-zone separation even though the amplitude of the forcing temperature wave was slightly smaller than in the standing-wave case.

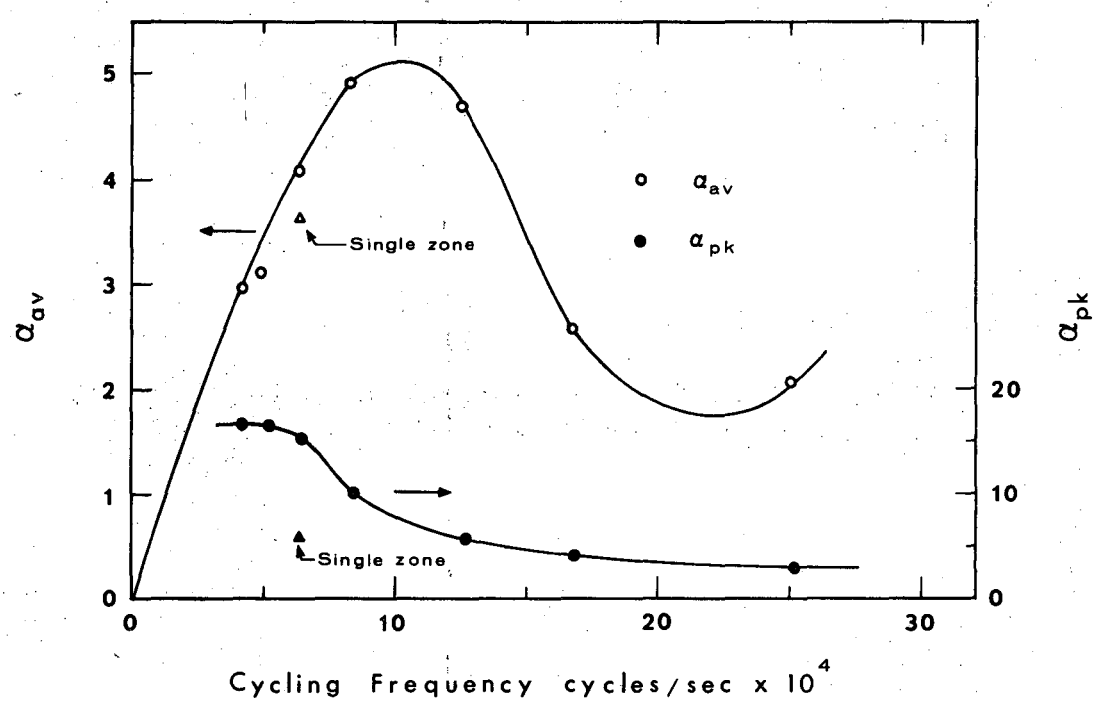

XBL 697-974

Figure 5-10. Separation factors for dual-zone standing square-wave cycling - effect of frequency.

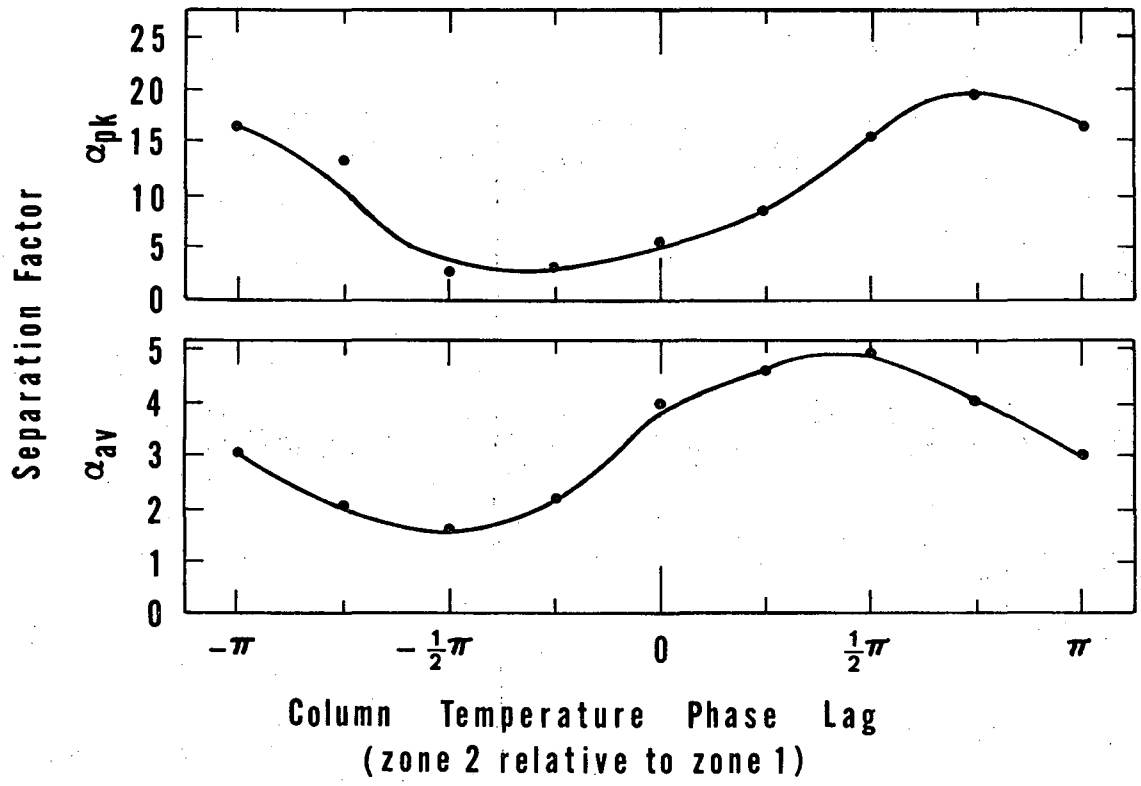

XBL 697-1051

Figure 5-11. Separation factors for dual-zone standing square-wave cycling - effect of phase lag.

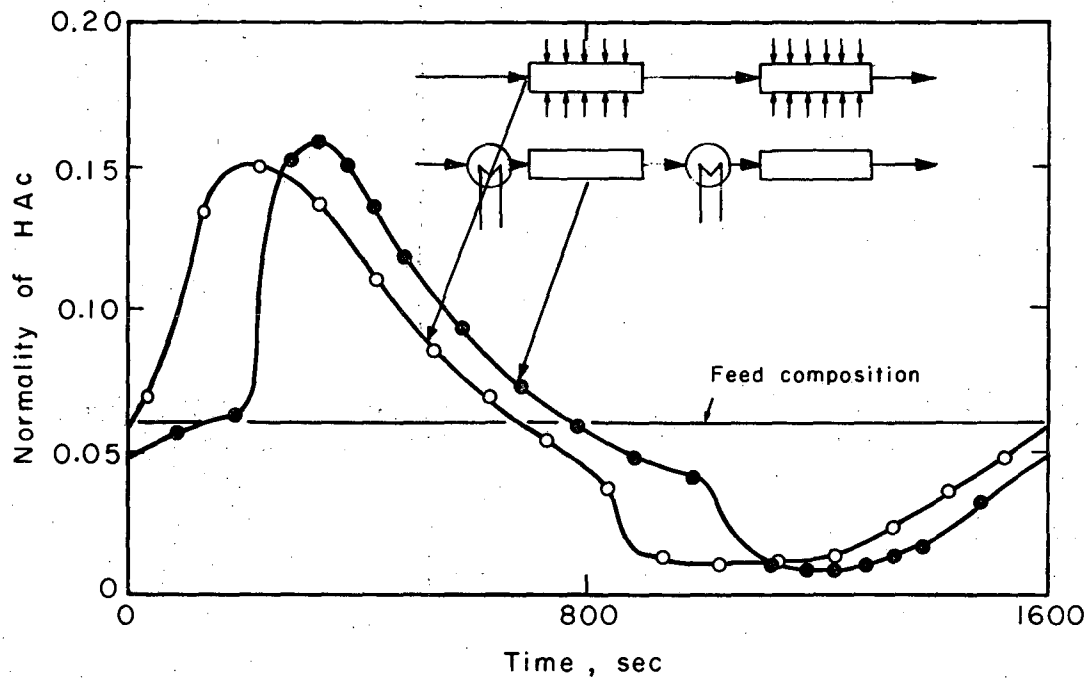

XBL 697-976

Figure 5-12. Comparison of standing and travelling square-wave cycling on dual-zone system.

APPENDIX TO CHAPTER 5

DETAILS OF EXPERIMENTAL CONDITIONS

Forcing: Step or square-wave cycling in all experiments.

Flow Rate: 6.90 ml/min in all experiments

Mesh: Refers to particle size.

Feed: Refers to concentration of feed.

Temp.: Refers to extreme values of experimental step or square-wave.

Freq.: Refers to frequency of cycling.

Phase Lag: Refers to phase lag of the temperature of Zone 2 relative to Zone 1; if negative, indicates a phase lead - this lag does not include residence-time lag between zones.

Single Zone

Standing-Wave Forcing - Figure 5-1a

(a) Step-Forcing Effluent-Concentration Profiles. See Figure 5-8a for Temperature Profiles.

Figure 5-3

Mesh: 50-140
Feed: .0610 N
Temp.: 3.5-58.9° C

Figure 5-4

Mesh: Variable
Feed: .0610 N
Temp.: 3.5-58.9° C

Figure 5-5

Mesh: 50-140
Feed: .0610 N
Temp.: Variable

Figure 5-6

Mesh: 50-140
Feed: Variable
Temp.: 3.5-58.9° C

(b) Cycling-Frequency Variation - Figure 5-7

$\alpha_{pk} = c_{pk}/c_{\ell,pk}$

$\alpha_{av} = c_{h,av}/c_{\ell,av}$

h - refers to $c > c_o$

ℓ - refers to $c < c_o$

Mesh: 50-140
Feed: .0610 N
Temp.: 3.5-58.9° C

Travelling-Wave Forcing - Figure 5-1b

Step-Forcing Effluent-Concentration and Temperature Profiles.

Figures 5-8a,b

Mesh: 50-140
Feed: .0610 N
Temp.: Nondimensionalized using 3.5°-58.9° C

Dual Zone

Standing-Wave Forcing - Figure 5-2a

Figure 5-9a,b

Mesh: 50-140
Feed: .0647 N
Temp.: Shown
Freq.: .030 cycles/min
Phase Lag: π radians

Figure 5-10

Mesh: 20-40
Feed: .0610 N
Temp.: 3.5-58.9°
Freq.: .030 cycles/min
Phase Lag: Variable

Travelling-Wave Forcing - Figure 5-2b

Figure 5-12

Mesh: 20-40
Feed: .0610 N
Temp.: Standing wave - 3.5-58.9° C

[Temp.] Travelling wave

Zone 1: 7.3-60.0° C entrance
Zone 2: 8.5-59.0° C entrance

Freq.: .038 cycles/min

Phase Lag: π radians

CHAPTER 6

CONCLUSIONS

It has been demonstrated theoretically and on a laboratory scale that the cycling zone adsorption process is feasible. Significant separations are predicted mathematically using the equilibrium theory, at least when the isotherms are not too nonlinear. Experimentally, significant but by no means complete separations were obtained using a system with nonlinear isotherms. Particularly evident was the predicted increase in separation power gained by using multiple zones in series. Furthermore, it was demonstrated that the cyclic transfer of thermal energy in and out of the zones, which is essential to the process, can be accomplished very efficiently in liquid-solid systems by the use of the natural travelling thermal wave properties of the zones.

On the basis of these conclusions and with the advice of the Atomic Energy Commission, a patent application on the process has been filed.

On the other hand, certain difficulties in the process are evident. First, the small shift in the equilibrium isotherms for moderate temperature changes means that at least several zones will be required for significant separations. Since the addition of each zone means an additional heat duty, the thermal requirements for the

process may be high. Internal reuse of the heat is certainly possible, however, though there seem to be problems in using heat regenerators for this purpose (Appendix B).

The experimental results and the predictions of Chapter 3 indicate that low mass-transfer rates markedly attenuate the separation from that predicted using the equilibrium theory. In order to decrease this attenuation effect for this intraparticle diffusion-controlled system, one must operate at low flow rates or with fine adsorbent particles, thus restricting the throughput possible with the process. This problem is aggravated in the event that a large number of zones are required from the equilibrium theory.

The presence of dispersion caused by the nonlinear isotherms and finite mass transfer rates indicates that some recycle may be necessary. In other words, one may want to recover only the peak concentration during the cycle, returning the rest to the feed stream to be refed to the zone at the proper time in the cycle. This, however, would increase equipment and operating costs.

The procedure of using imposed thermal travelling waves is, presently, only a theoretical idea, which can be demonstrated mathematically to be very advantageous. According to Chapter 3, there is no point in using such an imposed wave instead of the natural thermal wave unless there are a large number of transfer units; in this case, there is a significant advantage. The physical feasibility of imposing

the travelling wave has not been investigated in this thesis. If experimentation should prove that it is not physically feasible to impose a travelling thermal wave, the effect still occurs for any intensive variable that shifts the solid-fluid equilibrium. Certain variables such as electrical or concentration fields may be more practical than thermal fields to impose as travelling waves, and thus amplify a small separation effect.

It is the present conclusion that cycling zone adsorption is an attractive process which may economically solve many difficult separation problems, particularly the intermediate scale separation of biological and isotopic materials which now must be performed chromatographically.

Two immediate goals of future research on the cycling zone adsorption process should be a more detailed analysis of the mass transfer aspects of the process and an experimental investigation of the amplification effect of the interaction between the travelling thermal and concentration waves. This should provide enough information for a cost estimation of several possible commercial-scale separations using the presently evolved form of the process. If these results are encouraging, the separation of a system of several adsorbed solutes should be investigated.

NOMENCLATURE

(Dimensionless unless specified)

A = solid-fluid equilibrium distribution parameter, units depend on function.

A' = $\rho_s A(1 - \varepsilon) + \varepsilon$, lumped solid-fluid equilibrium distribution parameter.

C = heat capacity, cal/g - °C.

D = $\alpha/(1 - \alpha)\rho_s A c_o^{k-1}$, mobile fluid-solid equilibrium mass capacity ratio.

D_{eff} = $\varepsilon_I D_I$, effective intraparticle diffusivity, cm^2/min

D_M = mass molecular diffusivity, cm^2/min.

D_T = thermal molecular diffusivity, cm^2/min.

E = $\alpha/(1 - \alpha)\varepsilon$, mobile-immobile fluid mass capacity ratio.

E_D = eddy axial dispersion, cm^2/min.

F = volumetric flow rate, ml/min.

G = superficial velocity, cm/min.

ΔH_{ads} = differential heat of adsorption, cal/mole.

Im = imaginary number operator.

K = m_o/NTU, mass transfer units.

N_M = mass flux, moles/min-cm^2.

N_T = heat flux, cal/min-cm^2

NTU = number of transfer units.

P = $v\ Z_o/(E_D + D_T)$, thermal axial dispersion parameter.

Pe_{disp} = $d_p v/E_D$, axial dispersion Péclet number.

$Pe_{flow,I}$ = $d_p F/D_I$, flow Péclet number.

P' = $h_w a_w Z_o / \alpha v \rho_f C_f$, radial thermal loss parameter.

R = gas constant, cal/gmole-°C.

Re = real number operator.

S = cross-sectional area (of bed if not subscripted), cm^2.

T = temperature, °C.

V_o = volume of solution, liters.

V_T = total volume of bed, cm^3.

W_o = weight of active adsorbent in bed.

W_{tot} = weight of total packing in bed.

X = $\rho_s A c^* (1-\varepsilon) + \varepsilon c^*$, lumped solid-phase concentration, moles/liter of solid.

Z_o = length of bed, cm.

a = surface area / bed volume ratio, cm^{-1}.

c = fluid concentration, moles/liter.

c^* = fluid concentration in equilibrium with solid-phase concentration, moles/liter.

d_p = particle diameter, cm.

d' = $A_o \rho_s (1-\varepsilon) \Delta H_{ads}(T_H - T_o) / (A_o \rho_s (1-\varepsilon) + \varepsilon) R T_o^2$.

$f(x)$ = arbitrary function of arbitrary parameter.

f_{ads} = $\rho_s c_s (1-\varepsilon) \Delta H_{ads}(q'_{max} - q'_o) / (T_H - T_o)(\rho_s c_s (1-\varepsilon) + \rho_f c_f \varepsilon)$, heat of adsorption parameter.

$g(y)$ = nonlinear equilibrium distribution function.

h = heat transfer coefficient, cal/cm^2-min-°C.

k = exponent in Freundlich isotherm.

k_M = mass transfer coefficient, cm/sec.

k_T = thermal conductivity, cal/cm-min-°C.

m = $\frac{1-\alpha}{\alpha} A'$, solid-fluid mass capacity ratio parameter.

n = zone number.

P_1 = $P/4u_{th}t$, axial dispersion parameter.

p_2 = $Pu_{th}t/4$, axial dispersion parameter.

per(ωt) = general periodic function of frequency ω.

q = amplification factor.

q' = solid-phase concentration, moles/kg dry solid.

$\bar{q}$ = $(q' - q_o')/(q'_{max} - q_o')$, solid concentration.

r = radius of bed wall.

t' = time, min.

t = $t'v/Z_o$, time in bed residence times.

t_c = cycle period.

u = wave velocity.

u_o = average concentration wave velocity.

v = interstitial fluid velocity, cm/min.

y = c/c_o, concentration in fractions of feed concentration.

y^* = maximum in concentration.

$\langle y \rangle$ = cycle-averaged concentration.

z = z/Z_o, axial distance in fractions of bed length.

z' = axial distance, cm.

α = interparticle void fraction.

α_{pk} = $y_{h,pk}/y_{\ell,pk}$, peak separation factor.

α_{av} = $\langle y_h \rangle / \langle y_\ell \rangle$, cycle-averaged separation factor.

β = concentration velocity deviation variable.

γ = phase lag, radians (if negative, refers to phase lead).

ε = intraparticle void fraction.

ε_I = effectiveness factor for diffusion through solid.

ζ = z, axial distance.

θ = $(T - T_o)(/T_H - T_o)$, temperature.

ρ = density, g/cm^3.

ρ_p = particle density of solid including intraparticle void, g/cm^3.

ρ_s = structural density of solid, g/cm^3.

σ = S_w/S, wall-to-bed cross-sectional area or volume fraction.

τ = $t - z/u_{th}$, time.

τ^* = z-coordinate of maximum in concentration.

φ = $(c - c_o)/c_o$, fluid-phase concentration deviation.

$\bar{\varphi}$ = the z-only dependent part of φ.

χ = $(X/A_o' - c_o)/c_o$, solid-phase concentration.

$\bar{\chi}$ = the z-only dependent part of χ.

ω' = frequency, radians/min.

ω = $\omega' Z_o/v$, frequency.

Ω = ωK, frequency-mass transfer parameter.

<u>Subscripts</u>

ads = adsorption

air refers to environment outside of system.

av = cycle-averaged.

C = cold.

c = concentration.

f = feed condition.

H = hot.

h = high.

I refers to nature of transport: I = M, mass; I = T, heat.

i = conditions after a concentration characteristic crosses a temperature boundary.

i - 1 = conditions before a concentration characteristic crosses a temperature boundary; if i = hot, i - 1 = cold, and vice versa.

ins = insulation.

ℓ = low.

max = maximum.

n = zone number.

o = average condition or feed condition.

p = particle.

pk = peak.

s = solid.

sh = concentration shock.

w = wall.

th = thermal

<u>Superscripts</u>

C = cold.

H = hot.

M = mass.

T = temperature.

REFERENCES

Berg, C. 1946. Hypersorption Process for Separation of Light Gases, Trans. A.I.Ch.E. 42, 665.

Bohrer, B. B. 1965. Multicomponent Separation Process, U.S. Patent 3,233,748 (December 14, 1965).

Cassidy, H. G. 1951. "Adsorption and Chromatography," Interscience, New York.

Carberry, S. S., Bretton, R. H. 1958. Axial Dispersion of Mass in Flow Through Fixed Beds, A.I.Ch.E. J. 4, 367.

De Vault, Don. 1943. The Theory of Chromatography, J. Amer. Chem. Soc. 65, 532.

Dryden, C. E., Kay, W. B. 1954. Kinetics of Batch Adsorption and Desorption, Ind. Eng. Chem. 46, 2294.

Goldstein, F. R. S. 1953. On the Mathematics of Exchange Processes in Fixed Columns, II, Proc. Roy. Soc. A219, 151.

Helfferich, Friedrich. 1962. "Ion Exchange," McGraw-Hill, New York.

Jenczewski, T. S., Myers, A. L. 1968. Parametric Pumping Separates Gas Phase Mixtures, A.I.Ch.E. J. 14, 509.

Kipling, J. J. 1965. "Adsorption from Solutions of Non-Electrolytes," Academic Press, New York.

Kraus, K. A., Raridon, R. S. 1959. Temperature Dependence of Some Cation Exchange Equilibria in the Range 0 to 200°, J. Phys. Chem. 63, 1901.

Kreith, Frank. 1965. "Principles of Heat Transfer," p. 577, International Textbook, Scranton, Pa.

———. 1965b. Ibid. p. 15.

Lapidus, L., Amundson, N. R. 1952. Mathematics of Adsorption in Beds, VI. The Effect of Longitudinal Diffusion in Ion Exchange and Chromatographic Columns, J. Phys. Chem. 56, 984.

Mantell, C. L. 1951. "Adsorption," McGraw-Hill, New York.

Othmer, D. F., Thakar, M. S. 1953. Correlating Diffusion Coefficients in Liquids. Ind. Eng. Chem. 45, 589.

Perry, J. A. 1963a. "Chemical Engineer's Handbook," 4th ed. (R. H. Perry, C. H. Chilton, and S. D. Kirkpatrick, eds.), McGraw-Hill Book Company, Inc., New York, 1963, Section 16.

———, 1963b. Ibid., p. 16-15.

———, 1963c. Ibid., p. 23-58.

———, 1963d. Ibid., p. 23-55.

———, 1963e. Ibid., p. 12-39.

Pfann, W. G. 1966. "Zone Melting," Chapter 4, John Wiley and Sons, New York.

Pigford, R. L., Baker, B. III, and Blum, D. E. 1969a. An Equilibrium Theory of the Parametric Pump, Ind. Eng. Chem., Fundam. 8, 144.

———, 1969b. Cycling Zone Adsorption, A New Separation Process, UCRL-18848 (May 1969; also accepted for Ind. Eng. Chem., Fundam.

Rolke, R. W., and Wilhelm, R. H. 1969. Recuperative Parametric Pumping, Model Development and Experimental Evaluation, Ind. Eng. Chem., Fundam. 8, 235.

Ross, Sidney, and Oliver, J. P. 1964. "On Physical Adsorption," Interscience, New York.

Sherwood, T. K., and Reid, R. C. 1958. "Properties of Gases and Liquids," p. 52, McGraw-Hill Book Company, New York.

Skarstrom, C. W. 1959. Use of Adsorption Phenomena in Automatic Plant-Type Gas Analyzers, Ann. N.Y. Acad. Sci. 72, 751.

Sneddon, Ian N. 1957. "Elements of Partial Differential Equations," Chapters 1, 2, McGraw-Hill Book Company, Inc., New York.

Stack, R., and Rice, C. B. 1967. "Chromatographic Methods" Chapman and Hall, London.

Sweed, N. H., and Wilhelm, R. H. 1969. Parametric Pumping Separations via Direct Thermal Mode, Ind. Eng. Chem., Fundam. 8, 221.

Timmins, R. S., Mir, L., and Ryan, J. M. 1969. Large Scale Chromatography: New Separation Tool, Chem. Eng. 170, (May 19, 1969).

Vermeulen, T. 1969. Personal communication.

Weiss, D. E., Bolto, B. A., McNeill, R., Macpherson, A. S., Siudak, R., Swinton, E. A., Willis, D. 1966a. An Ion-Exchange Process with Thermal Regeneration, II. Properties of Weakly Basic Resins, Aust. J. Chem. 19, 561.

———. 1966b. III. Properties of Weakly Acidic Ion-Exchange Resins, ibid., p. 589.

———. 1966c. IV. Equilibria in a Mixed Bed of Weak-Electrolyte Resins, ibid., p. 765.

———. 1966d. V. Multistage Operation, ibid., p. 791.

Weiss, D. E., New C.S.I.R.O. Approach to Water Demineralization, Royal Aust. Chem. Inst. Proceedings 32, 287 (1965).

Weiss, D. E., Bolton, B. A., McNeill, R., Macpherson, A. S., Siudak, R., Swinton, E. A., Willis, D. 1966. Thermally Regenerated Ion-Exchange Process - An Aid to Water Management, Water Pollut. Control Fed. J., 1784 (November, 1966).

Weiss, D. E. 1943. On the Theory of Chromatography, J. Chem. Soc., 297.

Wilhelm, R. H., Rice, A. W., and Bendelius, A. R. 1966. Parametric Pumping, A Dynamic Principle for Separating Fluid Mixtures. Ind. Eng. Chem., Fundam. 5, 141.

Wilhelm, R. H., Rice, A. W., Rolke, R. W., and Sweed, N. H. 1968. Parametric Pumping, A Dynamic Principle for Separating Fluid Mixtures, ibid. 7, 337.

APPENDIX A

THE CALCULATION OF TRANSPORT PROPERTIES AND HEAT OF ADSORPTION EFFECTS FOR THE PROCESS

Transport Parameters

The general correlation of transport properties in fixed-bed systems due to Vermeulen and presented in Figure 16-9* of Perry (1963a) is used to determine the controlling modes of mass and heat transfer in the experimental system and to calculate estimates of the height of a transfer unit, HTU, in the column for these transport processes. The flow Péclet number is calculated for the average diameter, d_p, for the two particle sizes. The value of the HAc-water diffusivity coefficient was found in Dryden and Kay (1954) as was the effectiveness factor for porous carbon. The latter is only approximate for the activated carbon of this experiment, since it is not from the same manufacturer as that of the Dryden and Kay study. The variation of the diffusivity with temperature for dilute aqueous acetic acid solutions was estimated from Othmer (1953) using the molal volume calculation of La Bas (see Sherwood and Reid, 1958). The thermal diffusivity of water was found in Kreith (1965).

The flow Péclet number and the effectiveness factor are defined as

$$Pe_{flow,I} = \frac{d_p\ F}{D_I\ S} \qquad (I = M \text{ or } T)$$

$$\varepsilon_I = \frac{D_{eff,I}}{D_I}$$

---

*The correction to Figure 16-9 made by Vermeulen (1969) is used.

where F = 6.94 ml/min, volumetric flow rate

S = 0.785 cm^2, superficial cross-sectional area of column

d_p = 0.06 cm, 20-40 mesh, average particle diameter

0.02 cm, 50-140 mesh, " " "

D_M = 7.88×10^{-4} cm^2/min, HAc-water diffusivity at 25°C

D_T = 8.55×10^{-2} cm^2/min, water thermal diffusivity at 25°C

D_{eff} = effective diffusivity in porous carbon

ε_M = 1.34×10^{-2}, effectiveness factor of carbon for mass transfer

ε_T = 1.0 , effectiveness factor of carbon for heat transfer

Note that the thermal effectiveness factor, ε_T, is estimated to be approximately unity since heat can be transferred through the carbon and also through the liquid-filled pores. The height of a transfer unit, HTU, is found from the graph using the relationship

$$HTU = \frac{Z_o}{NTU}$$

The results are shown in Table A-1. The variation of the mass diffusivity with temperature are shown in Table A-2.

Heat of Adsorption Effects

The importance of the heat of adsorption term in Equation 2-4 will be examined. Nondimensionalizing the dependent variables and rearranging, Equation 2-4 becomes

Table A-1. Mass and Thermal Transport Parameters for HAc-Water-Activated Carbon System

	Thermal			Mass		
Mesh size	$Pe_{flow,T}$	Mode	HTU, cm	$Pe_{flow,M}$	Mode	HTU, cm
50-140	2.7	Axial dispersion controlling	0.05	2.24×10^2	Particle diffusion controlling	4.0
20-40	6.2	Axial dispersion controlling	0.2	6.73×10^2	Particle diffusion controlling	60.

Table A-2. Dependence of HAc-Water Diffusivity on Temperature

Temperature, °C	Diffusivity, cm^2/sec
4	0.69
20	1.11
25	1.31
60	2.50

$$\frac{\partial}{\partial t'}\left(\theta_s - \frac{\rho_s C_s(1-\varepsilon)\ \Delta H_{ads}}{\rho_s C_s(1-\varepsilon) + \rho_f C_f \varepsilon} \cdot \frac{q'_{max} - q'_{min}}{T_H - T_o}\ \bar{q}\right) \qquad \text{(A-1)}$$

$$= \frac{-ha_p}{(\rho_s C_s(1-\varepsilon) + \rho_f C_f \varepsilon)(1-\alpha)}\ (\theta_s - \theta)$$

where

$\bar{q} = \dfrac{q' - q'_o}{q'_{max} - q'_o}$, solid concentration, dimensionless.

q'_{max}, q'_o , maximum and average solid-phase contrations encountered during the process.

Therefore, θ and $\bar{q}$ are of the order of magnitude of unity so that if

$$f_{ads} = \frac{\rho_s(1-\varepsilon)\ \Delta H_{ads}}{\rho_s C_s(1-\varepsilon) + \rho_f C_f \varepsilon} \cdot \frac{q'_{max} - q'_o}{T_H - T_o} << 1,$$

the term is negligible. Since

T_H ~ 60° C

T_o ~ 30° C

q'_{max} ~ 2 moles/kg

q'_o ~ 1 mole/kg

ρ_s = 1.820 g/cm^3

C_s ~ 0.25 kcal/kg

ε = .5702

ΔH_{ads} ~ 5 kcal/mole (an upper estimate for van der Waals adsorption for liquid-solid systems)

then

$$f_{ads} = 0.169$$

which may be considered negligible. However, this quantity is not so small that the effect could never be important in other fluid-solid systems.

APPENDIX B

THE USE OF INTERSTAGE HEAT REGENERATORS TO INCREASE THE THERMAL EFFICIENCY OF THE PROCESS

It is obvious that the multiple-zone arrangement will require additional heating and cooling for each successive zone. The use of countercurrent heat exchangers is possible, as was demonstrated in the experiments, and different streams in the process could be exchanged against each other to increase efficiency. However since the process itself is cyclic, the use of cyclic heat exchangers, namely heat regenerators, seems an attractive choice, and the idea is examined in this section.

From the theory in Chapter 2, the stream coming from zone 1 in Figure 2-2 in the time period $\tau = 0$, π/ω is hot and should enter zone 2 cold during this period. Thus it is necessary to change the stream from hot to cold, beginning at $\tau = 0$. Note that this $\tau = 0$ for the second zone can be delayed relative to the first zone by a residence time lag in an interstage exchanger, but when the fluid leaving the first zone at $\tau = 0$ does arrive at the entrance to zone 2, it must be cold. This can be done by making the exchanger have thermal capacity, so that the thermal wave through the exchanger is delayed because of heat exchange between the stream and the packed bed of glass spheres or other particles having no mass adsorption capacity. The desired situation is shown in Figure B-1, assuming that the thermal equilibrium travelling wave equation, 2-11, is valid for the heat

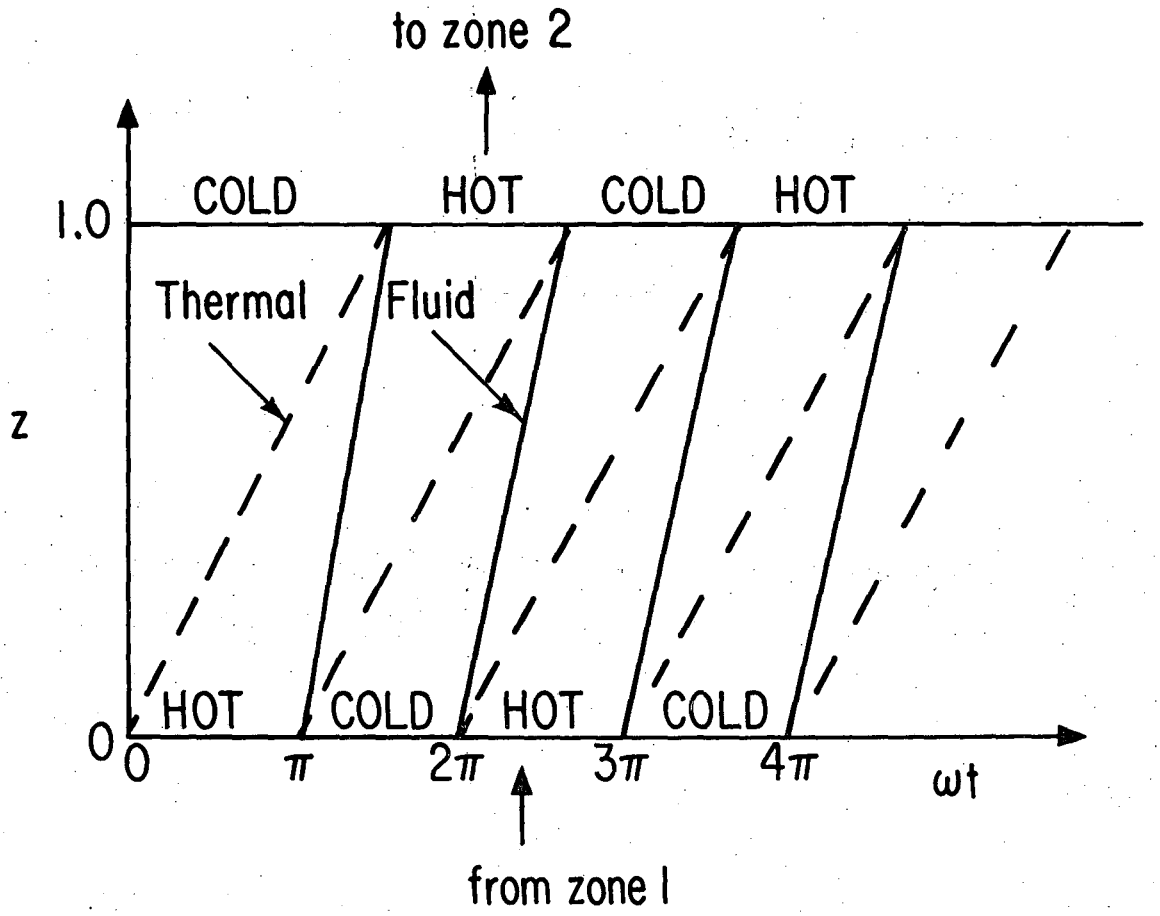

XBL 697-936

Figure B-1. Characteristics for interstage heat regenerator to reuse heat in multiple-zone cycling zone adsorption.

regenerator. The concentration characteristics travel at the fluid velocity since there is no mass adsorption. In the diagram, t and z are nondimensionalized using the length and residence time of the exchanger. It is necessary to have the regenerator larger than a zone, or to have it filled with material having a very high heat capacity, in order to have a thermal characteristic from one switch point intersect the fluid characteristic from the successive switch point at the exit of the regenerator.

The two main problems encountered in implementing the scheme experimentally are the thermal axial dispersion and the thermal losses through the walls.

Axial Dispersion

Since the residence time in the exchanger is larger than in the column, the thermal wave passes more slowly through it, allowing time for axial dispersive effects to occur; hence Equation 2-11 is not obeyed. If local equilibrium is assumed, Equations 2-2 and 2-4, after being nondimensionalized, reduce to (neglecting the effect of a small heat loss):

$$\frac{1}{u_{th}} \frac{\partial\theta}{\partial t} + \frac{\partial\theta}{\partial z} - \frac{1}{P} \frac{\partial^2\theta}{\partial z^2} = 0 \qquad \text{(B-1)}$$

with the conditions for a cold thermal wave passing through an initially hot regenerator being

$$\begin{array}{lll} \theta = 1 & z \longrightarrow \infty & t > 0 \\ \theta = -1 & z = 0 & t > 0 \\ \theta = 1 & t = 0 & z > 0 \end{array}$$

where $P = v\, z_o / (E_D + D_T)$.

The solution, outlined by Lapidus and Amundson (1952) is:

$$\theta = 1 - \text{erfc}\,(p_1^{1/2} - p_2^{1/2}) - e^P\,\text{erfc}\,(p_1^{1/2} + p_2^{1/2}) \qquad \text{(B-2)}$$

where $p_1 = P/4\,u_{th}\,t$

$p_2 = P\,u_{th}\,t/4$

Since e^P is very large while the erfc $(p_1^{1/2} + p_2^{1/2})$ is very small, the asymptotic expansion for erfc (x),

$$\text{erfc}\,(x) = \pi^{-1/2}\,e^{-x^2}\left(\frac{1}{x} - \frac{1}{2x^3} + \frac{1\cdot 3}{2^2\,x^5} - \frac{1\cdot 3\cdot 5}{2^3\,x^7} + \ldots\right)$$

is used.

Values of the axial eddy diffusivity are correlated by the group (Carberry and Bretton, 1958):

$$Pe_{disp} = \frac{d_p\,V}{E_D}\text{, the dispersion Péclet number,}$$

$$= 0.7 \text{, for liquids in laminar flow.}$$

For the phenolic plastic regenerator filled with glass spheres (d_p = 0.1 cm),

ρ_s	= 2.907 g/cm^3	mercury displacement
C_s	= 0.186 cal/g-°C,	Perry (1963c)
ρ_w	= 1.31 g/cm^3 ,	Perry (1963d)
C_w	= 0.23 cal/g-°C,	Perry (1963d)
α	= 0.37	
S	= 9.50 cm^2	
S_w	= 1.95 cm^2	
V	= 1.96 cm/min	

so that

$$u_{th} = 0.480, \quad \text{from Equation C-1.}$$

For this case

$$D_T = 8.55 \times 10^{-2} \text{ cm}^2/\text{min}$$
$$E_D = 2.80 \times 10^{-1} \text{ cm}^2/\text{min}$$
$$Z_o = 25.8 \text{ cm}$$
$$P = 1.38 \times 10^2$$

Equation B-2 and the experimental results are plotted in Figure B-2. The hot wave results are also plotted in reverse order for comparison; the increased mixing in this case is probably due to the instability of having hot fluid following cold fluid in upflow. Note that the amplitude attenuation effect is discussed in the next section; it is removed from this plot by normalizing both inlet and outlet temperatures about their own maximum and minimum values. The results indicate that the experimentally observed dispersion is due to axial dispersion; the restrictions this places on the regenerator scheme are discussed on page 118.

Radial Thermal Losses

The attenuation of the final (steady-state) amplitude of the travelling wave resulting from heat transfer through the insulated walls of the regenerator (or column) can be calculated from Equations 2-2 and 2-4. As $t \longrightarrow \infty$, these, nondimensionalized, reduce to

$$\frac{1}{P}\frac{d^2\theta}{dz^2} - \frac{d\theta}{dz} - P'\theta = -P'\theta_{air} \qquad \text{(B-3)}$$

with the conditions for a cold wave of

$$\theta = -1, \qquad z = 0 \qquad t \longrightarrow \infty$$
$$\theta = 1, \qquad z,t \longrightarrow \infty$$

which has the solution

$$\theta = e^{-f(P,P')} + \theta_{air}\left(1 - e^{-f(P,P')}\right)$$

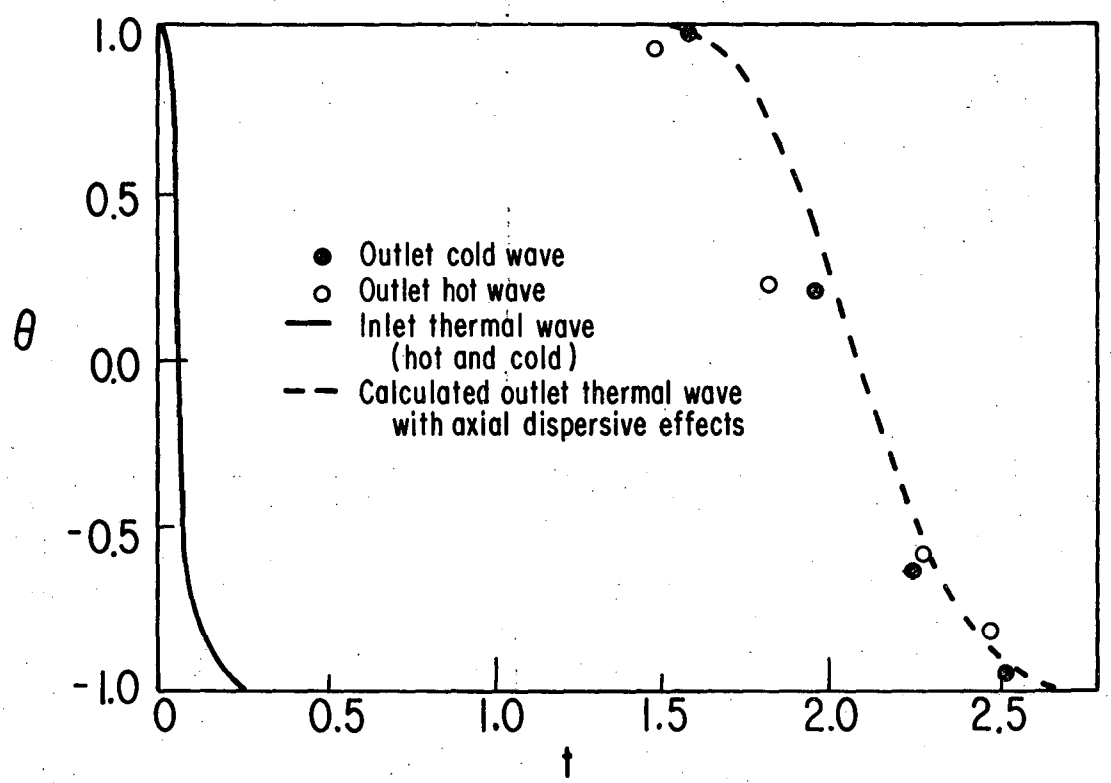

XBL 697-935

Figure B-2. Axial-dispersive effects in interstage heat regenerator for cycling zone adsorption.

where $$f(P,P') = \frac{P}{2}\left[1 - \left(1 + 4\,\frac{P'}{P}\right)^{1/2}\right]$$

$$\simeq P'\left(1 - \frac{P'}{P}\right)$$

(since $P'/P \ll 1$, using the binomial expansion)

where

$P' = h_w\, a_w\, Z_o / \alpha\, v\, \rho_f\, C_f$, thermal loss parameter

θ_{air} = dimensionless temperature of the surroundings (T_{air} = 24.5°C)

a_w = surface area of insulation/bed volume, 2.94 cm^{-1}

Under the assumption that heat transfer from the fluid to the wall is not controlling,

$$h_w = 1 \Big/ \left(\frac{r_3}{k_{T,w}} \ln \frac{r_2}{r_1} + \frac{r_3}{k_{T,ins}} \ln \frac{r_3}{r_2} + \frac{1}{h_{air}}\right)$$

where r_1 = inside radius of regenerator wall, 1.74 cm

r_2 = outside radius of regenerator wall, 1.91 cm

r_3 = outside radius of insulating wall, 4.45 cm

h_{air} = 12.21×10^{-3} cal/cm^2-min-°C, insulation to air transfer coefficient (Kreith, 1965b)

$k_{T,w}$ = 3.720×10^{-2} cal/cm-min-°C, wall conductivity (phenolic plastic) (Perry, 1963d)

$k_{T,ins}$ = 4.710×10^{-3} cal/cm-min-°C, insulation conductivity (polyurethane foam) (Perry, 1963d)

so that

$h_w = 1.115 \times 10^{-3}$ cal/cm^2-min-°C

$P' = 0.1170$

For T_C = 9.9°C, the exit temperature calculated from

Equation B-3 is 11.6°C, which compares with 11.4°C found experimentally. This 10 percent loss in amplitude could have been reduced to less than one percent by using multilayer insulation in a high vacuum ($k_{T,ins}$ = 2.48 x 10^{-5} cal/min-cm-°C.

Dual-Zone Experiment with Regenerator

The results of an experiment in which the first zone was forced with a standing temperature wave at a frequency of 0.30 cycles/min and the above interstage regenerator was used, followed by the second zone, is shown in Figures B-3a and B-3b. The effect of thermal axial dispersion and loss is evident in Figure B-3a, although not all the loss occurred in the regenerator; some took place in the interstage tubing. In comparison with Figure 5-9b, the separation is impaired, particularly during the enriched half cycle. Though these experiments were not carried any further, the conclusion is that the regenerator scheme may work if the intraparticle mass transfer is not too much poorer than the heat transfer, since, then, the flow rates will be fast enough that axial dispersion will not be a problem. Otherwise, as in this case, the separation will not be as good as with external exchangers. The radial heat losses will probably not be of any importance in large-scale (i.e. large-diameter) systems.

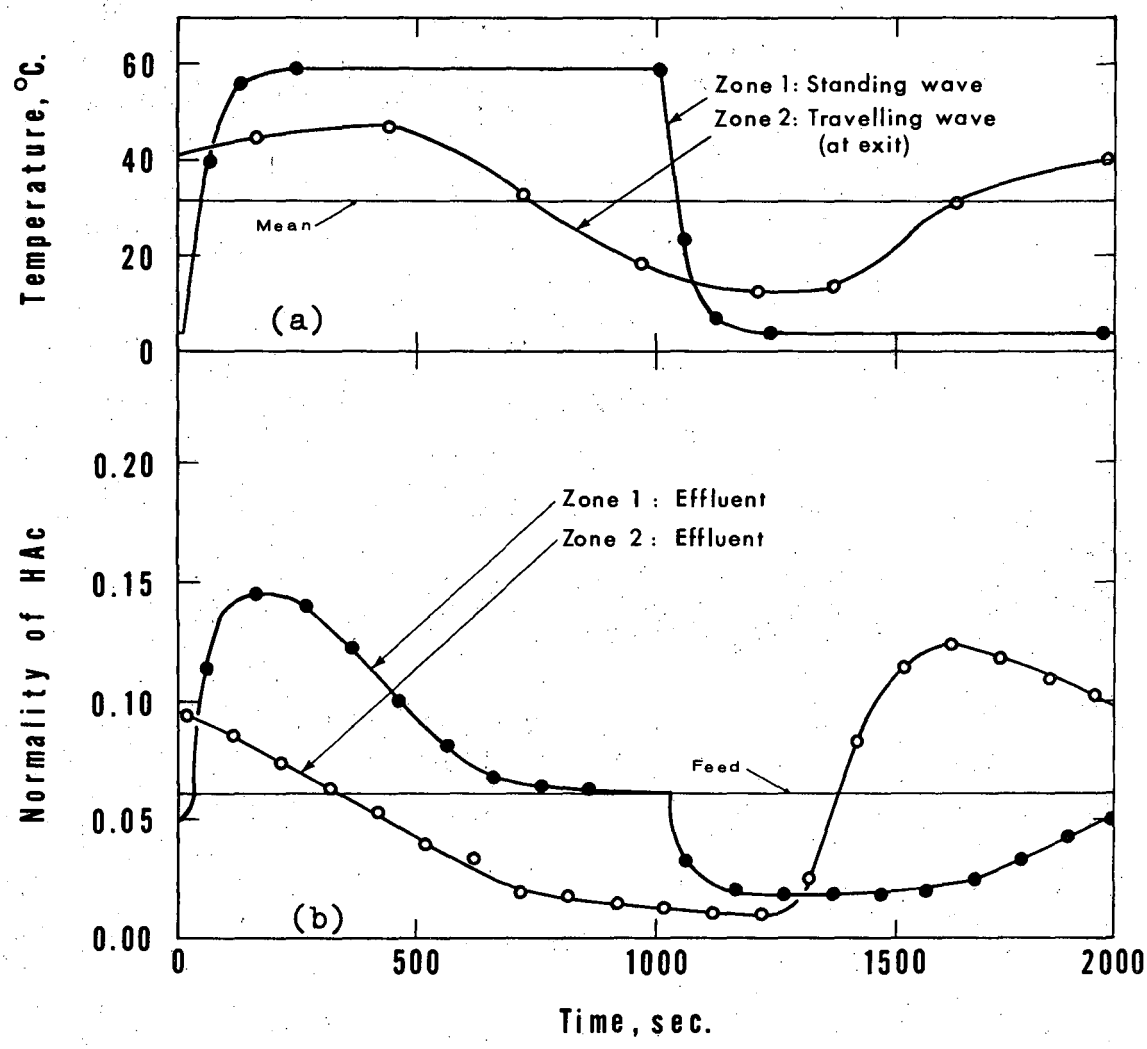

XBL 697-1052

Figure B-3. Dual-zone cycling zone adsorption, using standing square-wave forcing in the first zone and an interstage heat regenerator before the second zone.

(a) Temperature profiles.

(b) Effluent-concentration profiles.

APPENDIX C

THE EXPERIMENTAL PRODUCTION OF TRAVELLING THERMAL WAVES OF ARBITRARY VELOCITY

In Chapter 2 it was predicted that the use of a travelling thermal wave of approximately the velocity of the concentration waves would have a very desirable amplification effect on the separation. Although the experimental verification will be left to future research, some guidelines can be suggested. There are three possible ways of producing such waves.

(1) The most obvious is to have a moving external jacket similar to the stationary jacket used to produce the standing waves. The physical apparatus might be similar to the equipment used in the conventional process of zone refining, although the separation principle is different in the two cases. In his book on zone refining, Pfann (1966) suggests several techniques for creating such travelling thermal zones; these would not seem to be economically feasible on a large scale, however.

(2) Another method would be to increase the thermal capacity of the walls of the column in order to slow down the natural thermal wave moving through the column. If the wall thermal capacity is important, instead of the expression in Chapter 2,

$$u_{th} = \frac{\rho_f C_f \alpha}{\rho_s C_s (1-\varepsilon)(1-\alpha) + \rho_f C_f \varepsilon (1-\alpha) + \rho_f C_f \alpha + \rho_w C_w \sigma} \qquad \text{(C-1)}$$

where $\sigma = S_s/S$, the ratio of the wall cross-sectional area to the bed cross-sectional area.

This could be accomplished by making the column wall thicker or by inserting fins extending from the wall into the column. In some cases, slowing down the thermal wave could cause axial-dispersion problems in the wall or in the liquid, similar to those discussed in Appendix B. Both these two methods shift the thermal wave toward the concentration wave.

(3) A third method would shift the concentration wave toward the thermal wave by replacing some of the mass adsorptive packing with inert packing such as glass or metal spheres having only heat capacity. Obviously, in the standing wave case, this would be undesirable; because the preferential adsorption isotherm has effectively been reduced by the factor W_o/W_T, where W_T is the weight of the total packing, the separation would be reduced. Curiously, in the travelling-wave case, this disadvantage is outweighed by the enhancement of having the thermal and concentration waves closer together. Furthermore, the thermal axial-dispersion problem does not become more important, as the thermal wave is not slowed down as in the second method, and the heat transfer is more efficient than in the first method.

ACKNOWLEDGMENT

I would particularly like to thank Professor R. L. Pigford for his guidance, assistance, and enthusiasm in this project.

Also, I thank my fellow student Dwain Blum for his ideas and suggestions, and my typist, Mrs. Edith Taylor, for her thoroughness and concern.

Financial assistance for equipment expenses was provided through AEC Contract W-7405-eng-48 and by the Computer Center, University of California, Berkeley. Personal support by a University of California Fellowship, a NASA Predoctoral Traineeship (NSG(T)-117-2), and a Shell Companies' Foundation Grant is gratefully acknowledged.

LEGAL NOTICE

This report was prepared as an account of Government sponsored work. Neither the United States, nor the Commission, nor any person acting on behalf of the Commission:

A. Makes any warranty or representation, expressed or implied, with respect to the accuracy, completeness, or usefulness of the information contained in this report, or that the use of any information, apparatus, method, or process disclosed in this report may not infringe privately owned rights; or

B. Assumes any liabilities with respect to the use of, or for damages resulting from the use of any information, apparatus, method, or process disclosed in this report.

As used in the above, "person acting on behalf of the Commission" includes any employee or contractor of the Commission, or employee of such contractor, to the extent that such employee or contractor of the Commission, or employee of such contractor prepares, disseminates, or provides access to, any information pursuant to his employment or contract with the Commission, or his employment with such contractor.

TECHNICAL INFORMATION DIVISION
LAWRENCE RADIATION LABORATORY
UNIVERSITY OF CALIFORNIA
BERKELEY, CALIFORNIA 94720